Chem Soc Rev

Functional Crystalline Porous Framework Materials Based on Supramolecular Macrocycles

Journal:	*Chemical Society Reviews*
Manuscript ID	CS-SYN-10-2023-000939.R2
Article Type:	Review Article
Date Submitted by the Author:	02-Jan-2025
Complete List of Authors:	Wu, Yitao; Zhejiang University, Department of Chemistry Tang, Meiqi ; Zhejiang University, Department of Chemistry Barsoum, Michael L.; Northwestern University, Materials Science and Engineering Chen, Zhijie; Zhejiang University, Department of Chemistry Huang, Feihe; Zhejiang University, Department of Chemistry

Journal Name ARTICLE

Functional Crystalline Porous Framework Materials Based on Supramolecular Macrocycles

Received 00th January 20xx,
Accepted 00th January 20xx

DOI: 10.1039/x0xx00000x

www.rsc.org/

Yitao Wu,[a,b] Meiqi Tang,[a] Michael L. Barsoum,[c] Zhijie Chen,[a,b,*] Feihe Huang[a,b,*]

Crystalline porous framework materials like metal–organic frameworks (MOFs) and covalent–organic frameworks (COFs) possess periodic extended structures, high porosity, tunability and designability, making them good candidates for sensing, catalysis, gas adsorption and separation, etc. Despite their many advantages there are still problems affecting their applicability. For example, most of them lack specific recognition sites for guest uptake. Supramolecular macrocycles are typical hosts for guest uptake in solution. Macrocycle-based crystalline porous framework materials, in which macrocycles are incorporated into framework materials, are growing into an emerging area as they combine reticular chemistry and supramolecular chemistry. Organic building blocks which incorporate macrocycles endow the framework materials with guest recognition sites in the solid state through supramolecular interactions. Distinguished from solution-state molecular recognition, the complexation in the solid state is ordered and structurally achievable. This allows for determination of the mechanism of molecular recognition through noncovalent interactions while that of the traditional recognition in solution is ambiguous. Furthermore, crystalline porous framework materials in the solid state are well-defined and recyclable, and can realize what is not possible in solution. In this review, we summarize the progress of the incorporation of macrocycles into functional crystalline porous frameworks (i.e., MOFs and COFs) for their solid state applications such as molecular recognition, chiral separation and catalysis. We focus on the design and synthesis of organic building blocks with macrocycles, and then illustrate the applications of framework materials with macrocycles. Finally, we propose the future directions of macrocycle-based framework materials as reliable carriers for specific molecular recognition, guiding the crystalline porous frameworks with their chemistry, applications and commercialization.

1. Introduction

Crystalline porous framework materials are periodic frameworks formed by coordination bonds or covalent bonds.[1-25] These materials have their own unique advantages, such as ordered framework structures, high porosity, and ease of post-synthetic modification and functionalization.[26-28] Combining these merits, crystalline porous framework materials like metal–organic frameworks (MOFs) and covalent–organic frameworks (COFs) have found many uses in various fields, such as adsorption, separation and catalysis.[29-37] This class of materials have been developed rapidly over the last twenty years and many have been brought to commercial applications.[9,13,38] For example, MOF Technologies made efforts to improve fruit packaging using MOFs, and Numat/Merck are selling cylinders which can safely store highly volatile gases at lower pressures utilizing these materials.[39-48] Additionally, governments have increased interest in the framework materials. For example, the U.S. Department of Energy is supporting the realization of direct air capture through crystalline porous framework materials, which can directly recover carbon dioxide from a concentration of 0.04 percent in the atmosphere at a low cost.[49-52] In general, the use of crystalline porous framework materials is expected to reach many industries and see far reaching applications outside the laboratory.

Despite increased usage in industrial and commercial markets many problems have yet been solved using conventional crystalline porous frameworks. For example, up to now, a thorough understanding of the geometry of nanopores in porous materials is still not fully realized and there are challenges in precisely controlling the pore size.[53-61] In traditional porous framework materials, nanopores are generated by the formation of a network structure between ligand molecules.[62-72] Porous framework materials provide nanopores with high free volume due to their rigid skeletons, but the pore size and environment can be influenced by solvent and temperature, which can lead to pore collapse.[65,73-77] Therefore, due to the poorly defined pores in traditional porous materials, the direct fabrication and precise control of crystalline porous framework materials with permanent nanopores is still an area of active interest.[78-81] Supramolecular macrocycles with permanent pores have the potential to conquer this challenge.[82-90] Macrocycles, a kind of molecular materials binding small molecular guests through supramolecular interactions, are undergoing a recent boom in progress due to the simple synthesis and easy functionalization.[91-104] During the last decade, macrocycle-based crystalline porous frameworks have been developed to some extent.[53,54,72,105-112] Different from traditional framework materials, these macrocycle-based frameworks bind guest molecules with specific interactions. These interactions can utilize the pore aperture and internal surface area to accommodate guest molecules in the sorting domain (the pores

[a] Stoddart Institute of Molecular Science, Department of Chemistry, Zhejiang University, Hangzhou 310027, P. R. China. E-mail: zhijiechen@zju.edu.cn; fhuang@zju.edu.cn.
[b] Zhejiang-Israel Joint Laboratory of Self-Assembling Functional Materials, ZJU-Hangzhou Global Scientific and Technological Innovation Center, Hangzhou 311215, P. R. China.
[c] Department of Materials Science and Engineering, Northwestern University, 2145 Sheridan Road, Evanston, Illinois 60208-3113, USA.

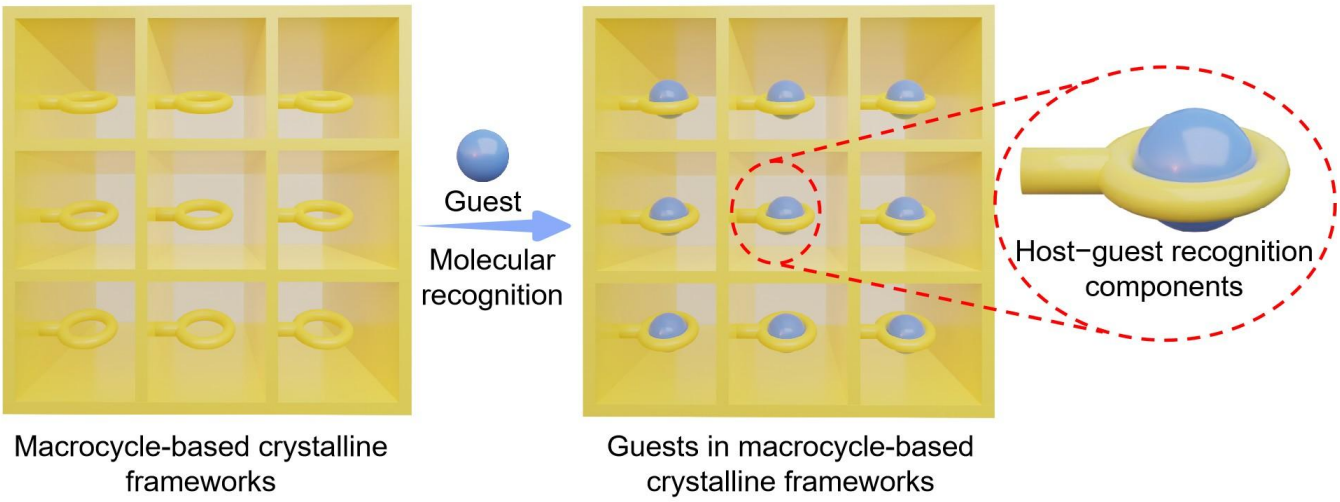

Fig. 1 Schematic representation of molecular recognition in the macrocycle-based crystalline porous framework materials.

can incorporate guest molecules with size-selectivity) and the coverage domain (the struts and joints within pores can interact with guest molecules).[27,113] Macrocycle-based frameworks recognize incoming guests with controlled cavities in the active domain.[114-118] This kind of recognition is sensitive to size, shape, and electric charge, allowing for randomly distributed guests in solution to access the permanent pores of framework materials and be ordered within the pores (Fig. 1).[114] The high degree of ordered guests in macrocycle-based frameworks allows for clear structure determination of the guest-containing frameworks while traditional crystalline porous framework materials like MOFs often contains guest molecule in the disordered forms.[114,119,120]

Therefore, much effort has been done to synthesize these framework materials for molecular recognition applied in various fields through a bottom-up "pre-porous macrocycle to porous framework" approach. Early examples of macrocycle-based framework materials use crown ethers.[114,121-126] Flexible crown ethers were firstly introduced to zinc-based MOFs to provide active domain for binding positively charged molecules like paraquat (**PQT**) derivatives.[114] Then a series of crown ether-based MOFs were also systematically investigated to reveal the mechanism of molecular recognition in the interior of frameworks, giving a comprehensive explanation from structures to applications.[42-47] In more recent years, pillararenes, a new generation of macrocycles, exhibited their potential in chiral separation and gas adsorption due to the planar chirality and adaptive pores for molecular recognition, showing the possibility of being applied in crystalline porous frameworks.[87, 127,128] Other macrocycles such as cyclodextrins,[129,130] calixarenes,[131,132] and cucurbiturils[133,134] have similarly established their foundation in the macrocycle-based reticular chemistry by combining the merits of their own characteristics. However, the full potential of these materials remains to be explored because of the difficulty in incorporating macrocycles into frameworks.[54] Remaining challenges in the molecular recognition field include balancing many material characteristics such as of efficiency, selectivity, system-level operation, and cost.[54]

In this review, we summarize the major progress of crystalline porous frameworks based on supramolecular macrocycles. This comprehensive review of the macrocycle-based crystalline porous frameworks detailedly narrates their development history, existing problems and future opportunities. A discussion on the precise regulation of the macrocycles in framework materials is conducted for recognizing specific molecules and improving the output of these materials for the future commercial applications.

2. Design and synthesis of macrocycle-based crystalline porous frameworks

In this section, we introduce the design principles of crystalline porous framework materials incorporating macrocycles. Macrocycles and crystalline porous framework materials have many synergistic effects including, but is not limited to: (1) crystallinity allows the ordered arrangement of macrocycles, (2) porosity permits the accessibility of specific interaction sites of macrocycles, and (3) macrocycles bring a high degree of recognition for host–guest interactions.

2.1. Difference between crystalline porous frameworks with and without supramolecular macrocycles

As discussed previously, crystalline porous framework materials without macrocycles still have some problems, such as the lack of specific recognition sites which makes selective interactions more difficult. In 2009, the Yaghi group introduced supramolecular macrocycles into the crystalline framework materials to overcome this challenge.[114] They introduced the

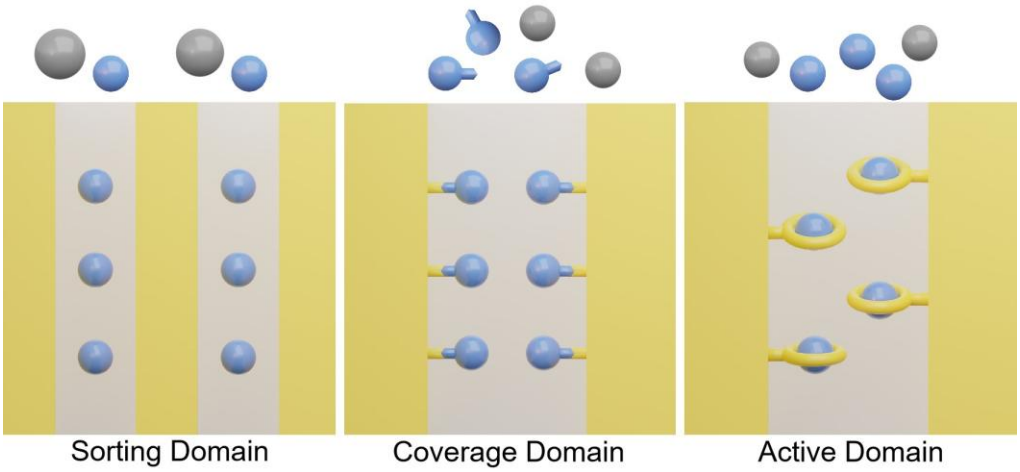

Fig. 2 Comparison between sorting domain, coverage domain and active domain. Sorting domain: the pores can incorporate guest molecules with size-selectivity. Coverage domain: the struts and joints within pores can interact with guest molecules. Active domain: the pores can recognize guest molecules with size-, shape-, and electronic-elements.

concept of architectural domain into framework materials, which can help to explain the selective phenomena of supramolecular macrocycles. To date , most of the crystalline framework materials can be considered to have three important structural domains: 1) The sorting domain where guest molecules can enter the pores of crystalline framework materials according to the pore sizes;[114,135,136] 2) the coverage domain where the guest molecules can enter the inside of the frameworks according to some non-specific interactions on the interface of crystalline framework materials and, in some cases, for example, these interactions may come from open metal sites in the pores;[137,138] 3) the active domain where the size, shape and charge of the incoming guest molecules are considered in the interactions.[114,119] Supramolecular macrocycles with specific recognition sites in the crystalline framework materials can act as active domains to create binding sites where guest molecules can dock in a highly specific fashion,[119] while sorting domain and coverage domain do not show the specific recognition in the conventional crystalline framework materials (Fig. 2). Therefore, macrocycle-incorporated crystalline framework materials bring new opportunities to solid state molecular recognition. In other word, this is what supramolecular chemistry brings to reticular chemistry.[139,140]

2.2. Preparations and structures of macrocycle-based crystalline porous frameworks

In this section, strategies of designing organic struts for constructing crystalline frameworks are discussed. It is known that the design and synthesis of macrocycle-incorporated ligands is the key to fabricate macrocycle-based crystalline frameworks. However, the macrocycle-containing moiety is often challenging to synthesize. In some cases, chelate units on macrocycles, such as cyclodextrins, calixarenes, and cucurbiturils, can be used as organic struts directly (Fig. 3).[141-143] However, other macrocycles need further synthetic modification to functionalize the macrocycles through classical Suzuki coupling and Sonogashira coupling, etc.[114] Most importantly, the types, sizes and lengths of the macrocycles in the ligands can be further adjusted according to different needs, which is more conducive to the future commercialization. A summary of strategies for incorporating such macrocycles into crystalline porous frameworks is summarized in Fig. 3.

Herein we summarize the design and synthesis of macrocycle-incorporated components. There are three main strategies for introducing supramolecular macrocycles into crystalline framework materials (Fig. 3): 1) The reaction groups on supramolecular macrocycles can be modified with carboxylic, hydroxyl and pyridine coordination groups for MOF preparation,[114,119,120] while for the COF preparation, amino, aldehyde and boric acid groups can be modified on the macrocycles.[144,145] In this strategy, the cavity of the supramolecular macrocycles in the crystalline frameworks materials is generally unoccupied.[114] Therefore, the molecular recognition ability of crystalline framework materials can be significantly improved after the incorporation of accessible supramolecular macrocycles. For example, the introduction of crown ethers to crystalline frameworks materials will endow them the ability of binding ions; 2) a pre-organized supramolecular macrocycle-incorporated host–guest complex can also be established for preparing MOFs and COFs.[146-148] These macrocyclic complexes on the reaction components can be rotaxanes and catenanes.[125,149] In these cases, on account of the pre-organized recognition components and adjustable supramolecular interactions, the dynamics of crystalline frameworks can be investigated in the solid state and the performance of them can be regulated with the incorporation of highly adjustable components; 3) supramolecular

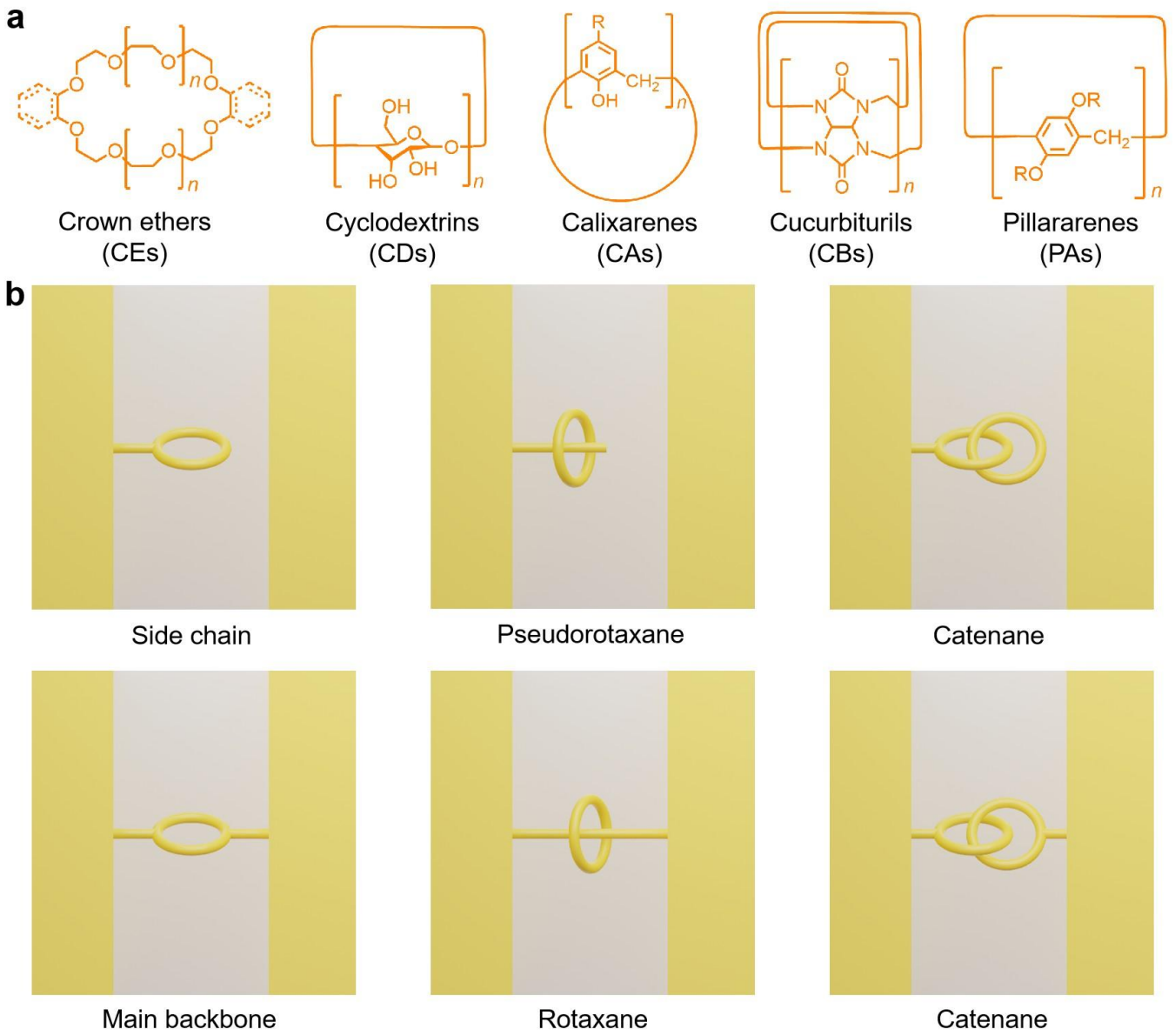

Fig. 3 (a) Typical supramolecular macrocycles involved in this review. (b) Cartoon representations of macrocycle-incorporated components involved in this review for preparing crystalline framework materials. The strategies of incorporating macrocyclic components into crystalline frameworks include introducing these components as side chain, main backbone, pseudorotaxane, rotaxane and catenane units.

moieties can also be attached on the surface or in the interior of the crystalline framework materials through supramolecular interactions.[150] Using this strategy, the modified macrocycles attached on the crystalline framework materials can provide additional recognition sites for improving the performance of extended drug release and selective catalysis.[150-156]

3. Crown ether-based crystalline porous framework materials

Crown ethers (CEs) are the first generation of supramolecular macrocycles and have been used as flexible hosts to prepare solid materials due to their favorable stability, activity, and recyclability.[92,157-159] Many examples of CE-based framework materials have been reported, especially MOFs and COFs.[125,160] The CE-based MOFs and COFs not only reveal the host–guest mechanisms in the frameworks but also have been demonstrated in a wide range of applications including: molecular recognition, catalysis, chiral separation, molecular machines and many others.[122,126,161-165] Herein we summarize some of the prototypical examples of CE-based framework materials as well as their organic units (Fig. 4), and they are broken into the subsections according to their applications as discussed below.

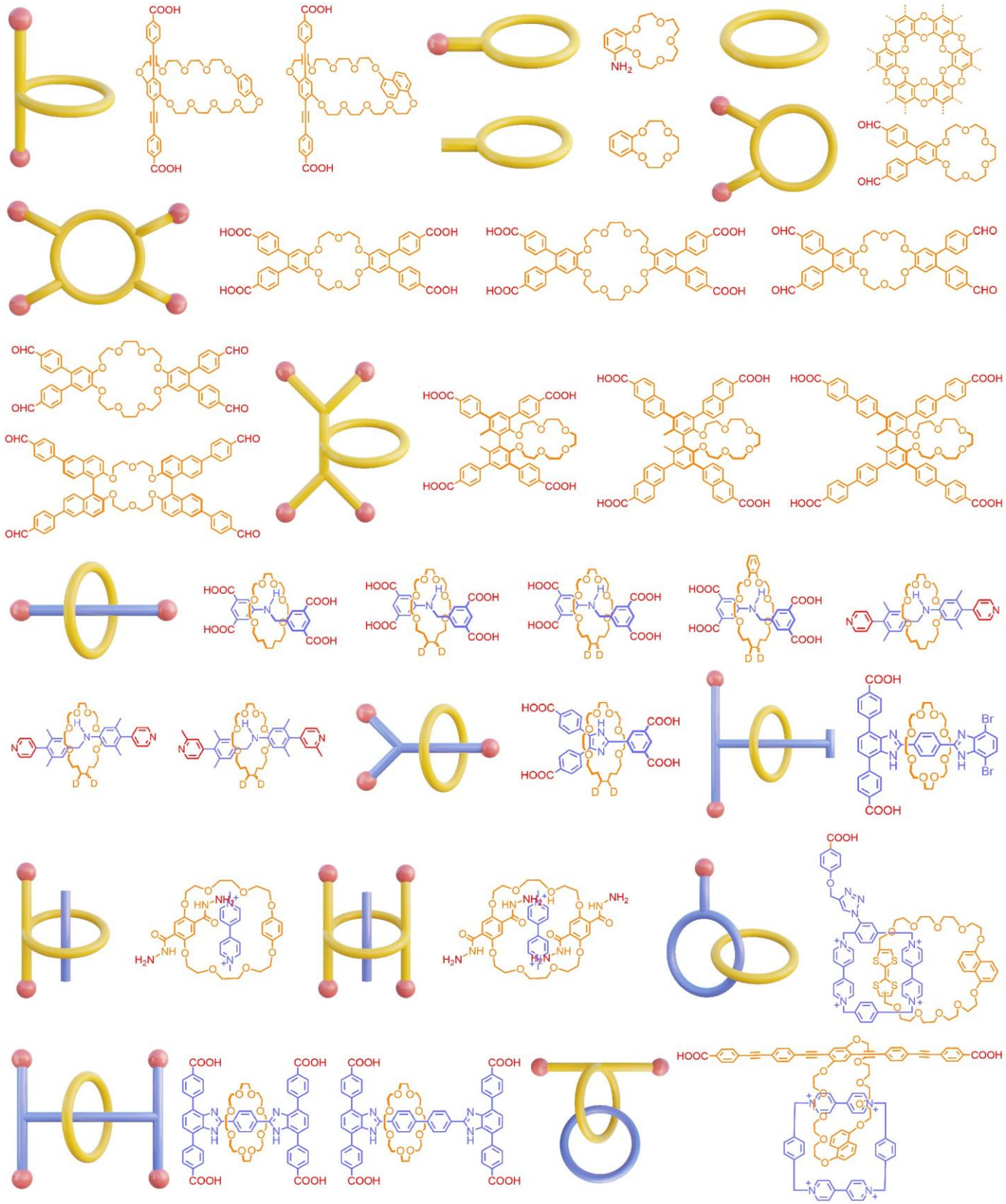

Fig. 4 Cartoon representations and chemical structures of CE-incorporated components involved in this review for preparing crystalline framework materials.

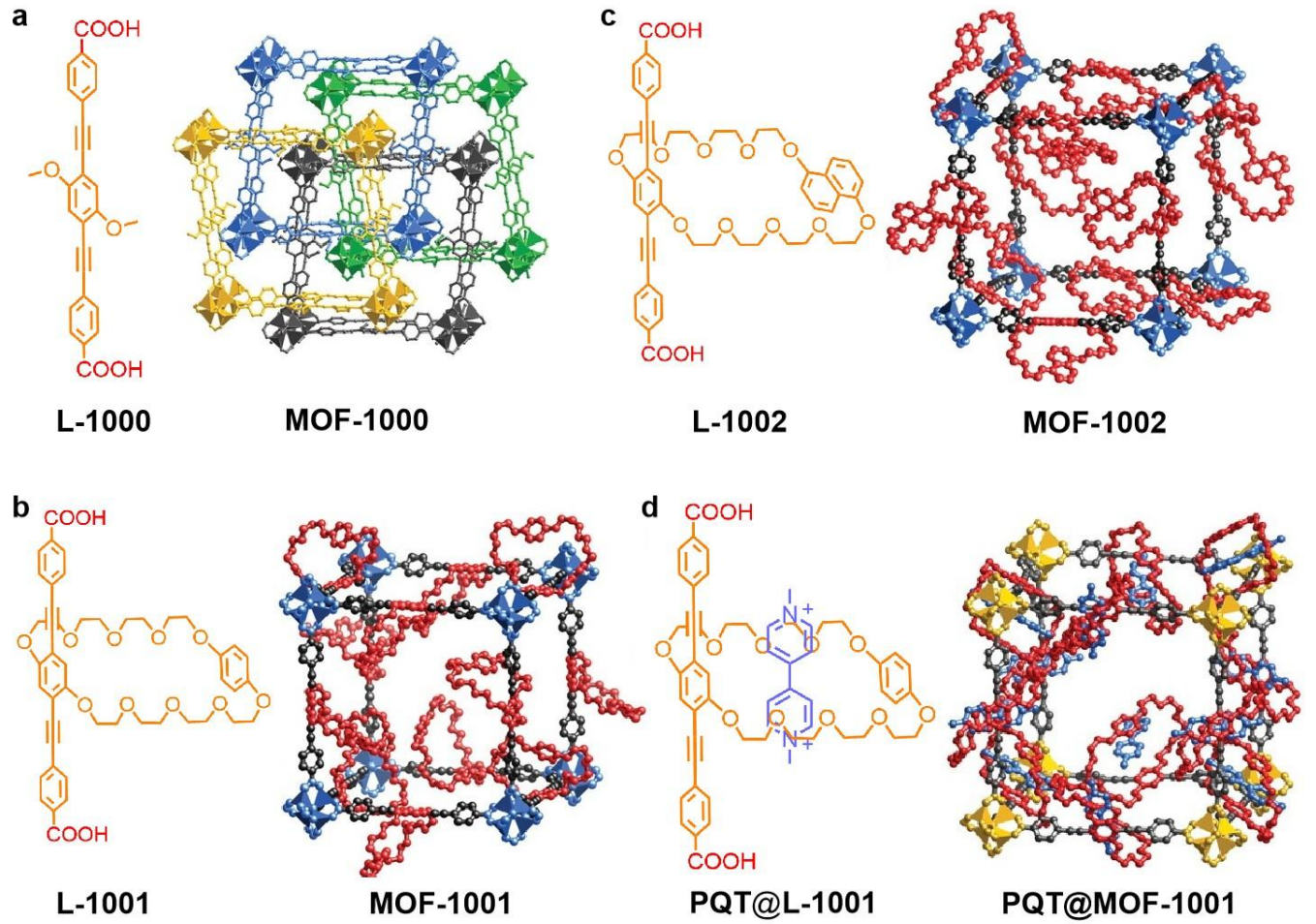

Fig. 5 Chemical structures and crystal structures of (a) **L-1000** and **MOF-1000**, (b) **L-1001** and **MOF-1001**, and (c) **L-1002** and **MOF-1002**. (d) Chemical structure and calculated structure of **PQT@L-1001** and **PQT@MOF-1001**. Reproduced from ref. 114 with permission from American Association for the Advancement of Science, copyright 2009.[114]

3.1. Crown ether-based MOFs

The applications of CE-based MOFs mainly focus on molecular recognition, artificial membranes and chiral separation. Due to the ease of material modifications, the strategies for constructing CE-based MOFs are very diverse.

3.1.1. Molecular recognition

In 2009, the Yaghi group reported a number of quintessential CE-based MOFs.[114] Using organic struts containing 34- and 36-membered CEs as ligands, they constructed several CE-based MOFs named **MOF-1001** and **MOF-1002** with **pcu** networks (Fig. 5). For comparison they also constructed an isostructural system without CE units named **MOF-1000** (Fig. 5). These MOFs are consisted of organic struts and $Zn_4O(CO_2)_6$ cluster joints. Their structures were solved using single crystal X-ray diffraction (SCXRD). The SCXRD results revealed that **MOF-1000** showed four-fold interpenetrated networks while **MOF-1001** and **MOF-1002** showed open frameworks due to the existence of CE units. Among the CE-incorporated MOFs, **MOF-1001** was capable of recognizing electron-deficient **PQT** guests. They quantitatively characterized **PQT@MOF-1001** and **PQT@L-1001** complexes by SCXRD and solid state nuclear magnetic resonance (ssNMR) method. The ssNMR studies confirmed that **MOF-1001** could complex **PQT** in a specific manner. By comparison, another model MOF (**MOF-177**) without incorporation of CEs revealed that the adsorption of **PQT** was negligible, indicating the importance of CE units for **PQT** complexation in MOFs. The recognition exhibited in these frameworks is similar to the drug molecule recognition by protein receptors, as it is highly selective.[114] Perhaps more importantly, this work introduces the concept of architectural domains in reticular chemistry, establishing the theoretical foundation of macrocycle-based crystalline porous frameworks.

Yaghi's work revealed the crown ether–cation recognition components in the MOFs. It is well known that MOFs have shown unique advantages in gas storage.[71,166] However, gas storage usually needs to be carried out at low temperature and high pressure.[71,167] Gas storage at room temperature still remains a challenge.[71,167] The Suh group introduced CE (benzo-18-crown-6, **B18C6**) components into the MOF structures and

developed a zinc-based MOF **Zn-B18C6-MOF** from **B18C6-4PhCOOH** for hydrogen storage, which contains **B18C6** units to provide specific cation binding sites (Fig. 6).[161] The single crystal structure of **Zn-B18C6-MOF** reveals a two-fold interpenetrated networks, producing one dimension channels along the *c*-axis (Fig. 6). The estimated solvent accessible void volume in **Zn-B18C6-MOF** accounted for 39.2% of the whole structure. After the complexation of CE units with K^+, NH_4^+ and **PQT**, the electrostatic interactions between **Zn-B18C6-MOF** and N_2/H_2 significantly increased, which improved the gas storage capacity (e.g., the H_2 uptake increase from 1.06 wt% to 1.19 wt% after **Zn-B18C6-MOF** complexing with K^+). Supercritical CO_2-activated **Zn-B18C6-MOF** has a isosteric heat (Q_{st}) of hydrogen storage (7.70 kJ mol^{-1}). In the K^+-complexed **Zn-B18C6-MOF**, the K^+ ions have an effect on increasing the Q_{st} of H_2 adsorption (9.92 kJ mol^{-1}) due to the accessible open metal sites on K^+.[161] Their work provides an evidence for CE-incorporated MOFs in increasing the recognition ability of guest molecules.

Fig. 6 Synthesis and crystal structure of **Zn-B18C6-MOF**. C atoms are grey, O atoms are red, Zn atoms are blue, and H atoms are omitted for clarity.[161]

Ion recognition has importance in a number of separation applications.[126,168-170] For example, strontium (II) (Sr^{2+}) is commonly found in nuclear waste streams, the presence of this ion can cause serious radioactive contamination.[171,172] Designing efficient adsorbents for the separation of Sr^{2+} is the key to the removal of radioactive strontium. Accordingly, Suh's **Zn-B18C6-MOF** is not stable enough for this separation. Based on the work of the Suh group, Li's group reported a Ni-MOF named **Ni-B18C6-MOF** using the same ligand, and this MOF can be used for the removal of Sr^{2+} through the **B18C6** units in **Ni-B18C6-MOF**.[150] Compared with the conventional MOFs, **Ni-B18C6-MOF** has independent and evenly distributed **B18C6** cavities in the channels. Each asymmetric unit contains three Ni^{2+} and two **B18C6-4PhCOOH** units. Structural analysis showed that **Ni-B18C6-MOF** has an estimated solvent accessible void volume of 51.5% of the entire structure, suggesting that **Ni-B18C6-MOF** can provide more volume for Sr^{2+} due to the ordered non-interpenetrated framework. This property of **Ni-B18C6-MOF** can effectively complex Sr^{2+} through the channels and prevent Sr^{2+} from blocking the pores (Fig. 7). Thus, with these specific recognition sites, they achieved a 99.73% removal selectivity of Sr^{2+} in simulated nuclear wastewater. This work further expands the application of designing highly efficient CE-based MOF adsorbents for separating specific substances from complicated environments.[150]

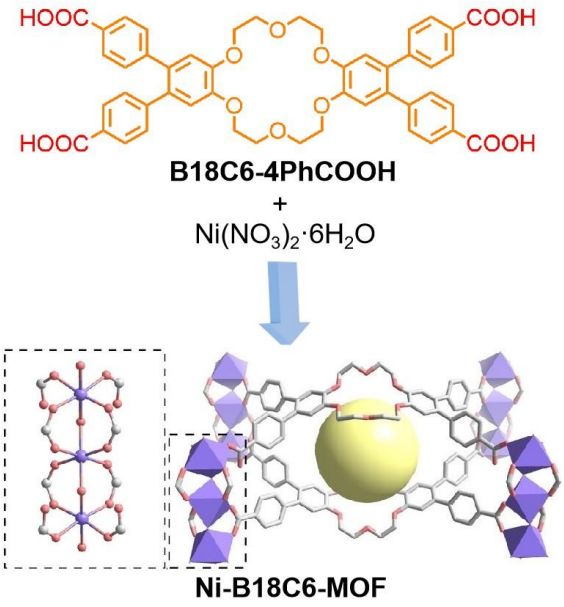

Fig. 7 Synthesis and crystal structure of **Ni-B18C6-MOF**. C atoms are grey, O atoms are red, Zn clusters are purple, and H atoms are omitted for clarity. Reproduced from ref. 150 with permission from John Wiley & Sons, copyright 2023.[150]

Xiao's group also successfully introduced **B18C6** and benzo-24-crown-8 (**B24C8**) units into MOFs. They designed and synthesized more stable zirconium (Zr)-based MOFs, named **Zr-B18C6-MOF** and **Zr-B24C8-MOF**, respectively (Fig. 8).[173] SCXRD analysis revealed that **Zr-B18C6-MOF** is consisted of octahedral Zr_6 nodes, each of which is composed of 6 Zr atoms, 4 μ_3-OH and 4 μ_3-O groups. The coordination network is further assembled into a one-dimensional channel along the *c*-axis. The connection between the two Zr_6 clusters and the two ligands forms a two-dimensional layered structure. The pore structure results in a solvent accessible volume up to 55%. As comparison, **Zr-B24C8-MOF** is composed of two-fold interpenetrated frameworks. Each Zr_6 cluster is connected to eight deprotonated ligands, two of which are coordinated in a single-dentate manner and the remaining ligands are coordinated in a double-dentate manner. Both MOFs maintain the porosity and stability under various solvent and pH conditions. Brunauer–Emmett–Teller (BET) surface areas of **Zr-B18C6-MOF** and **Zr-B24C8-MOF** are 1145 m^2

g^{-1} and 440 m^2 g^{-1}, respectively. Similarly, **Zr-B18C6-MOF** and **Zr-B24C8-MOF** showed excellent adsorption properties for Sr^{2+} and Cs^{2+}, respectively. Their single crystal structures reveal the precise location of Sr^{2+} and Cs^{2+} in **Zr-B18C6-MOF** and **Zr-B24C8-MOF**, which illustrate the adsorption mechanisms. This work provides further support for utilizing the crown-ether MOFs for ion recognition and molecular/ionic separations.[173]

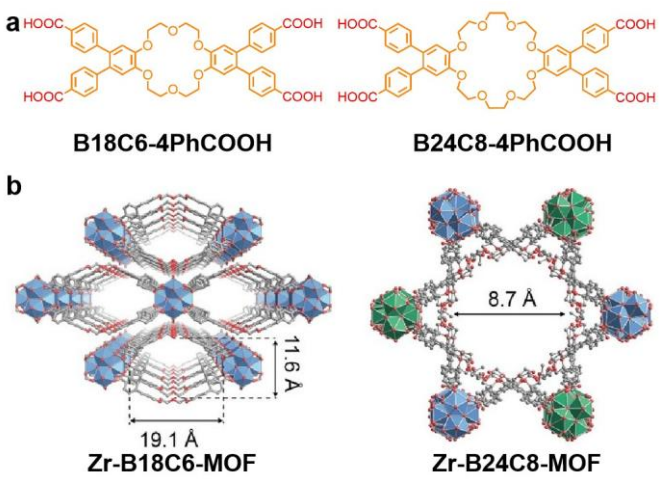

Fig. 8 (a) Chemical structures of **B18C6-4PhCOOH** and **B24C8-4PhCOOhH**. (b) Crystal structures of **Zr-B18C6-MOF** and **Zr-B24C8-MOF**. C atoms are light grey, O atoms are red, Zr clusters are blue or green, and H atoms are omitted for clarity.[173]

3.1.2. Chiral separation

The work mentioned above laid the foundation for the mechanism of MOF–guest recognition with CEs. Now, we turn our focus to chiral separations of racemic mixtures as it is significant in the chemical industry.[174-178] The application of chiral separation using crystalline framework materials has been extensively studied.[174-176] However, developing new chiral stationary phases (CSPs) for chiral resolution remains a challenge. Cui's group designed and synthesized a set of highly stable Zr-based MOFs that can be used as CSPs for high performance liquid chromatography (HPLC) (Fig. 9).[162] Through the synthesis of three tetracarboxylic ligands of the enantiomers 1,1'-biphenyl-20-crown-6 (**(*S*)-H_4L^1**, **(*S*)-H_4L^2** and **(*S*)-H_4L^3**), they prepared three chiral Zr-based MOFs denoted as **CE-1**, **CE-2** and **CE-3** that share the same **flu** topology but differ in channel sizes. **CE-1**, **CE-2** and **CE-3** have the same space group and topology. They crystallize in a chiral space group $P2_12_12_1$. Due to the symmetry of the frameworks and the disorders of the CE structures, the exact location of the CE units cannot be determined by SCXRD in the above cases. The chiral CE units in the MOFs are simulated and periodically arranged within the frameworks, allowing stereoselective recognition of guests through specific supramolecular interactions. These MOFs are stable in water, acid, and base environments. The Zr-MOF-filled HPLC column provides high resolution and selectivity for the chiral separation of a variety of racemic mixtures, including amino acids and *N*-containing drugs, and even outperforms several commercial chiral HPLC columns. Density functional theory (DFT) calculations reveal that these Zr-MOFs provide special microenvironments of chiral CE units, thus improving the selectivity of chiral separation.[162] Their work further establishes the practical applications of CE-based MOFs.

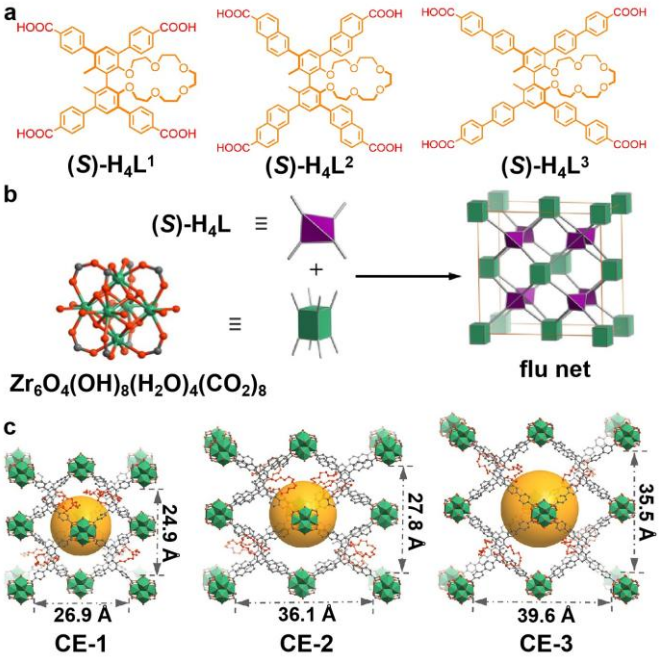

Fig. 9 (a) Chemical structures of ligands **(*S*)-H_4L^1**, **(*S*)-H_4L^2** and **(*S*)-H_4L^3**. (b) A **flu** framework constructed from 4-connected linkers (**(*S*)-H_4L^1**, **(*S*)-H_4L^2** and **(*S*)-H_4L^3**) and 8-connected Zr nodes. (c) Structures of **CE-1**, **CE-2**, and **CE-3**. Here the pores are highlighted by yellow spheres, C atoms are grey, O atoms are red, Zr clusters are green, and H atoms are omitted for clarity. Reproduced from ref. 162 with permission from American Chemical Society, copyright 2021.[162]

3.1.3. Mechanically interlocked molecules

The CE recognition units can also be complexed on aniline axles in MOFs as pre-organized host–guest components. These pre-organized host–guest complexes in MOFs are regarded as mechanically interlocked molecules. The dynamics of mechanically interlocked structures in solution have been well studied.[179-181] However, the molecules are randomly dispersed and do not show continuity in solution. The synthesis of MOFs through constructing CEs and cation complexed struts provides a new strategy for the study of dynamics of mechanically interlocked structures in the solid state. Based on this strategy, Loeb's group did a set of systematic works, they constructed a MOF named **UWDM-1**, which utilized a 24-crown-6 (**24C6**)-based [2]rotaxane (**L-1**) as an organic ligand and Cu (II) units as metal nodes (Fig. 10).[146] The molecular formula of **UWDM-1** is $[Cu_2(\mathbf{L\text{-}1})(H_2O)_2]\cdot 3H_2O$ as confirmed by SCXRD analysis. This MOF

has a **nbo** topology, in which water molecules occupy a small internal space (11%) in the crystal structure lattice. The activated material creates increased free space within relatively rigid frameworks, enabling the rapid rotation of CEs on the [2]rotaxane units. The dynamic changes inside the MOF were demonstrated by ^{13}C and ^{2}H ssNMR experiments. Their results provide a novel approach for the construction of solid state molecular machines based on pre-organized mechanically interlocked molecules in CE-based MOFs.[146]

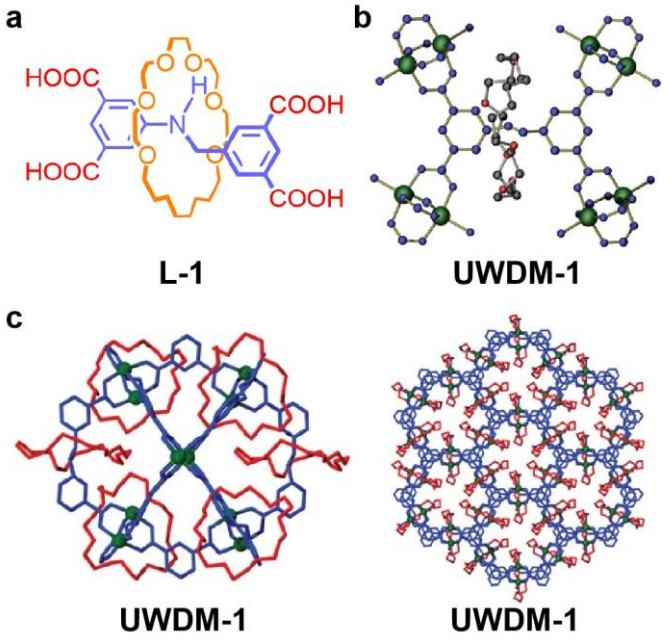

Fig. 10 (b) Chemical structure of ligand **L-1**. (a) Ball-and-stick representation of the single crystal structure of **UWDM-1** containing a **24C6** moiety. Here C and N atoms are blue, O atoms are red, Cu atoms are green, and H atoms are omitted for clarity. (c) Capped stick representations of the single crystal structure of **UWDM-1**. The coordinative ligands are blue, **24C6** components are red, and Cu nodes are green. Reproduced from ref. 146 with permission from Springer Nature, copyright 2012.[146]

Loeb's group also investigated the effect of the ring size of CE components on the dynamics within MOFs (Fig. 11).[182] Similar with Loeb's prior work discussed above, they constructed [2]rotaxanes based on CEs with different sizes (22-crown-6, **22C6**; 24-crown-6, **24C6**; benzo-24-crown-6, **B24C6**) and an aniline axle containing carboxylic acid ligands. Compared to **UWCM-1**, under the same synthetic conditions, ligands (**L-1**$_{(22)}$, **L-1**$_{(24)}$ or **L-1**$_{(B24)}$) react with $Cu(NO_3)_2{\cdot}H_2O$ to form similar structures with macrocycles of different sizes in **UWDM-1**. The molecular formula of **UWDM-1**$_{(22)}$ is $[Cu_2(\textbf{L-1}_{(22)})(H_2O)_2]{\cdot}4(H_2O)$ and crystallizes in the *R*3 space group as confirmed by SCXRD analysis. They compared the single crystal structures of **UWCM-1** (crown ether free) and **UWDM-1**$_{(22)}$**.** They found that the CE-containing structure produced a **nbo**-type MOF with enough space to allow the CEs to rotate within the MOF pores, while the CE-free structure produced a 12-linked **bcc** structure. The ^{2}H ssNMR showed that the CE units in **UWDM-1**$_{(22)}$, **UWDM-1**$_{(24)}$ and **UWDM-1**$_{(B24)}$ (synthesized from **22C6**, **24C6** and **B24C6**, respectively) rotate to different degrees according to their sizes and shapes.[182] This work is a systematic study of the dynamics within MOF materials using vary-sized CEs as movable components, further illustrating the high degree of tunability in CE-incorporated MOFs.[182]

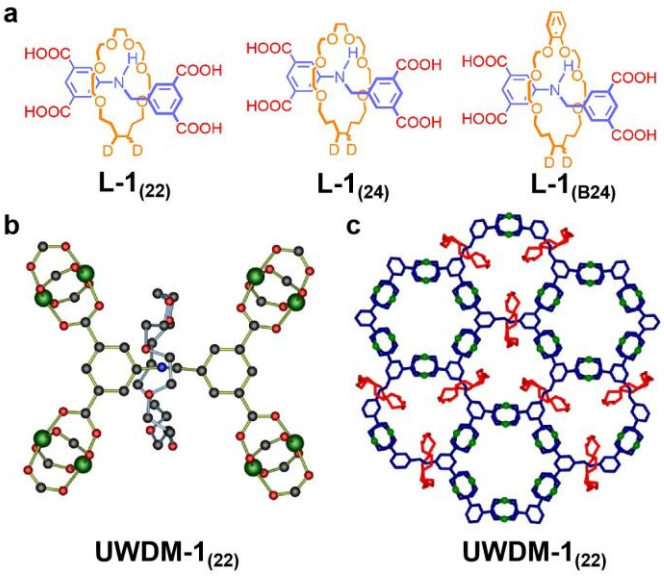

Fig. 11 (a) Chemical structures of ligands **L-1**$_{(22)}$, **L-1**$_{(24)}$ and **L-1**$_{(B24)}$. (b) Ball-and-stick representation of the single crystal structure of **UWDM-1**$_{(22)}$. Here C atoms are black, O atoms are red, N atom is blue, Cu atoms are green, and H atoms are omitted for clarity. (c) Capped stick representation of the single crystal structure of **UWDM-1**$_{(22)}$. Here frameworks are blue, **22C6** components are red, Cu nodes are green, and H atoms are omitted for clarity. Reproduced from ref.182 with permission from American Chemical Society, copyright 2015.[182]

Loeb's group continued to develop the mechanically interlocked CE-based structure (ligand **L-2**) in two MOFs using "pillar–layer" strategy [183,184] and denoted them as **UWDM-2** and **UWDM-3** with **pcu** topology (vary in "layering" and interpenetration) (Fig. 12).[147] The CE-based ligand is a [2]rotaxane containing a **24C6** unit and a pyridine group-terminated amine base axis. The MOF structures solved by SCXRD show that there is enough free space in the frameworks of **UWDM-2** and **UWDM-3** to accommodate the rotation of the interlocked **24C6** component, where the frameworks of **UWDM-2** are three-fold interpenetrated and **UWDM-3** are two-fold interpenetrated. They conducted variable temperature (VT) ^{2}H ssNMR experiments and showed that the **24C6** components in **UWDM-2** and **UWDM-3** could perform partially restricted motion but could not rotate freely. Additionally, VT powder X-ray diffraction (PXRD) showed that a reversible phase transition can occur after **UWDM-3** (denote as **UWDM-3*α***) was activated,

the new phase of **UWDM-3** (denote as **UWDM-3*δ***) still retained its crystallinity, and ^{2}H ssNMR showed that after undergoing the phase transition, the **24C6** moieties on the ligands had enough space to rotate freely. They demonstrated that the dynamics in crystalline framework materials could be controlled by reversible phase transitions for the first time.[147] This work provides an example for the design of molecular machines using CE-based MOFs.

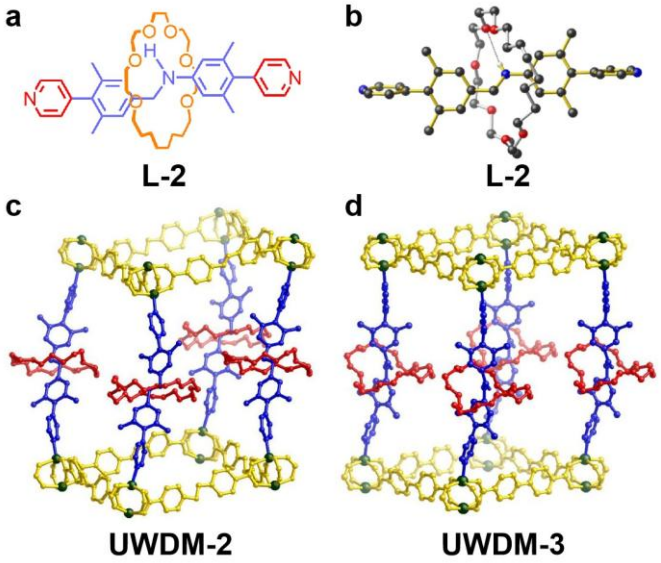

Fig. 12 (a) Chemical structure of ligand **L-2**. (b) Ball-and-stick representation of the single crystal structure of ligand **L-2**. (c and d) Ball-and-stick representations of the crystal structures of **UWDM-2** and **UWDM-3**. Aniline axles are blue, **24C6** wheels are red, carboxylate linkers are yellow, and Zn atoms are green. Reproduced from ref. 147 with permission from American Chemical Society, copyright 2014.[147]

Based on the above work, Loeb's group tried to study more complicated cases using CE-incorporated MOFs. A molecular shuttle is a mechanically interlocked complex that can move the macrocyclic units freely between different recognition sites.[185-187] At present, many molecular shuttles have been designed and synthesized, and exhibit complex functions that mimic switches and machines.[185-187] The Loeb group further applied a CE-based MOF to the synthesis of a molecular shuttle. They prepared a MOF named **UWDM-4** with the incorporation of 24-crown-8 (**24C8**) units which is composed of rigid molecular shuttle ligand **L-3** (Fig. 13).[188] The formula of **UWDM-4** was determined by SCXRD analysis as $[(Zn_4O)_2(\mathbf{L\text{-}3})_3(HBF_4)_3]\cdot 16EtOH$. Four carboxylate groups are coordinated to form a Zn_4O cluster. This MOF structure connects Zn_4O clusters using triphenyl-dicarboxylate linkers to give two-fold interpenetrated frameworks. They used ^{1}H-^{13}C cross-polarization/magic angle spinning (CP/MAS) and ^{13}C two-dimensional exchange correlation spectroscopy ssNMR to investigate ^{13}C-rich samples, demonstrating that the **24C8** units could shuttle rapidly along the rigid axles within the frameworks.[188] This work demonstrates the applicability of introducing molecular machines into MOFs through the integration of CE units.

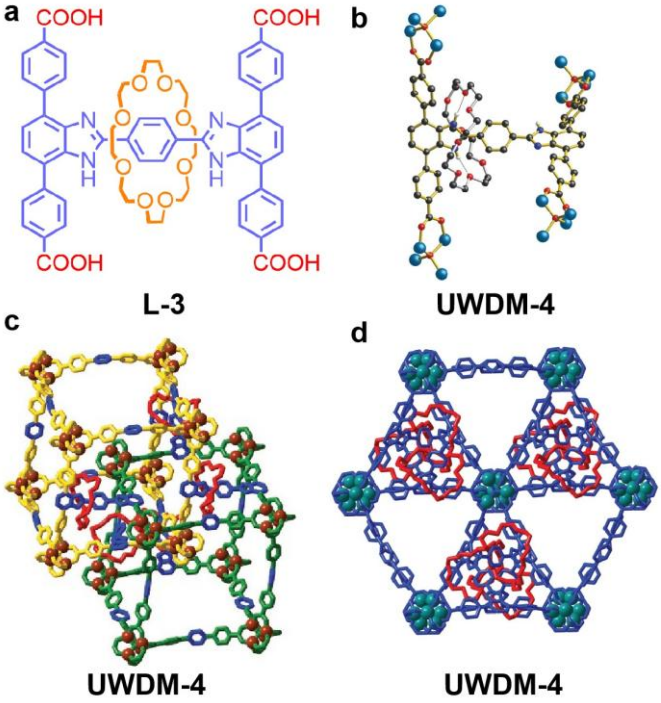

Fig. 13 (a) Chemical structure of ligand **L-3**. (b) Ball-and-stick representation of the single crystal structure of **UWDM-4**. Here C atoms are black, O atoms are red, N atoms are dark blue, H atoms are grey, and Zn atoms are light blue. The H atoms on N-H groups are shown while the other H atoms are omitted for clarity. (c) Two-fold interpenetrated single crystal structure of **UWDM-4** (green and yellow) with ligands. Partial **24C8** units are omitted for clarity. (d) Capped-stick representation of the single crystal structure of **UWDM-4**. Axles are blue, wheels are red, and Cu nodes are green. Reproduced from ref. 188 with permission from Springer Nature, copyright 2015.[188]

Loeb also prepared a new mechanical interlocked ligand (**L-4**) by clamping a **24C6** structural unit on an axis containing Y-type dibenzimidazole and isophthalic acid groups (Fig. 14).[189] They used this ligand and Zn ions to prepare **UWDM-5**. SCXRD results show that the structural formula of **UWDM-5** is $\{[Zn_2(\mathbf{L\text{-}4})(NO_3)(DEF)](DEF)(H_2O)\}$. They found an interesting phenomenon in **UWDM-5** where the imidazole unit in the rotaxane was protonated, producing a cationic imidazole recognition site surrounded by **24C6**. The positive charge on the cationic ligand is balanced by nitrate ions in the frameworks. The Y-shaped diphenyl-imidazole unit provides sufficient space between adjacent recognition sites to avoid interactions between adjacent **24C6** units. This allows the **24C6** structural units to rotate freely in **UWDM-5**. Moreover, **UWDM-5** is stable which allows them to study the thermally driven molecular dynamics of the interlocked **24C6** components inside **UWDM-5**. They

used VT ^{2}H ssNMR to characterize the motion of **24C6** units around the rigid axles in the frameworks. They found that the **24C6** structural unit of **UWDM-5** underwent rapid and thermally driven rotational motion around the axes in the lattice at a high temperature (over 150 °C). This work provides a case of regulating the macrocyclic motion in the MOFs by increasing the space between adjacent macrocyclic components.[189]

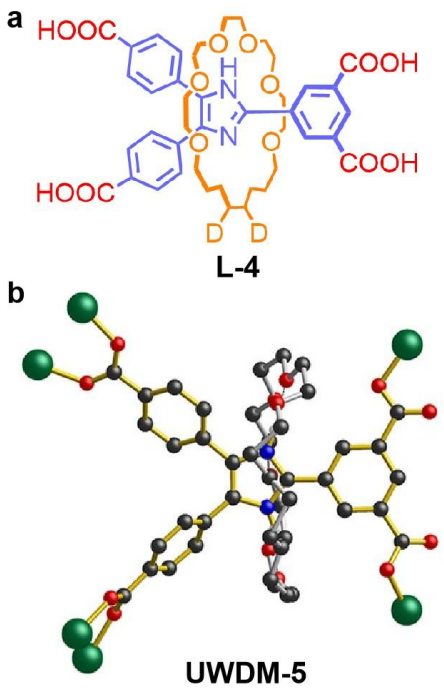

Fig. 14 (a) Chemical structure of ligand **L-4**. (b) Ball-and-stick representation of the single crystal structure of **UWDM-5**. C atoms are black, O atoms are red, N atoms are blue, Zn atoms are green, and H atoms are omitted for clarity.[189]

Loeb's group continued to prepare UWDM-MOFs (**UWDM-6** and **UWDM-7**) from porphyrinyl tetracarboxylate layers and [2]rotaxanes (**L-2** for **UWDM-6** and **L-5** for **UWDM-7**) with terminated pyridines (Fig. 15).[190] They characterized the structures of these two MOFs using SCXRD. Both **UWDM-6** and **UWDM-7** have a two-fold interpenetrated **fsc** topology, in which the porphyrins form two-dimensional layered structures as supported by [2]rotaxane pillars with an interlayer distance of 25 Å. They analysed the two structures using PLATON and found that the solvent accessible volumes of **UWDM-6** and **UWDM-7** were 49% and 47%, respectively. During the activation of *α*-**UWDM-6**, they found a third phase, *γ*-**UWDM-6**, which remained stable in the temperature range of 25 to 200 °C. The activation process did not significantly reduce the crystallinity of *γ*-**UWDM-6**, but affected the quality of single crystals. Despite the structural changes that occurred during the phase transition of **UWDM-6**, **UWDM-6** did not exhibit irreversible collapse of the frameworks or loss of the crystalline state. Both phenomena are commonly observed in pillar-layer MOFs and would greatly hinder the investigation of the dynamics of macrocycles. Compared with **UWDM-6**, the structure of **UWDM-7** is more stable. The structure of *α*-**UWDM-7** did not change during the heating process, and the PXRD pattern still revealed a crystalline state after activation. Both of these MOFs can undergo reversible phase transitions after removal of the solvent molecules to form *γ*-**UWDM-6** and *β*-**UWDM-7**. They studied the dynamics of **24C6** units in these two MOFs using VT ^{2}H ssNMR. Interestingly, only the solvent-containing *α*-**UWDM-7** showed unrestricted macrocyclic motion in the MOF pores. They also studied the dynamics of *α*-**UWDM-7** in different solvents and showed that its dynamic properties were solvent-independent.[190]

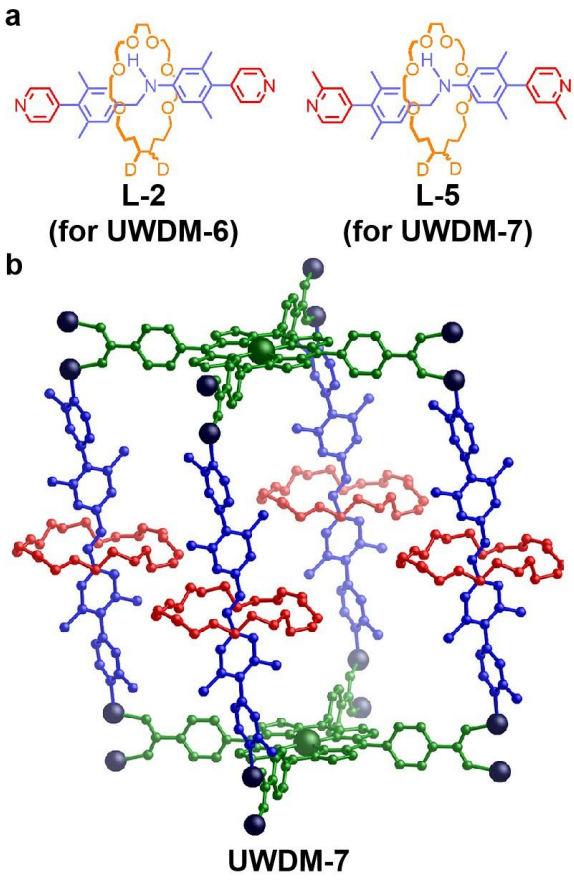

Fig. 15 (a) Chemical structure of ligand deuterated **L-2** (for preparing **UWDM-6**) and **L-5** (for preparing **UWDM-7**). (b) Ball-and-stick representation of the single crystal structure of **UWDM-7**. Pillared struts are blue, **24C6** units are red, layers are green, Zn atoms are dark blue, and H atoms are omitted for clarity. Reproduced from ref. 190 with permission from American Chemical Society, copyright 2019.[190]

The Loeb group then introduced a [2]rotaxane (**L-6**) with a biphenyl axis and a **24C8** unit into tetrahedral structures with the same topological structure as **UiO-68** (Fig. 16). They obtained three [2]rotaxane-containing MOFs (**UWDM-8**, **UWDM-9** and **UWDM-10**). The crystal structures of MOFs they prepared are the same with **UiO-68** topological networks, formulated by $[Zr_6(O)_4(OH)_4(L)_6]$ (L = dicarboxylate ligands). The H-shaped [2]rotaxane **6** was then inserted into these structures by substituting two primary ligands, giving the MOFs **UWDM-8**, **UWDM-9** and **UWDM-10** with the molecular

formula of $[Zr_6(O)_4(OH)_4(\mathbf{6})(L)_4]$. These MOFs were prepared by the solvent assisted ligand exchange (SALE) method, only 67% of the ligands could be exchanged. PXRD patterns showed that these dynamic MOFs have the same crystallinity as **UiO-68**. The MOFs have some structural characteristics: 1) **24C8** unit can move along the rotaxane axis from a benzimidazole recognition point to another site; 2) the limited volume of the tetrahedral pores may prevent the movement of the **24C8** unit and thus prevent its movement to the benzimidazole recognition site. Therefore, the rotation of different ligands can regulate the dynamics of **24C8**. They characterized the dynamics of different rotors in these MOFs using VT ssNMR. VT ^{13}C and ^{2}H ssNMR results showed that the translational position of **24C8** along the [2]rotaxane axis was influenced by the steric resistance and rotation direction of the ligand in the MOF. This work provides an example of using the steric hindrance of the ligands to regulate the motion of macrocycles in the crystalline frameworks.[191]

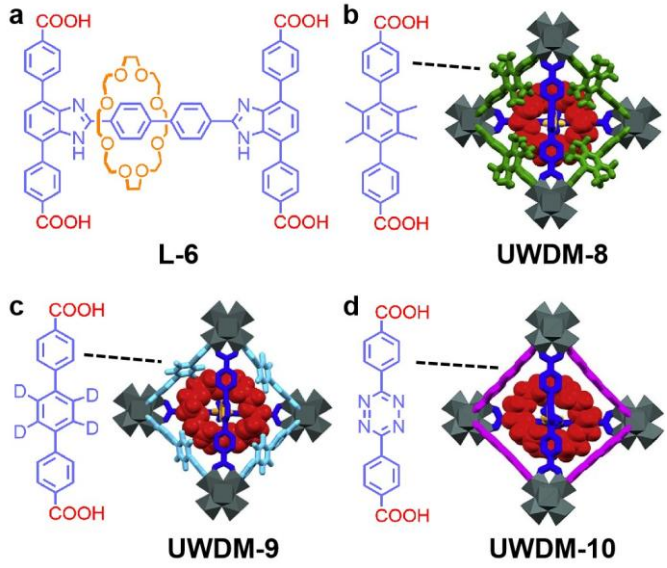

Fig. 16 (a) Chemical structure of ligand **L-6**. (b) Structures of **UWDM-8**, **UWDM-9** and **UWDM-10**. Here ligands **L-6** are blue, **24C8** units are brown, Zr clusters are grey, and other ligands are various color-coded as shown in the figure. Reproduced from ref. 191 with permission from Elsevier, copyright 2021. [191]

Loeb's research group further synthesized a molecular shuttle (**L-7**) containing **24C8** units (Fig. 17). They studied the dynamics of the molecular shuttle in solution, and SCXRD results confirmed its structure. They then used this ligand to synthesize a novel Zr MOF, **UWDM-11**, and studied the translational motion of the molecular shuttle in the solid state. They confirmed the integrity and crystallinity of **UWDM-11** by PXRD. Similarly, they used a ^{13}C MIM linker to track the dynamics of **UWDM-11**. When **UWDM-11** is in the solvent-free state, the molecular shuttle exhibits a rapid periodic movement. However, when mesitylene guest molecules were complexed into the pores of **UWDM-11**, the movement rate of the molecular shuttle slowed down to a certain extent, and VT ssNMR spectroscopy was used to elucidate the mechanism of this change. This work provides another strategy of using the guest molecules to regulate the movement of macrocyclic components in the MOFs.[192]

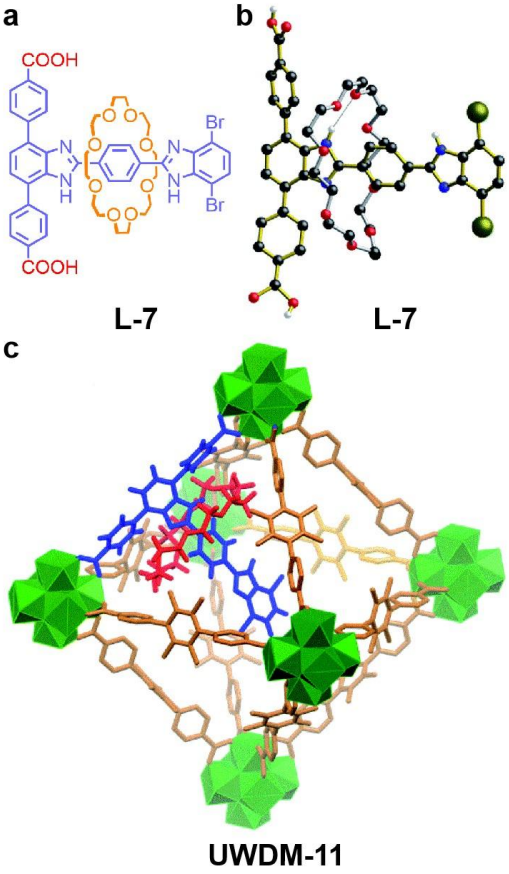

Fig. 17 (a) Chemical structure of ligand **L-7**. (b) Ball-and-stick representation of the single crystal structure of ligand **L-7**. Here C atoms are black, O atoms are red, N atoms are dark blue, H atoms are grey, and Br atoms are green. The H atoms on N-H groups are shown while the other H atoms are omitted for clarity. (c) Simulated structure of **UWDM-11** with ligands (axles are blue and brown while **24C8** unit is red). Zr clusters are shown in green.[192]

3.1.4. Artificial membrane

Aside for the first two strategies, the CE units can also be installed into MOFs through supramolecular interactions. Protein channels on biofilms are capable of controlling the ion transport by regulating the distribution of charge.[193-195] This idea can also be applied to artificial membranes. But simulating similar processes in artificial membranes remains a challenge. Yuan's team used a MOF (**ZIF-7**)-based membrane with charge-adjustable nanochannels to control the selectivity of ion transport.[196] Benzo-12-crown-4 (**B12C4**) can be introduced into **ZIF-7** and complexed by different cations. According to the CO_2 adsorption/desorption isotherms, the porosity of **B12C4@ZIF-7** is similar with that of **ZIF-7**. The pore size of **B12C4@ZIF-7** is 4.3 Å, 0.6 Å narrower than that of **ZIF-7**. The reduced surface area

and pore size distribution both confirmed the presence of **B12C4** in **ZIF-7**. Ions of different valence states can bind with **B12C4** units in the MOF channels, and the **B12C4** moieties can adjust the electron charge state of the channels from negative to positive by regulating the metal ions (M[**B12C4**]$^{n+}$**@ZIF-7** (M = Li^+, Mg^{2+}, Al^{3+})). Compared with negatively charged channels, positively charged channels significantly enhance the selectivity of Li^+/Mg^{2+}, due to the difference in electrostatic repulsion between ions and channels. Theoretical calculation showed that Mg^{2+} needed to overcome higher energy barrier than Li^+ through positively charged channels. Their research provides an ingenious strategy for regulating the charge state of artificial membranes, also providing a new application for CE-based MOFs.[196]

3.2. Crown ether-based COFs

Similar to CE-incorporated MOFs, COFs containing CEs also demonstrate a marked increase in the molecular recognition compared with traditional crystalline framework materials.[197-200] The applications of CE-incorporated materials mainly focus on molecular recognition, catalysis, chiral separation, and lithium metal batteries.[163,201-204] Surprisingly, CE-containing COFs even can be used to prepare nanosheets.[202] The detailed description is discussed below.

3.2.1 Molecular recognition

The introduction of CE units into COFs endows them with enhanced molecular recognition.[198] However, the synthesis COFs with flexible structure units remains a challenge. Liu's group synthesized two COFs based on modified pyrene (**Py**) with flexible **B18C6** and **B24C8** units, named **Py-B18C6-COF** and **Py-B24C8-COF**, respectively, then they demonstrated their applicability in alkali metal ion recognition (Fig. 18).[144] The porous structure is an important feature of COFs. The porosity of **Py-B18C6-COF** and **Py-B24C8-COF** was studied using N_2 adsorption/desorption isotherms at 77 K. Both COFs exhibit a typical I isotherm, indicating that they have microporous structural composition. The BET surface areas of **Py-B18C6-COF** and **Py-B24C8-COF** are calculated to be 1356 and 862 $m^2\ g^{-1}$, respectively. The pore volumes of **Py-B18C6-COF** and **Py-B24C8-COF** are 0.52 and 0.39 $cm^3\ g^{-1}$, respectively. These two COFs have high crystallinity and chemical stability as confirmed from PXRD patterns at various conditions. Both COFs with **B18C6** or **B24C8** units exhibited significant K^+ or Cs^{2+} complexation. Their work opens up new avenues for the application of COFs in molecular recognition with the incorporation of CEs.[144]

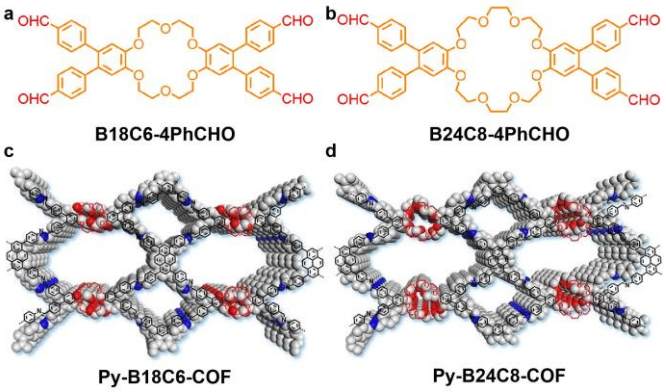

Fig. 18 (a) Chemical structures of **B18C6-4PhCHO** and **B24C8-4PhCHO**. (b) Simulated structures of **Py-B18C6-COF** and **Py-B24C8-COF**. C atoms are grey, O atoms are red, N atoms are blue, and H atoms are omitted for clarity.[144]

COFs with CE structural units have received extensive attention due to their applications in molecular recognition.[200,205] Shi's group prepared a one-dimensional (1D) COF with **B18C6** units incorporated (denoted as **Py-B18C6-COF-2**) with high crystallinity (Fig. 19). Hydrogen bond networks and π-π stacking hold the 1D COF together.[198] Experimental and computational results show that the hydrogen bond networks play a crucial role in the formation of **Py-B18C6-COF-2**. The BET surface area of **Py-B18C6-COF-2** was calculated to be 32 $m^2\ g^{-1}$. Similar to the **B18C6**-incorporated MOFs[150,173], **Py-B18C6-COF-2** prepared by Shi's group can also be used as the adsorbent for radioactive element strontium (Sr^{2+}), showing fast adsorption kinetics and high selectivity. Their work provides a prototypical example of the recognition of radioactive elements using COFs with flexible CE units.[198]

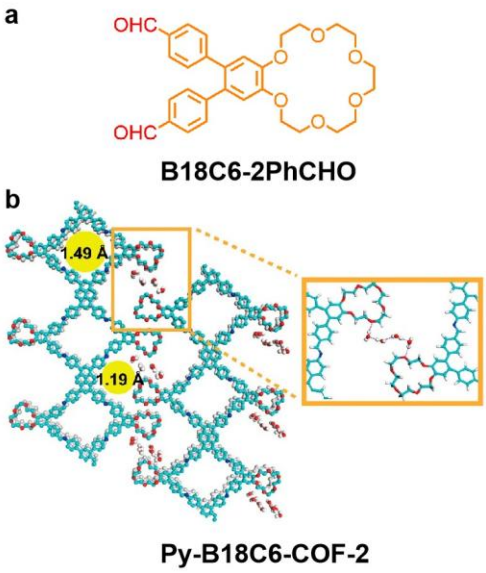

Fig. 19 (a) Chemical structure of **B18C6-2PhCHO**. (b) Simulated structure of **Py-B18C6-COF-2**. Reproduced from ref. 198 with permission from American Chemical Society, copyright 2024.[198]

In addition to the application of Sr^{2+} adsorption, Shi's group also used the *γ*-ray induced grafting strategy to fix the 15-crown-5 units (**B15C5-NH$_2$**) on a COF (denoted as **TzDa**).[206] They prepared a CE modified COF named [**B15C5**]$_{n\%}$-(**TzDa**-**GMA**-*x*%) and applied it to $^6Li/^7Li$ isotope separation (Fig. 20). Here *n*% represents the immobilization yield of **B15C5-NH$_2$** and **GMA**-*x*% is the grafting yield to **TzDa**. The modified COF showed rapid adsorption kinetics in the separation. The internal structure of the **TzDa** framework has enough space to accommodate the introduced glycidyl methacrylate (**GMA**) and CE units. Among them, [**B15C5**]$_{57\%}$-(**TzDa**-**GMA**-50%) has high crystallinity and stability, showing the best Li^+ adsorption and $^6Li/^7Li$ isotope separation performance. This COF can reach the Li^+ adsorption capacity of 3.6 mg g^{-1} within 30 min, the maximum adsorption capacity is 7.3 mg g^{-1}, and the separation factor for $^6Li/^7Li$ isotopes is 1.014 ± 0.001. This material can remove more than 99% of Li^+ from acetonitrile. This radiation-assisted synthesis strategy of CE modification is expected to be applied to $^6Li/^7Li$ isotope separation.[206] Their work shows a post-modified strategy for introducing CE units into COFs.

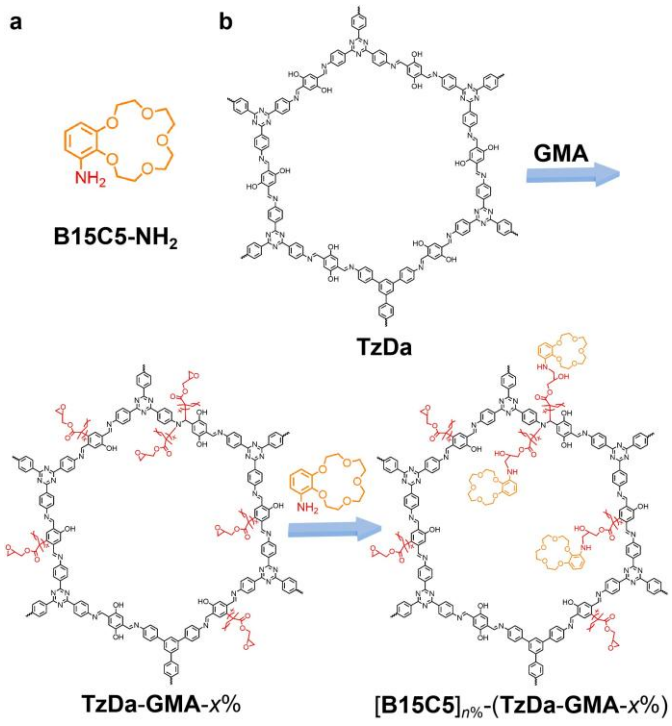

Fig. 20 (a) Chemical structure of **B15C5-NH$_2$**. (b) Synthetic route to [**B15C5**]$_{n\%}$-(**TzDa**-**GMA**-*x*%).[206]

3.2.2. Catalysis

Since CE-based COFs have favorable molecular recognition capabilities, they can also act as suitable catalysts.[163] It is known that the electrochemical reduction of CO_2 is of great significance for clean energy.[207] Metal porphyrin-based COFs are ideal catalysts for the CO_2 conversion to CO.[10] However, the hydrophobicity and poor electron transport of metal porphyrin-based COFs limit their catalytic performance. Liu's group prepared two COFs named **TAPP(H$_2$)-B18C6-COF** and **TAPP(Co)-B18C6-COF** based on **B18C6**-containing porphyrin, and demonstrated the applicability of **TAPP(Co)-B18C6-COF** for CO_2 reduction.[163] The **B18C6** units in this COF not only enhance the hydrophilicity of the material, but also promote the transfer of electrons from **B18C6** units to Co porphyrin moieties. In addition, the presence of **B18C6** units enhances the ability of the COF to bind CO_2. This work expands the application of COFs in electro-catalysis with the integration of CEs into frameworks.[163]

Lee's group proposed a new preparation method of CE-based COFs and they prepared an unique COF named **C$_2$O**, with **18C6** units in its internal structure (Fig. 21).[200] This COF could be prepared at gram scale, and showed high chemical stability in the presence of acids, bases and a variety of chemical solvents. It is worth mentioned that although **C$_2$O** is prepared by irreversible S_NAr reaction, it still has a crystalline state. The formation of this regular structure can be ascribed to the rigidity of the structural units and the directivity of the dioxin links. The porosity measured by N_2 at 77 K could be neglected due to the dense structure with small pores. The porosity of **C$_2$O** could be confirmed by a CO_2 adsorption isotherm with an adsorption capacity of 0.6 mmol·g^{-1}. Since the limbic hydroxyl groups in **C$_2$O** enhanced the affinity of CO_2. Through specific recognition of K^+ and **18C6**, **C$_2$O** could effectively activate KI, enhance the nucleophilicity of I^-, and thus improve its catalytic activity for epoxide-fixed CO_2. This increased the CO_2 conversion rates of epichlorohydrin and allyl glycidyl ether from 5.7% to 99.9% and 2.9% to 74.2%, respectively. In addition, **C$_2$O** has electrophilic and nucleophilic sites at the edge of its structure, allowing for chemical modification. The conversion of these modified materials for fixing CO_2 with allyl glycidyl ester increased from 97.2% to 99.9%, while the conversion of unmodified **C$_2$O** for CO_2 fixation was only 74.2%. This newly developed strategy provides another way of incorporating CE components into COFs for catalysis.[200]

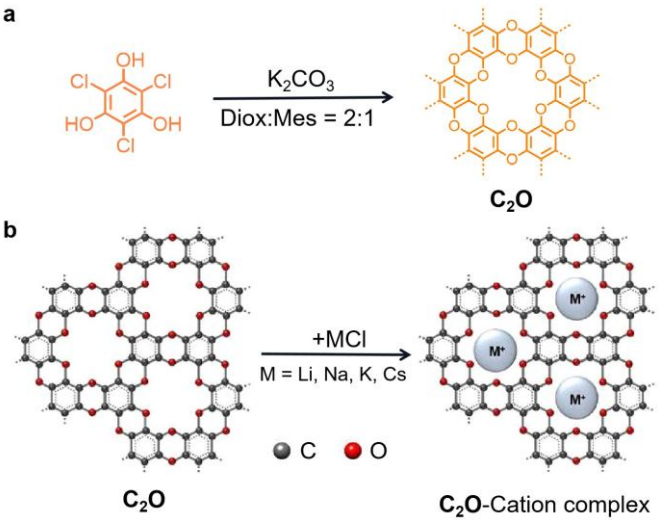

Fig. 21 (a) Synthesis of **C_2O**. (b) Cation binding behavior of **C_2O**. Reproduced from ref. 200 with permission from American Chemical Society, copyright 2024.[200]

3.2.3. Chiral separation

At present, the most widely used technique for chiral separations is HPLC and gas chromatography (GC), but there is no CSP that can be used for both liquid and gas chromatography.[208] Cui's group prepared two COFs (denoted as **CCOF-17** and **CCOF-18**) with chiral **N22C6-4PhCHO** components that can be used as general CSPs not only in GC but also in HPLC (Fig. 22).[201] The two COFs have similar two-dimensional layered structures and show high stability in water, organic solvents, acids, alkalis and other environments. PXRD patterns confirmed the crystallinity of **CCOF-17** and **CCOF-18**. The periodic arrangement of chiral CEs in the channels of COFs allows enantioselective recognition of guest molecules through supramolecular interactions. CE-based COF-filled columns exhibit high resolution, selectivity, and durability. In addition, they can be used to separate a wide range of racemic compounds, including amino acids, alcohols, lactones, esters, amides, ketones, aldehydes, and drug molecules. The resolution and versatility of these columns even surpasses most commercial chiral columns, and have a high potential prospect. Cui's work therefore advances the generality of CE-incorporated COFs as column CSPs.[201]

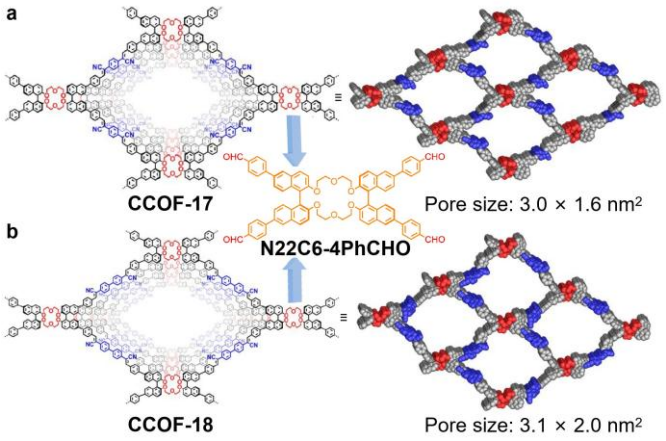

Fig. 22 (a) Structures of **N22C6-4PhCHO**, **CCOF-17** and **CCOF-18**.[201]

3.2.4. Lithium metal battery

Due to the enhanced specific recognition of cations by CEs, CE-incorporated COFs seem to be ideal candidates for lithium battery design.[209-211] In practice lithium batteries are inhibited by the accumulation of lithium dendrites and the consumption of active lithium, both reducing the overall battery life.[212-214] One effective strategy to inhibit the formation of lithium dendrites is to construct an artificial solid electrolyte layer in lithium anode, such as COFs, which can improve the overall cycling performance.[215-217] However, this strategy of implementing three-dimensional (3D) COFs as a protective layer has been rarely reported. Zeng's group prepared a 3D COF structure (denoted as **B18C6-N-COF**) with the incorporation of CE units by arranging the **B18C6** units in both parallel and vertical configurations along the electrode (Fig. 23).[203] They studied the precise structure of **B18C6-N-COF** by PXRD analysis. Based on the reticular chemistry theory, the marriage of 4-connected rectangular and 3-connected triangular linkers can be assembled into **ffc**, **tbo**, and **pto** topological networks. The calculation results clearly show that **B18C6-N-COF** has a two-fold interpenetrated **ffc** network in a *C*2/*m* space group. N_2 adsorption experiments confirmed that **B18C6-N-COF** maintained its porosity with a BET surface area of 757 $m^2\ g^{-1}$. The coupling effect between **B18C6** units and Li^+ cations accelerates the diffusion kinetics of Li^+ cations and makes the Li^+ flux uniform. These elements facilitate the deposition of Li^+ cations in three dimensions. As a result, in over 340 cycles, the Li/COF-Cu battery showed a low Li nucleation overpotential (17.4 mV) and an average coulombic efficiency of close to 98.6%. This work provides a new approach for the design of energy storage systems based on COFs using CE units as recognition sites.[203]

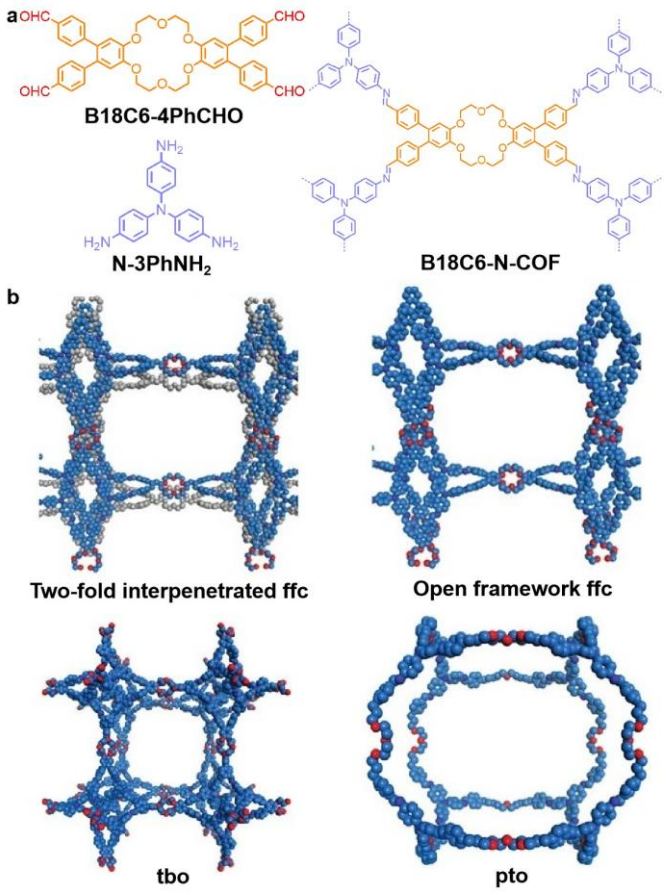

Fig. 23 (a) Chemical structures of **B18C6-4PhCHO**, **N-3PhNH$_2$** and **B18C6-N-COF**. (b) Possible topological structures (**fcc**, **tbo** and **pto**

networks) of **B18C6-N-COF**. Reproduced from ref. 203 with permission from John Wiley & Sons, copyright 2024.[203]

3.2.5. Nanosheets

Besides, CE-based COFs are capable of expanding the applications of traditional COFs. The design of COF building blocks is expected to realize the construction of functional and pore-controlled two-dimensional materials, whether in single or multi-layered forms.[218-220] However, constructing uniform COF sheets in two dimensions remains a challenge. The Loh group adopted a strategy of increasing the interlayer space of COFs by adding pseudorotaxane units to the skeletons of two COFs (named **MCOF-1** and **MCOF-0**) (Fig. 22).[202] The layered COFs are formed by the reaction of acylhydrazine building blocks based on benzo-34-crown-10 (**B34C10**) units with aldehyde groups. The results of PXRD showed that the addition of the hosts will not destroy the in-plane or out-of-plane crystallinity in the absence of the guests. They simulated anti-parallel, overlapped, and cross-stacked bilayer structures to infer the crystal structure of **MCOF-1**. The simulation results of the anti-parallel structure agree well with the experimental results, which indicates that **MCOF-1** may have an anti-parallel stacked structure. When the **PQT** units are introduced, the formation of the host–guest complexes promotes the self-exfoliation between the COF layers, forming monolayer and bilayer crystals (**RCOF-1** and **RCOF-0**), respectively. This work creatively provides a new strategy for the preparation of bilayer- and monolayer-packed COFs.[202]

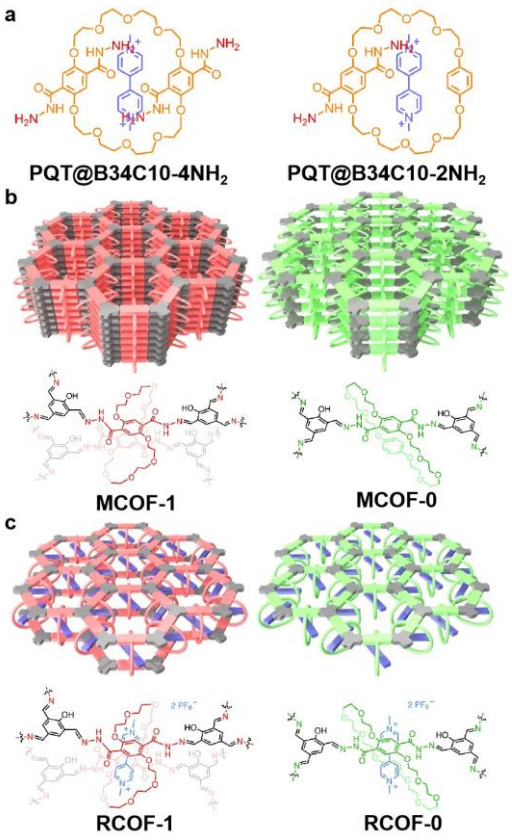

Fig. 24 (a) Chemical structures of **PQT@B34C10-4NH$_2$** and **PQT@B34C10-2NH$_2$**. (b) Cartoon representations and chemical structures of layer-packed **MCOF-1** and **MCOF-0**. (c) Cartoon representations and chemical structures of monolayer- and bilayer-packed **RCOF-1** and **RCOF-0** with pseudorotaxane units. Reproduced from ref. 200 with permission from Springer Nature, copyright 2020.[202]

4. Cyclodextrin-based crystalline porous framework materials

Cyclodextrins (CDs), a general term for a series of cyclic oligosaccharides produced from amylose.[221-225] A cyclodextrin molecule has a hollow cylindrical stereoscopic structure with a slightly conical shape (Fig 25).[226] In the hollow structure, the larger opening is composed of the secondary hydroxyl groups of C_2 and C_3, and the smaller opening is composed of the primary hydroxyl groups of C_6, which is hydrophilic (Fig 26).[227] The hydrophobic region is formed in the cavity due to the shielding effect of C–H bonds.[227] Since the outer edge of a cyclodextrin is hydrophilic and the inner cavity is hydrophobic, it can provide a hydrophobic binding site similar to an enzyme. The main body can envelope various appropriate guests, such as organic molecules, inorganic ions, and gas molecules.[141,223,228] Due to their hydrophobic inner cavities and hydrophilic rims, cyclodextrins can form inclusive complexes and molecular assembly systems according to van der Waals forces, hydrophobic interactions, and host–guest interactions.[224] Cyclodextrin-based crystalline porous framework materials have been well investigated and applied in separation/purification, gas storage, ion recognition, molecular transport, and circularly polarized luminescence.[141,229-231] Several selected examples of cyclodextrin-based crystalline porous framework materials are discussed in detail below. These sections are broken down based upon applications of these cyclodextrin-based frameworks.

4.1. Cyclodextrin-based MOFs

Most of the MOFs reported to date are composed of non-renewable struts and transition metal nodes.[232-236] The natural products are not suitable for preparing MOFs because of the asymmetry of their structural units.[225] Stoddart's group first reported a strategy for preparing MOFs using *γ*-cyclodextrin (***γ*-CD**), a symmetric cyclic oligosaccharide consisting of eight *D*-glucose residues (Fig. 26).[141] They used these ***γ*-CD** structural units to construct a cyclodextrin-based MOF named **CD-MOF-1** with the formula $[(C_{48}H_{80}O_{40})(KOH)_2]_n$ using K^+ coordination in water at room temperature. This MOF can be prepared entirely from food-grade ***γ*-CD** combined with a KCl or potassium benzoate and grain alcohol (EtOH) in water to produce edible

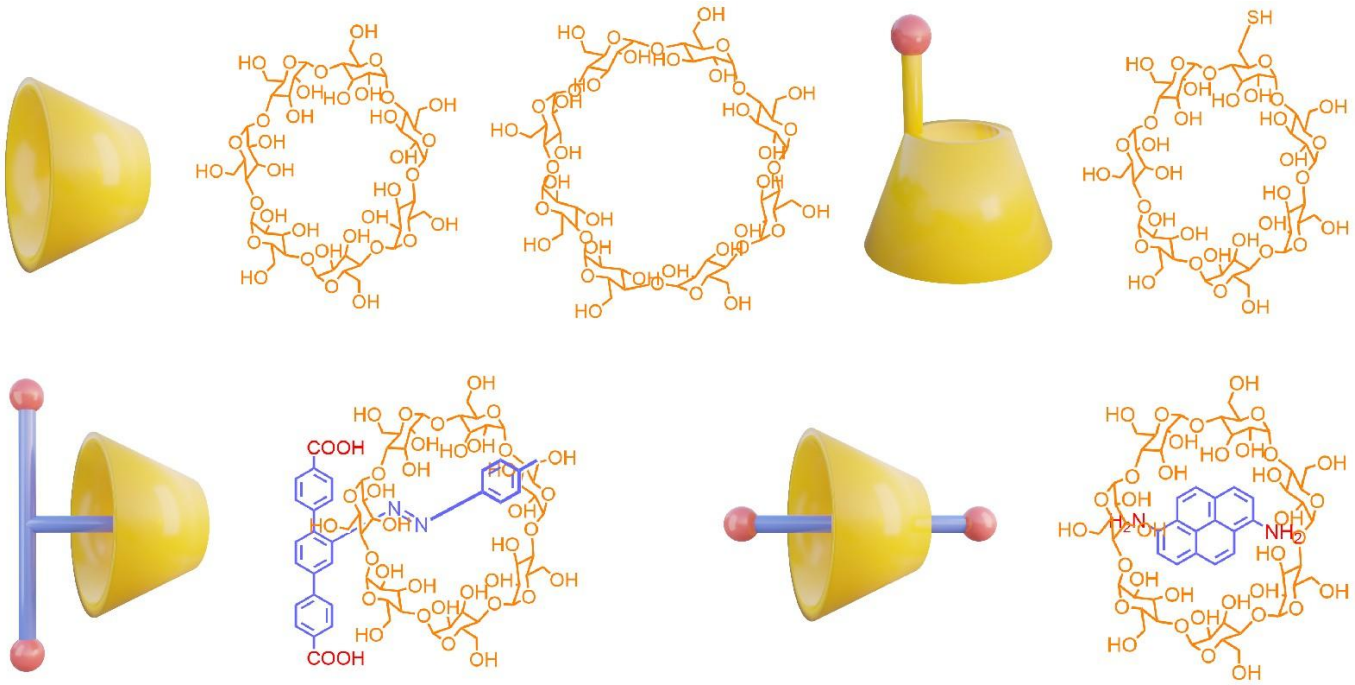

Fig. 25 Cartoon representations and chemical structures of CD-incorporated components involved in this review for preparing crystalline framework materials.

MOFs.[141] **CD-MOF-1** has a topological network structure of **rra**, which has not been observed before. Each (***γ*-CD**)$_6$ cube has a large hole in the center with a diameter of 1.7 nm, and the entire structure forms a porous framework. In addition, with each macropore expanding in the direction (111) and an edge aperture of 0.42 nm, the total pore volume of **CD-MOF-1** is estimated to be 54%. N_2 adsorption experiments demonstrated the permanent porosity of activated **CD-MOF-1**. The adsorption isotherm showed that **CD-MOF-1** absorbed most N_2 at the low pressure region (P/P_0 < 0.05), and the BET surface area of **CD-MOF-1** was 1220 $m^2\ g^{-1}$. The corresponding pore density was 0.47 g cm^{-3}. The PXRD pattern of **CD-MOF-1** after activation also proved that it remained crystalline after activation. Based on this pioneering work, the CD-MOF families have undergone significant development in recent years. The most important cases are selected and discussed as below.

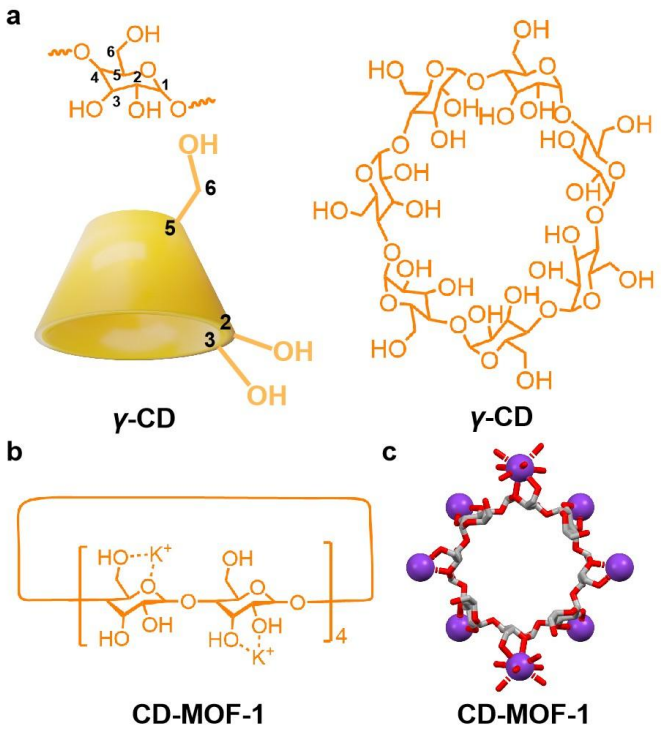

Fig. 26 (a) Structure representations of the asymmetric unit of *α*-1,4-linked *D*-glucose residue, ***γ*-CD** and cartoon representation of ***γ*-CD**. (b) Chemical structure representation of **CD-MOF-1**, showing the coordination with K^+. (c) Crystal structure of **CD-MOF-1** with the **rra** net. C atoms are grey, O atoms are red, K atoms are purple, and H atoms are omitted for clarity.[141]

4.1.1. Gas storage

The capture and storage of greenhouse gas CO_2 is an important environmental issue as it is directly related to our planet's warming.[71,237-239] While MOFs have been shown to selectively adsorb CO_2, but CO_2 is not typically covalently captured.[240] Stoddart's group reported the highly selective adsorption of CO_2 by **CD-MOF-2**, a greenly synthesized MOF prepared from renewable CDs and RbOH, which can fix carbon through carbonate decomposition at room temperature (Fig. 27).[241] The CO_2 absorption experiment of **CD-MOF-2** showed that there was an atypical strong affinity between CO_2 and **CD-MOF-2** at low pressure, which proved that it was a chemisorption process at low pressure. However, chemisorption gave way to physical adsorption under high pressure. When the CO_2 content of **CD-MOF-2** was 23 cm^3/g, the absorption mechanism changed, and this process was completely reversible at room temperature. They also added a pH indicator to **CD-MOF-2** to illustrate the formation of carbonic acid within the frameworks, and monitored this process using ^{13}C ssNMR spectroscopy and colorimetry.[241] Their work provides a reliable method for CO_2 storage with the advantage of low-cost raw materials.

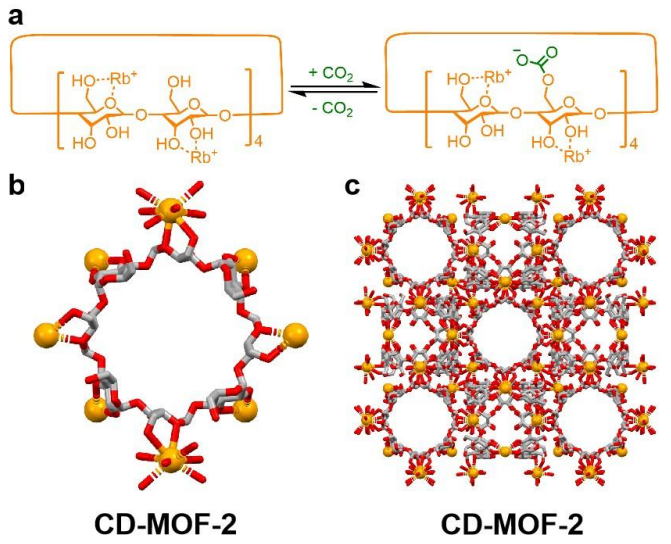

Fig. 27 (a) The mechanism of CO_2 adsorption by **CD-MOF-2**. (b) Crystal structure of **CD-MOF-2**. Rb^+ coordinates with (***γ*-CD**)$_6$ units, forming a 3D **bcc** topology. (c) Packing structure of **CD-MOF-2**. C atoms are grey, O atoms are red, Rb atoms are orange, and H atoms are omitted for clarity.[241]

As shown above, **CD-MOF-2** is a cubic structure containing six CD units that are jointed together in a cube form by Rb^+. The free primary hydroxyl groups in **CD-MOF-2** can react with gaseous CO_2 to form alkyl carbonate functional groups. After adsorption of CO_2, the dynamic covalent C–O bonds associated with this chemisorption process can release CO_2 at a low activation energy. Because of this dynamic chemical reaction, CO_2 can be selectively detected by **CD-MOF-2** in the atmosphere by electrochemical impedance spectroscopy. **CD-MOF-2** has a high proton conductivity in the pore filled with methanol, while its ionic conductivity decreases by 550 times after binding with CO_2. This feature can be used as a sensor to quantitatively measure CO_2 concentrations in the environment.[242]

The Stoddart group also determined the adsorption enthalpy of CO_2 on **CD-MOF-2** by adsorption calorimetry.[243] Their calorimetric method is more accurate than the adsorption enthalpy measurements calculated by adsorption isotherms, especially for systems with complex exothermic adsorption behavior. The differential enthalpy of CO_2 adsorption aligns with the enthalpy of chemisorption behavior. They observed an irreversible binding site with an enthalpy of −113.5 kJ/mol CO_2, followed by a reversible binding site of −65.4 kJ/mol. These sites can be adsorbed on stronger and weaker hydroxyl groups, respectively. In addition, there is a binding site with an enthalpy of −40.1 kJ/mol, which is attributed to physical absorption of CO_2. Calorimetric data confirmed the existence of at least two CO_2 chemisorption sites with different energies on **CD-MOF-2**.[243] This work elucidates the mechanism of CO_2 adsorption using **CD-MOF-2**.

The arrangement of macrocyclic -OCCO- and -OCCN- chelating units in supramolecular chemistry is responsible for their high complexation constants with the complexes of transition metal cations.[88,244] CDs extracted from starch also exhibit -OCCO- structure on their primary and secondary units. Stoddart's group continued their research and reported the self-assembly formation of network structures in water, known as CD-MOF, in which CDs form MOFs with metal cations through coordination.[229] **CD-MOF-1** and **CD-MOF-2** are prepared using KOH and RbOH, respectively, which can form body-centered cubic arrangements of alkali metal cation-linked (***γ*-CD**)$_6$ cubes.[229] The solvents in these CD-MOFs can be removed, with a specific surface area of around 1200 $m^2\ g^{-1}$. Therefore, these CD-MOFs are able to store gases and small molecules in their pores. However, ***γ*-CD**'s -OCCO- structure units are not prearranged well that favor the complexation of metal cations, so they prepared other CD-MOFs with different topologies from Cs^+, Na^+, and Sr^{2+} salts (Figs. 28 and 29). During the growth of the cubic crystals of **CD-MOF-3**, they observed another kind of unique crystals whose morphology was quite different from the cubic shape of the **CD-MOF-3** crystals. They named it **CD-MOF-4**, and this crystal structure consisted of ***γ*-CD** cavities with Cs^+ coordination is able to form channels along the crystallographic *c*-axis. In **CD-MOF-4**, in addition to connecting these ***γ*-CD** molecules in a checkerboard pattern on the ab plane, Cs^+ also connects CD units end to end along the *c*-axis. **CD-MOF-3** has the same cubic topology as observed in **CD-MOF-1** and **CD-MOF-2**, while **CD-MOF-4** shows a channel-like structure in which ***γ*-CD** is stacked in one dimension, and the coordination

of metal ions increases the stability of the structure. **CD-MOF-5** (coordinated with Na^+) reveals a similar channel-like structure with **CD-MOF-4**. In this case, the MOF channels are stacked in an offset fashion along the *a*-axis. The ***γ*-CD** cavities are interconnected by sodium cations only with their second-order coordination, producing tail-to-tail channels. These channels are further connected by more sodium cations in two-dimensional sheets, forming a network of square grids (**sql**). Additionally, the cationic-coordinated structure of **CD-MOF-6** (coordinated with Sr^{2+}) is different from that of the ***γ*-CD** torus bound to alkali metal cations. The ***γ*-CD** cavities are spatially arranged in a triangular slider-stacked structure, resulting in a nonlinear channel structure along the *c*-axis. The maximum and minimum diameters of the pores inside the crystal structure are 6.8 and 3.2 Å, respectively. It has a **bto** topology. The Sr^{2+} are nine-connected species and binds to three ***γ*-CD** units. These CD-MOFs suggest that CDs can be used as ligands for alkaline earth metal cations with function similarly to CEs. Their work provides a low-budget and green method to prepare crystalline porous materials entirely from food-grade ingredients.[229]

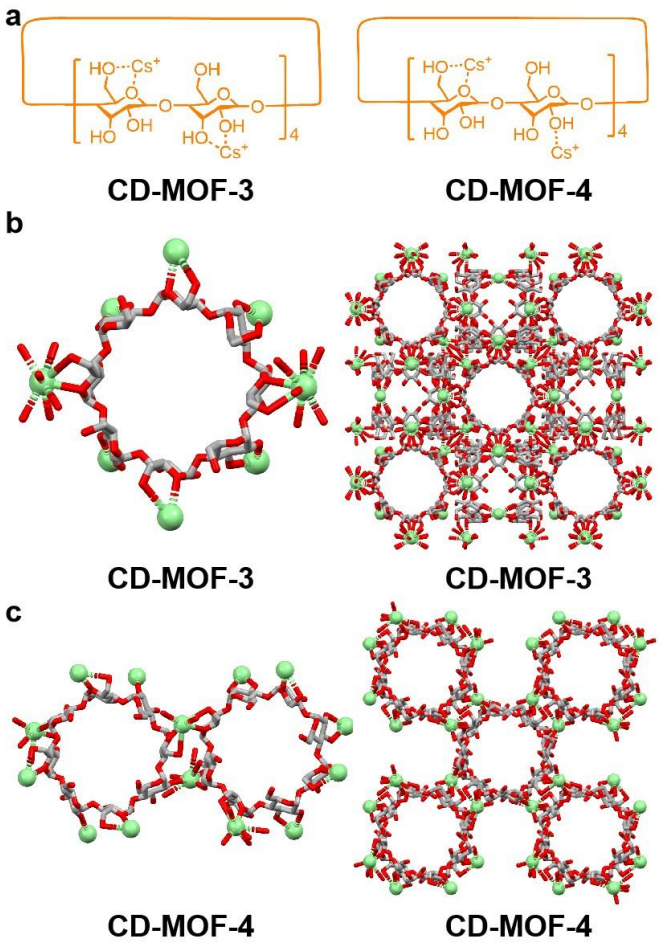

Fig. 28 (a) Chemical structures of **CD-MOF-3** and **CD-MOF-4**. Single crystal structures of the structural units and packing modes of (b) **CD-MOF-3** and (c) **CD-MOF-4**. C atoms are grey, O atoms are red, Cs atoms are light green, and H atoms are omitted for clarity.[229]

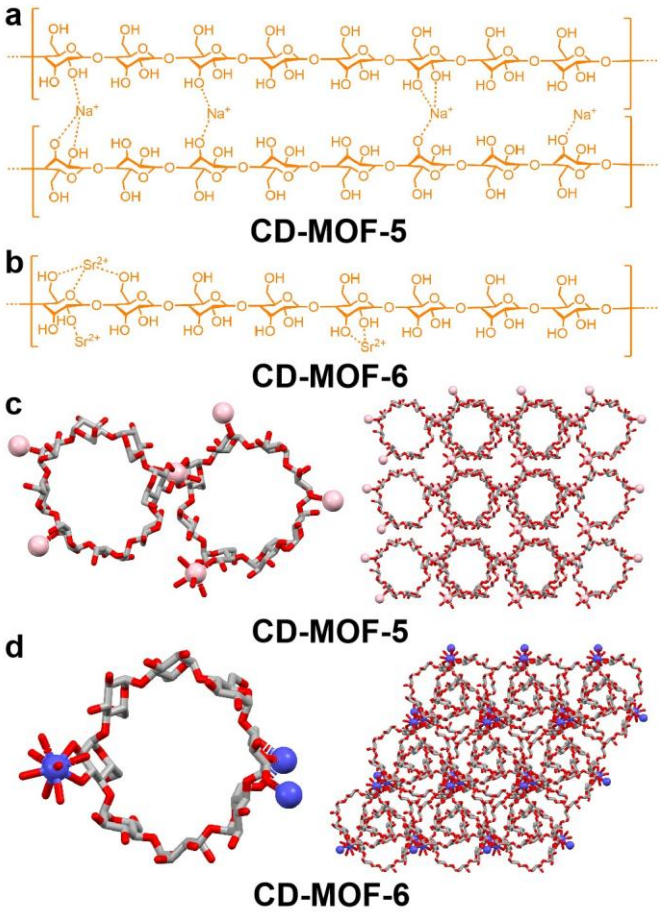

Fig. 29 Chemical structures of (a) **CD-MOF-5** and (b) **CD-MOF-6**. Single crystal structures of the structural units and packing modes of (c) **CD-MOF-5** and (d) **CD-MOF-6**. C atoms are grey, O atoms are red, Na atoms are light pink, Sr atoms are blue, and H atoms are omitted for clarity.[229]

Stoddart's group further investigated the multi-metal coordinative CD-MOFs.[245] When K^+ and Li^+ co-crystallize with ***γ*-CD**, Li^+ would replace some of the positions of K^+, maintaining the structural integrity and permanent porosity of **CD-MOF-1**. In order to obtain a high ratio of Li^+ in **CD-MOF-1**, they conducted a series of experiments in which the ratio of K^+/Li^+ changed with the ratio of ***γ*-CD** (Fig. 30).[245] They confirmed the presence of Li^+ in **CD-MOF-1** by calculating the K^+ vacancy and the cation/***γ*-CD** ratio in **CD-MOF-1** *via* SCXRD analysis. **Li/K-CD-MOF** has a triangular space group of *R*32. Compared with **CD-MOF-1**, the two adjacent K^+ on the ***γ*-CD** torus are partially occupied by Li^+, and the occupancy are 0.47 and 0.53, respectively. PXRD experiments of **CD-MOF-1** and **Li/K-CD-MOF** showed that their structures remain intact after Li^+ ions replace some K^+ sites. The BET surface areas of **CD-MOF-1** and **Li/K-CD-MOF** are 1145 and 1205 $m^2\ g^{-1}$, respectively. Elemental analysis also confirmed the proportion of Li^+ in **CD-MOF-1**. This synthetic method is promising for preparing mixed metal-containing CD-MOFs, in addition to MOFs that cannot be prepared directly. Finally the ability of Li^+ substituted **CD-MOF-1** to capture CO_2

and H_2 was shown which had the highest adsorption capacity reported among CD-MOFs.[245] This work provides a reliable strategy for preparing mixed-metal coordinated CD-MOFs as functional materials.

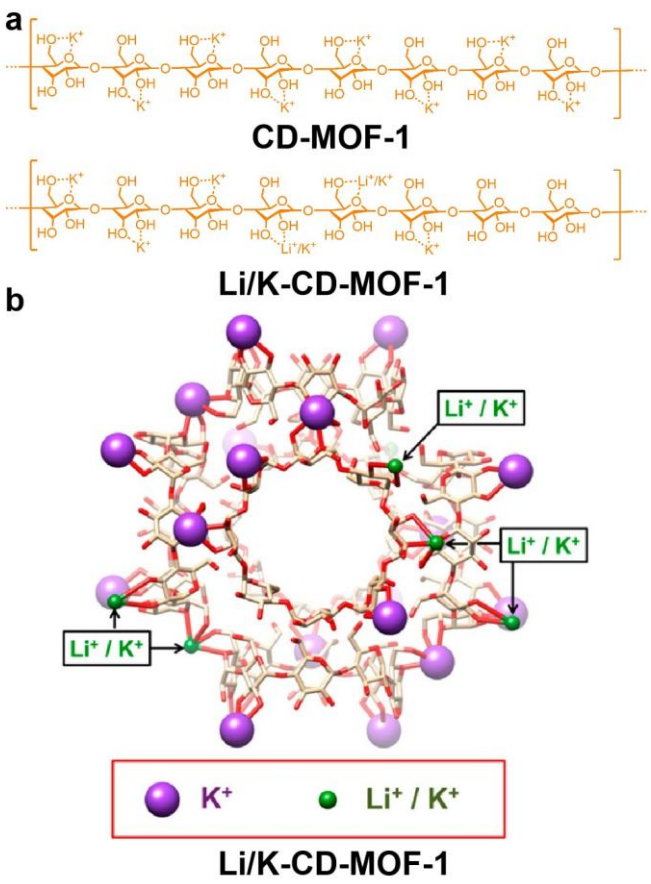

Fig. 30 (a) Chemical structures of **CD-MOF-1** and **Li/K-CD-MOF-1**, respectively. (b) Single crystal structure of **Li/K-CD-MOF-1**. C atoms are pale yellow, O atoms are red, K atoms are purple, Li atoms are green, and H atoms are omitted for clarity.[245]

4.1.2. Separation and purification

MOFs can be used for energy-saving separation of chemical raw materials.[166,239,246-249] For example, Stoddart's group reported that CD-MOFs showed high selectivity for aromatic compounds.[250] These MOFs composed of ***γ*-CD** and alkali metal cations can separate various xylene compounds. The results of adsorption isotherms and liquid chromatography showed that the separation order was *o*-xylene (***o*X**) > *m*-xylene (***m*X**) > *p*-xylene (***p*X**) by **CD-MOF-2**. They also observed regional selectivity in liquid chromatography of ethyltoluene and cymene regioisomers. Therefore, the molecular shape selectivity of CD-MOFs can be used to separate industrially relevant systems like BTEX (benzene, toluene, ethylbenzene and xylene isomers) mixtures. The high selectivity of CD-MOFs for benzene and these alkyl benzenes provides an efficient, reliable, and green alternative to current separation strategies. Furthermore, this separation of aromatic compounds highlights the specificity of shape selectivity exhibited by CD-MOFs. Single-component static vapor adsorption isotherms and grand canonical Monte Carlo simulations demonstrated the mechanisms of shape selectivity, providing new insights into the use of CD-MOFs as a renewable multifunctional separation platform.[250]

The CD-MOFs reported by Stoddart's group have been shown to facilitate the separation of alkyl aromatic compound mixtures, which have important implications for petrochemicals. For example, they reported the ability of **CD-MOF-1** to separate various mixtures, including ethylbenzene, styrene, halogenated aromatics, terpenes, pinene, and other chiral compounds.[251] **CD-MOF-1** tends to retain saturated compounds to a greater extent. In addition, the positions of the intramolecular double bonds in these compounds also affect their retention within the frameworks, as shown in the case of structure isomers of pinene and terpinine. These isomers with outer ring double bonds are better retained by **CD-MOF-1**. Additionally, **CD-MOF-1** is a homochiral framework, it can be applied to the enantiomers of dissociative analytes, including limonene and 1-phenylethanol. In comparison to other standard CSPs, **CD-MOF-1** is more cheap and easier to prepare.[251]

4.1.3. Catalysis

Other than separation and purification, CD-MOFs also show their potential in catalysis. An active site of the enzyme can catalyze chemical reactions between substrates efficiently and quickly.[252-254] Stoddart's group reported that 1-anthracene esters (**1-AC**$^-$) could be bound to **CD-MOF-1** and provided one of four possible isomers prior to [4+4] photo-dimerization between pairs of substrate molecules (Fig. 31).[255] This was one of the highest yielding regional isomers they reported that possessed optical activity. The structure of potassium 1-anthracene (**1-ACK**) co-crystallized with **CD-MOF-1** showed that the pair of substrate molecules could be stabilized in the channels of **CD-MOF-1** between the spherical cavities. In addition to forming hydrogen bonds with the C_2 and C_3 hydroxyl groups on the *D*-glucose residues in the CDs, hydrophobic and electrostatic interactions can also be formed with the carboxyl groups and the four K^+ cations. These non-covalent interactions induce the preferential conformation of regional isomers, which is the driving force for enantioselective [4+4] cycloaddition during optical radiation as confirmed by theoretical calculations.[255] Compared to **CD-MOF-1**, single ***γ*-CD** revealed no selectivity to this reaction. This strategy indicates that the integration of ***γ*-CD** into MOFs shows increased performance in catalyzing chemical reactions.

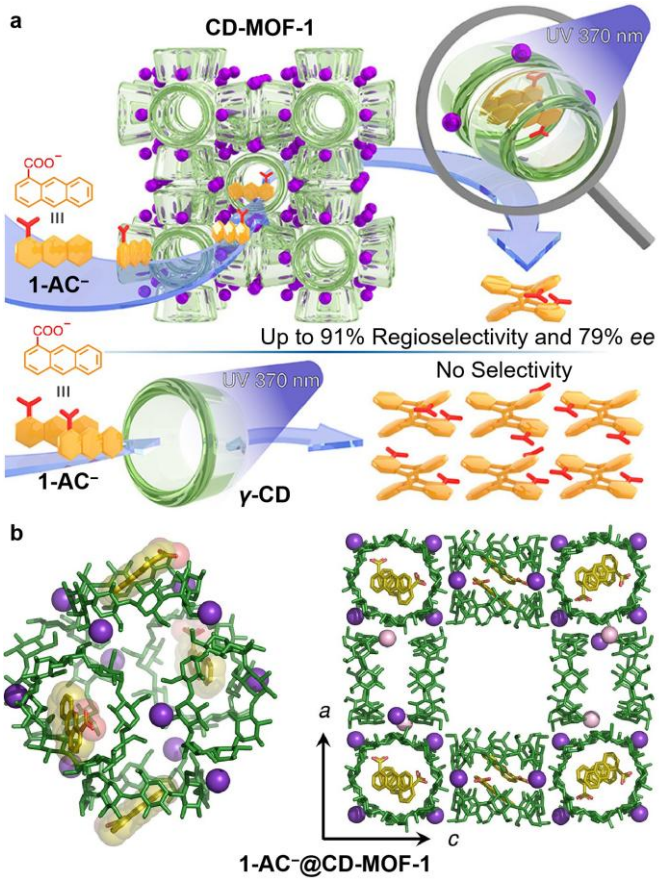

Fig. 31 (a) Schematic representation of photo-catalyzed **1-AC⁻** by **CD-MOF-1** and ***γ*-CD**. (b) Single crystal structure of **1-Ac⁻@CD-MOF-1**. Reproduced from ref. 255 with permission from American Chemical Society, copyright 2021.[255]

4.1.4. Circularly polarized luminescence

The chirality of CD-MOFs has not been revealed before. Through host–guest interactions between CD-MOFs and achiral luminescent groups with different charges and sizes, Liu's group demonstrated the unique chirality of the hollow cavity of **CD-MOF-1** and the effect of size on inducing circularly polarized luminescence (CPL).[231] Many achiral luminescent groups (**lum**) can be integrated into **CD-MOF-1** and exhibit significantly increased CPL. Small-sized guests can be complexed in the inherent void of the ***γ*-CDs**, while large-sized guests are selectively packaged into the cubic void of **CD-MOF-1**. When the sizes of luminescent groups on the guest are close to the cube size, **CD-MOF-1** can exhibit strong negative CPL. Otherwise, the disordered packing of **γ-CDs** would induce the loss of the host–guest interactions between the luminescent groups and ***γ*-CDs** which caused weak CPL or no CPL in the amorphous powders of **lum@CD-MOF-1**. In the **lum@CD-MOF-1** crystals, the order of ***γ*-CDs** and the tight confinement in the chiral cubic channels and two ***γ*-CD** pores with a rotaxane-like form contribute to the enhancement of CPL.[231] Their work revealed the chiral property of CD-MOFs.

4.1.5. Electrical device

The CD component can also be introduced into MOFs through host–guest complexation. Stoddart's group studied the electrochemical properties of CD-MOF.[256] They grew MOFs on the surface of a glass substrate in an epitaxial manner, which was modified by a self-assembled monolayer (SAM) of ***γ*-CD** molecules. SAMs are produced by the host–guest complexation between ***γ*-CD** molecules and functional pyrene units. The CD-MOF film they prepared has a continuous crystalline morphology. The film area is a few square millimeters, and the thickness is about 2 μm. In addition, their host–guest strategy has been applied to the growth of microparticle shells, and they integrated CD-MOF films into electrochemical devices for CO_2 sensing. These CD-MOF thin film-based devices exhibited a 300-fold increase in proton conductivity compared to devices prepared with CD-MOF crystalline powders. Their CD-MOF thin-film devices have fast and highly reversible CO_2 sensing cycles under environmental conditions.[256] This work provides a strategy for preparing films of CD-MOFs in electrical device.

4.1.6. Cargo release

At present, stimulus-responsive MOFs have attracted the attention of scientists because of their applications in many fields.[17,257-261] Wang's group reported the preparation of a light-responsive Zr-based MOF (denoted as **UiO-68-Azo**).[262] The SCXRD results showed that **UiO-68-Azo** has a ***Fm*3*m*** space group. Due to the disordered and flexible position of the overhanging substituents, the azobenzene group cannot be located in the crystal structure. N_2 adsorption/desorption experiment proved its permanent porosity. BET analysis revealed that **UiO-68-Azo** has a surface area of up to 2900 $m^2\ g^{-1}$ and a pore volume of 1.24 $cm^3\ g^{-1}$. Such a great porosity indicated the material had potential applications in cargo storage. This MOF could be used as a storage tank to store goods in water, and the cargoes loaded within this MOF could be stabilized by capping it with *β*-cyclodextrin (***β*-CD**) macrocylces on the azobenzene units on the surface of the MOF. The resulting MOF then released the cargoes by ultraviolet irradiation or the addition of a competing agent. Their research provides a simple strategy for building stimulus-responsive MOFs that supplies a viable MOF platform for on-demand drug delivery in the future.[262] This work also provides a new vision for introducing CDs into MOFs through a pseudorotaxane strategy.

4.2. Cyclodextrin-based COFs

Differently from CD-MOFs, the integration of CDs into COFs mainly depends on host–guest complexation and modification of CDs. The applications of CD-COFs are primarily focused on transmembrane transport, chiral nanomaterials and chiral separations.[263-265] The specific cases are discussed below.

4.2.1. 2D chiral nanomaterials

Liu's group proposed a strategy to prepare 2D chiral polyrotaxane (**2D-CPR**) layers with manipulable CPL activity using ***β*-CD** as a chiral wheel and a light-emitting dynamic COF (composed of **C3** and **Pyr**) as a 2D polymer skeleton (Fig. 32).[266] Their method combines host–guest chemistry and dynamic covalent chemistry to directly construct super-sized **2D-CPR** monolayers, while giving **2D-CPR** structural chirality to generate CPL activity. By changing the amount of ***β*-CD**, not only the structure of the COF network can be adjusted, but also the CPL performance can be further controlled. This work aids in understanding the excited state chirality of two-dimensional chiral materials.[266]

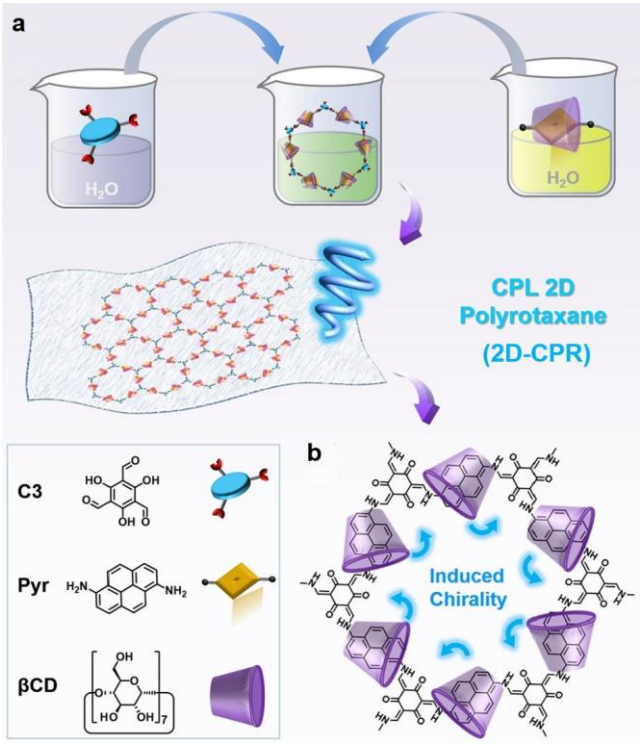

Fig. 32 (a) Schematic representation of the construction of **2D-CPR** and structures of **C3**, **Pyr** and ***β*-CD**. (b) Host–guest induced chirality which promotes CPL for **2D-CPR** monolayers. Reproduced from ref. 266 with permission from John Wiley & Sons, copyright 2022.[266]

4.2.2. Chiral separation

CD-COFs are crystalline framework materials with customizable channels, which have great potential in molecular transport.[267-271] Cui's group demonstrated that two-dimensional COFs (denoted as **CD-COF-1** and **CD-COF-2**) could be used as efficient solid state nanochannels for specific amino acid transport (Fig. 33).[264] By reacting C_3-symmetric trialdehyde with or without divinyl-containing diamine mixtures, they prepared two vinyl-functionalized COFs **CD-COF-1** and **CD-COF-2**. Both COFs have straight one-dimensional channels formed by stacking of layered hexagonal networks. They calculated the PXRD patterns of the two COFs and proposed the possible structures of **CD-COF-1** and **CD-COF-2**. They studied the porosity of two kinds of COFs by N_2 adsorption/desorption experiments. Nonlocal density functional theory (NLDFT) results revealed an average aperture of 23.0 Å for both **CD-COF-1** and **CD-COF-2**, corresponding to the simulated values of **CD-COF-1** (26 Å) and **CD-COF-2** (12−29 Å). The BET surface areas of **COF-1** and **COF-2** (without CDs introduced) reduced from 801 $m^2\ g^{-1}$ to 614 $m^2\ g^{-1}$ and from 592 $m^2\ g^{-1}$ to 415 $m^2\ g^{-1}$, respectively. The pore volumes decreased from 1.70 $cm^3\ g^{-1}$ to 0.91 $cm^3\ g^{-1}$ and 0.83 $cm^3\ g^{-1}$ to 0.23 $cm^3\ g^{-1}$, respectively. These phenomena were induced from the occupied space after incorporating ***β*-CD**. Chiral ***β*-CD** could be modified to COFs through sulfhydryl groups, and COFs could be further prepared into mixed matrix membranes (MMMs) with the ability to transport amino acids. They confirmed this result by monitoring changes in the concentration of the osmotic substrate. In their membrane system, the AA-stacked COF has stronger chiral recognition of histidine enantiomers (***L*-His** and ***D*-His**) than the AB-stacked COF, because its uniform channels are modified by ***β*-CD**. Their research demonstrates that COF nanochannels can be used for selective transport of small molecules and even solid biomolecules.[264]

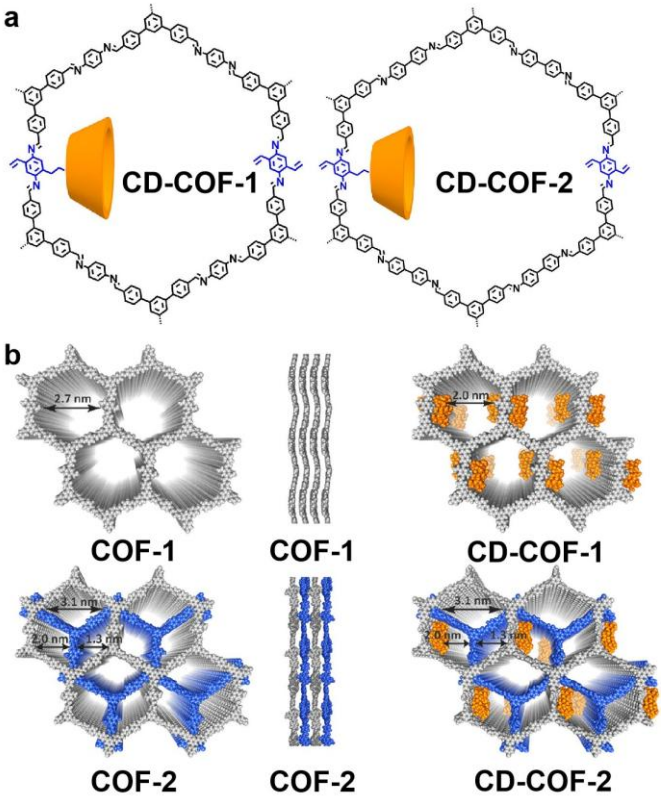

Fig. 33 (a) Chemical structures of **CD-COF-1** and **CD-COF-2**. Yellow circular cone represents ***β*-CD**. (b) Calculated structures of **COF-1**, **COF-2**, **CD-COF-1** and **CD-COF-2**. Reproduced from ref. 264 with permission from American Chemical Society, copyright 2019.[264]

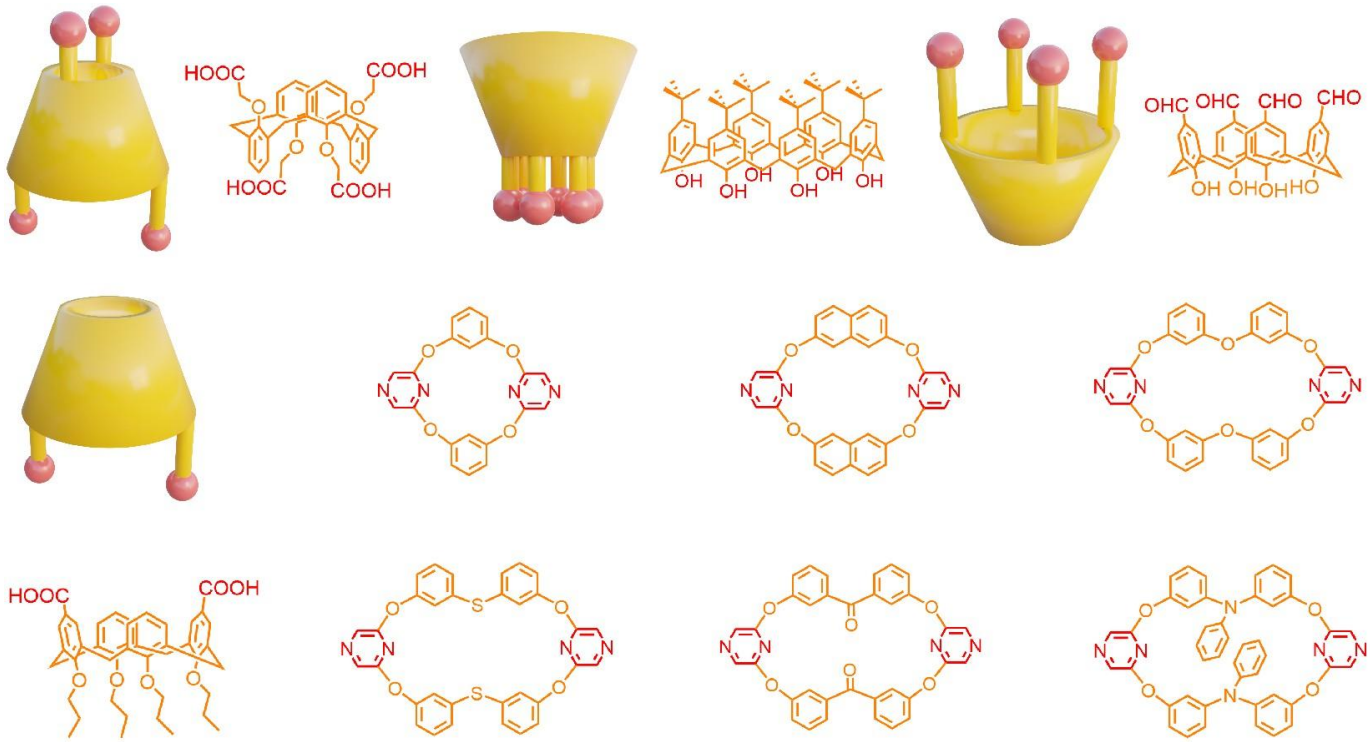

Fig. 34 Cartoon representations and chemical structures of CA-incorporated components involved in this review for preparing crystalline framework materials.

Combined with the low density, large specific surface area, permanent porosity and high chemical stability, COFs can also be used in CSPs.[272-275] Wang's group prepared a silica-modified COF by a solvothermal method, named **Sil-COF**.[265] They further used thiophene-based click chemistry to modify thiolated ***β*-CD** onto **Sil-COF** for chiral separation, known as **Sil-CD-COF**. They identified the successful construction of **Sil-CD-COF** through a series of characterizations. The crystallinity of **Sil-CD-COF** was confirmed by PXRD. The BET surface area of **Sil-COF** was calculated to be 328 $m^2\ g^{-1}$. Three non-polar substances can then achieve baseline separation on the **Sil-CD-COF**. Two compounds, 2-phenylpropionic acid and 1-phenyl-1-propanol, were selected as model enantiomers to further verify the chirality recognition ability of **Sil-CD-COF** columns. They compared the silica gel column with the commercial ***β*-CD** column and demonstrated superior recognition of the chiral column they prepared. The **Sil-CD-COF** modified columns they prepared also showed high reproducibility. Wang's research gave a strategy of covalently modified ***β*-CD** onto chiral COF-based stationary phase chromatography and increasing the chiral recognition ability.[265]

4.2.3. Li^+ conduction

3D COFs is a promising crystalline material with high porosity and low density. However, the limited nature of building blocks hinders their development. Wang's group used ***γ*-CD** as the structural unit to build 3D COFs (denoted as **Li-CD-COF**) by connecting to a tetrakis(spiroborate) tetrahedra with different counter-ions. They studied the porosity of **Li-CD-COF** using an Ar adsorption isotherm measured at 87 K. **Li-CD-COF** produced a typical type I adsorption isotherm at low pressure, which explained the microporous properties of this material. The calculated BET surface area was 760 m^2/g and the total pore volume was 0.39 cm^3/g. NLDFT analysis showed that the pore size of **Li-CD-COF** was 0.64 nm. Based on the **rra** topology of the *I*432 space group, they simulated the crystal structure of **Li-CD-COF**. The introduction of ***γ*-CD** in rigid frameworks gives **Li-CD-COF** dynamic properties, resulting in Li^+ conductivity up to 2.7 ms/cm at 30 °C and excellent Li^+ strip-off/plating stability. This COF can effectively regulate the interactions between the frameworks and CO_2 molecules by exchanging the counter-ions in the pores.[108]

5. Calixarene-based crystalline porous framework materials

Calixarenes (CAs) are macrocyclic compounds composed of methylene-bridged phenol units at meta-positions.[90,132,276-279] They were synthesized by Zinke for the first time in 1942, and named calixarenes by Gutscht because their structures are similar to that of a wine-glass.[280-282] CAs have a “cavity” with adjustable sizes. Compared with CDs and CEs, CAs can form host–guest complexes with both ions and neutral molecules, which are a class of more widely adaptable enzyme analogs.[283, 284] They are regarded as the third generation of supramolecular macrocycles after CEs and CDs, and many CAs have been commercialized.[285,286] The formation of crystalline porous

framework materials with CA-based ligands allows for the formation of hierarchical frameworks, combining two levels of porosity in respect to the ligand and the structural framework.[287] At present, the exploration of CA-based crystalline porous framework materials is still in its infancy. We highlight several prototypical examples of calixarene-based framework materials, categorized by a variety of applications as shown below (Fig. 34).

5.1. Calixarene-based MOFs

The study of CA-based MOFs remains challenging. Only a handful of calixarene-based MOFs have been reported, likely due to their asymmetric structures. The applications reported mainly focus on molecular recognition, gas detection, and membranes.[142,287-289]

5.1.1. Molecular recognition

The Thurston group prepared four MOFs using the rim-functionalized calix[4]arene with dicarboxylic acid (**H_2Caldc**). Three of them were extensively characterized and formed 2D or 3D network structures. They are $[Cu_2$(**Caldc**$)_2(DMF)_2]$ (**Cu-CA-MOF-1**), $[Zn_2$(**Caldc**$)_2(DMF)_2]$ (**Zn-CA-MOF-1**), $[Cd_2$(**Caldc**$)_2(DMF)_2]\cdot$3DMF (**Cd-CA-MOF-1**), and $[Co_5$(**Caldc**$)_4(OH)_2(H_2O)_4]\cdot$8DMF (**Co-CA-MOF-1**).[142] Simulation results showed that the specific surface areas of these structures are relatively small, and the calculated values of N_2 adsorption for **Cu-CA-MOF-1**, **Cd-CA-MOF-1** and **Co-CA-MOF-1** are 190 $m^2\ g^{-1}$, 410 $m^2\ g^{-1}$ and 441 $m^2\ g^{-1}$, respectively. Due to the collapse and porosity loss of MOFs after removal of coordinated DMF molecules, their experimental specific surface areas are quite low, which limits the further applications of these MOFs. This work provides a precedent for CA-based MOF preparation but still required further study to develop their applications.[142]

5.1.2. Gas detection

Schaate's group explored the gas detection properties of a stable CA-based MOF (Fig. 35).[287] They prepared a CA-based MOF named **Zr-CA-MOF-2** with an apparent BET surface area of 670 $m^2\ g^{-1}$ and characterized it by SCXRD. This structure is formulated by $[Zr_6O_4(OH)_4(FA)_6]_2$(**CA**$)_3$ (FA = formic acid) with a space group of *Ia*3*d*. The resulting framework has a **gar** topological network with a 4,6 connected network. Guest molecules can enter the cavities of calixarenes through MOF voids. **Zr-CA-MOF-2** allowed for the capture of NO_2 to form dark charge transfer complexes, which could be used to visually detect and encapsulate NO_2. They then analyzed the selective complexation of **Zr-CA-MOF-2** by UV/vis and infrared spectroscopy, and confirmed the stability of **Zr-CA-MOF-2** by PXRD and ^{1}H NMR spectroscopy. Finally, they installed **Zr-CA-MOF-2** as the sensing material in a homemade battery sensor, which showed high sensitivity to NO_2. This material provides a new way to detect gases with CAs incorporated.[287]

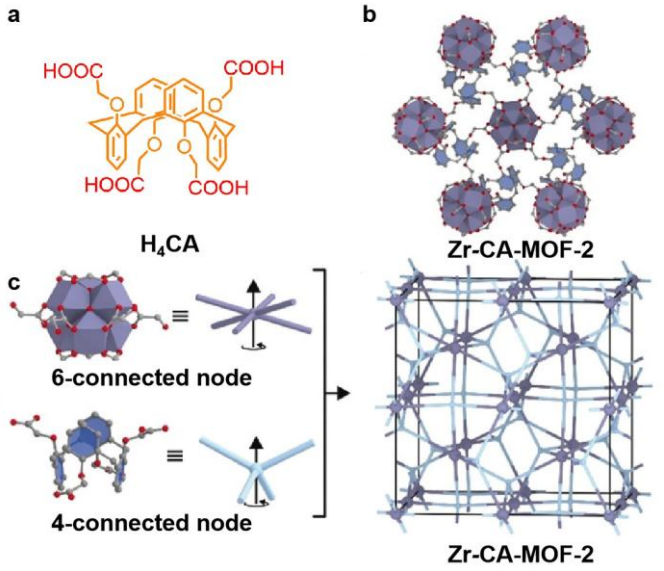

Fig. 35 (a) Chemical structure of calixarene ligand **H_4CA**. (b) Single crystal structure of CA-incorporated MOF $[Zr_6O_4(OH)_4(FA)_6]_2$(**CA**$)_3$(**Zr-CA-MOF-2**). Here FA is formic acid. (c) Structure illustration of the topological composition of **Zr-CA-MOF-2**. Purple polyhedras are metal nodes and blue nodes are CA ligands. C atoms are grey, O atoms are red, and Zr clusters are dark blue. Reproduced from ref. 287 with permission from John Wiley & Sons, copyright 2018.[287]

Tang's group further investigated the photo-chemical property of CA-containing MOFs (Fig. 36).[289] They reported that a butterfly molecule of oxacalix[2]arene[2]pyrazine (**OAP**) showed aggregation induced emission (AIE) characteristics through the restriction of intramolecular vibration (RIV) mechanism.[289] Unlike other AIE molecules, **OAP** AIEgens (**OAP-1** to **OAP-6**) could be synthesized in a simple one-step process using commercially available materials. Notably, **OAP** AIEgens are ideal ligands for constructing MOFs because they have pyrazine coordination sites. Using **OAP** AIEgens and CuI as ligands and metals, they prepared a series of **OAP**-based MOFs with different structures (**OAP-MOF-1** to **OAP-MOF-8**). **OAP-MOF-1** and **OAP-MOF-2** are 1D chain-like structures, and the **OAP** ligands are bridged by Cu_2I_2 clusters. **OAP-MOF-3** to **OAP-MOF-7** are two-dimensional layered structures, and **OAP** ligands are bridged by Cu_2I_2, Cu_4I_4 and Cu_6I_6 clusters, respectively. **OAP-MOF-8** is a three-dimensional structure with infinite CuI units connected together to form an 1D Cu_nI_n chain and **OAP-5** acts as a linear ligand to connect two adjacent Cu_nI_n chains. The **OAP**-based MOFs (**OAP-MOF-1** to **OAP-MOF-8**) they reported have multiple potential applications in the construction of reversible gas (MeOH) response and white light emitting devices. Their work, based on RIV-type AIEgens, provides additional choice of ligands for the construction of

luminous MOFs, and provides a novel idea for the applications of luminous MOFs.[289]

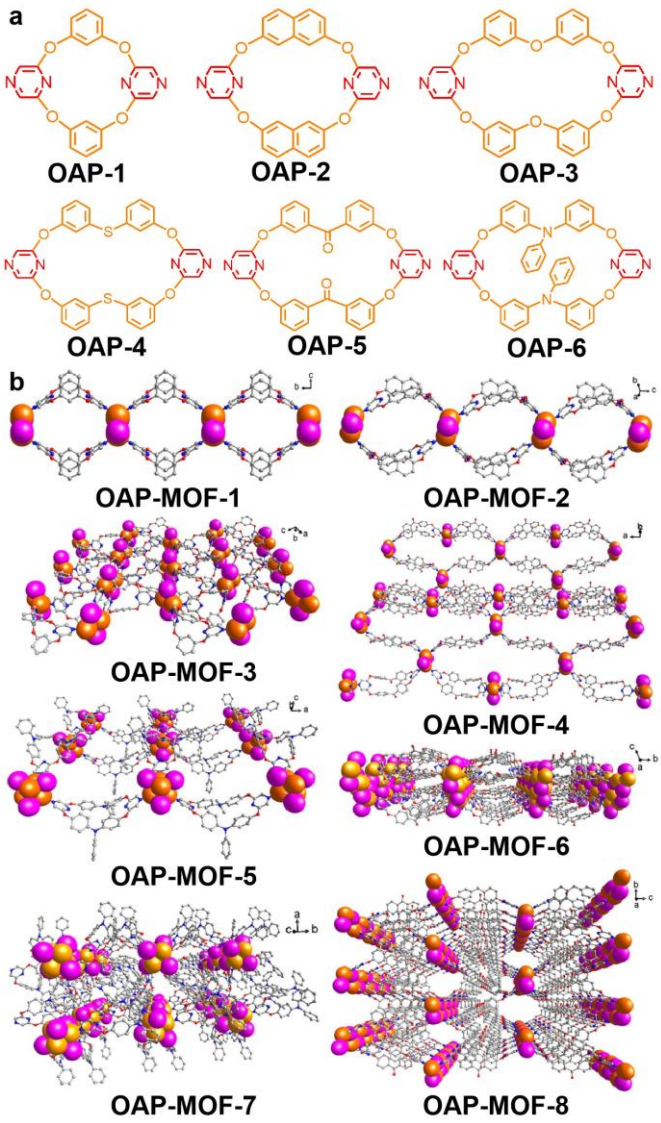

Fig. 36 (a) Chemical structures of calixarene ligands **OAP-1** to **OAP-6**. (b) Single crystal structures of calixarene-incorporated MOFs **OAP-MOF-1** to **OAP-MOF-8**. C atoms are grey, O atoms are red, N atoms are blue, Cu atoms are orange, I atoms are purple, and H atoms are omitted for clarity. Reproduced from ref. 289 with permission from John Wiley & Sons, copyright 2021.[289]

5.1.3. Membrane

Synthesizing MOFs that are stable in non-polar media is not as simple as the manufacturing of inorganic nanoparticles. Yavuz's group reported that calix[6]arene-stabilized **UiO-66** nanoparticles without clogging pores could allow the formation of stable colloid dispersions with a narrower size distribution.[286] Using an **UiO-66** dispersion solution, they demonstrated that smooth films could be prepared from immiscible polystyrene.[288] To verify the porosity of **UiO-66**, they tested the adsorption of N_2 by **UiO-66** at 77 K to calculate the specific surface area. The calculation results showed that the specific surface area of **UiO-66** coated with calix[6]arene (1385 m^2/g) was higher than that of natural **UiO-66** (1245 m^2/g). Commonly, the specific surface area of the material will be reduced after the incorporation of macrocycles. However, in this case, the specific surface area increased after macrocycles are introduced to **UiO-66**, which is relatively rare in macrocycle-incorporated crystalline frameworks. Their work expands the applications for preparing membranes using CA-based MOFs.

5.2. Calixarene-based COFs

CAs are ideal building blocks for building COFs because they are electron rich and have bowl-shaped π cavities that give them electronic and adsorption properties.[90] However, the synthesis and structural confirmation of CA-incorporated COFs remains a challenge due to the asymmetrical CA structures. Two cases are given below which highlight their applications in lithium isotope separation and pollution removal.[290, 291]

5.2.1. Lithium isotope separation

As mentioned previously, the lithium isotope has received a lot of attention due to its important role in nuclear fusion and fission reactions.[292-297] However, the chemical properties between lithium isotopes is very similar, so separating the lithium isotopes (^6Li and ^7Li) remains a huge challenge.[298] The Shi group designed three COFs (denoted as **C4A-COF-1-BD**, **C4A-COF-1-BD(OH)$_2$**, and **C4A-COF-1-DPT**) based on calix[4]arenes (**C4A**) for the adsorption of lithium and separation of its isotopes (Fig. 37).[290] N_2 adsorption experiment results showed that **C4A-COF-1-BD** has a specific surface area of 59 $m^2\ g^{-1}$ and an average pore size of 1.27 nm. The specific surface areas of **COF-1-BD(OH)$_2$** and **C4A-COF-1-DPT** are 50 and 25 $m^2\ g^{-1}$ with pore sizes of 1.36 nm and 1.59 nm, respectively. Compared with **C4A-COF-1-BD** and **C4A-COF-1-BD(OH)$_2$**, the decrease in surface area of **C4A-COF-1-DPT** may be related to the increase in lattice volume. For **C4A-COF-1-BD**, they built a single-layer model of the structure based on the **sql** topology. Considering the bowl-like structure of calix[4]arenes, two different interlayer stacking models AA-stacking and AB-stacking were proposed. The simulated PXRD patterns showed that the AA-stacking structure was in good agreement with the experimental results. After constructing the structure models, they continued the exploration of lithium isotope separation using these MOFs. Their study showed that the adsorption capacity of these COFs for lithium was as high as 94.66 mg g^{-1}. This high adsorption capacity was due to the abundance of calix[4]arene adsorption sites in COFs. Their study demonstrated that the calixarene units in **C4A-COF-1-BD** could separate lithium isotopes with a separation factor of up to 1.053 ± 0.002 for the first time, which was comparable to solid phase lithium separation adsorbents. Theoretical calculations as confirmed that calixarene units played an crucial role in the

adsorption of lithium. Their work expands the applications of CA-based COFs in isotope separation.[290]

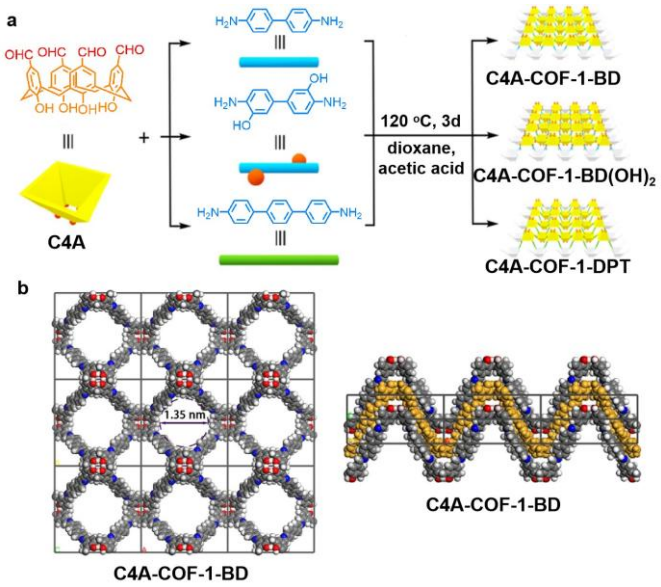

Fig. 37 (a) Synthetic routes to **C4A-COF-1-BD**, **C4A-COF-1-BD(OH)$_2$**, and **C4A-COF-1-DPT**. (b) Simulated structure of **C4A-COF-1-BD**. Reproduced from ref. 290 with permission from American Chemical Society, copyright 2023.[290]

5.2.2. Pollution removal

CA-containing COFs can also be used in catalysis.[115,299-301] Using 5,11,17,23-tetrahydroxycalix[4]arene (**CHO-C4A**) as the electron donor and 4,7-bis(4-aminophenyl)-2,1,3-benzothiazole (**BTD**) as the electron acceptor, the Li group synthesized a two-dimensional COF (denoted as **C4A-COF-2**) (Fig. 38).[291] PXRD and crystal structure theoretical simulations showed that **C4A-COF-2** possessed high crystallinity and formed a two-dimensional layered structure. The simulation results and experimental data of PXRD showed that the space group of **C4A-COF-2** is *P*-4*m*2. It has a two-dimensional layered structure with a AA stacking mode. The results of adsorption/desorption experiments of N_2 and CO_2 at 77 K and 195 K confirmed that, in the low pressure range of $P/P_0 < 0.8$, **C4A-COF-2** exhibited a lower N_2 adsorption capacity. The PXRD pattern of **C4A-COF-2** before and after activation revealed no obvious change, indicating that it still has a crystalline state. Therefore, the low N_2 adsorption was not caused by the collapse of the **C4A-COF-2** framework structure. The reason for this phenomenon may be the diffusion resistance of N_2 molecules in one-dimensional channels. The adsorption of CO_2 by **C4A-COF-2** showed that at $P/P_0 = 0.95$, the adsorption capacity of CO_2 reached 95 $cm^3\ g^{-1}$, and the pore size distribution was 0.9 nm and 1.6 nm, which matched well with the predicted pore size. The calculated BET specific surface area was 268 $m^2\ g^{-1}$, which proved the microporous property of **C4A-COF-2**. DFT calculations, transient photocurrent measurements and electrochemical impedance spectroscopy confirmed that **C4A-COF-2** had an intramolecular charge transfer behavior, so it had superior photocatalytic activity. Compared with conventional hydrogen electrodes, **C4A-COF-2** has a narrow band gap of 1.99 eV and a band conduction energy of −0.37 V. The removal rates of **C4A-COF-2** for organic pollutants such as rhodamine B, bisphenol A and methylene blue were 85%, 66% and 99%, respectively.[291] These results indicated that the CA-containing COFs had potential applications in pollution removal.

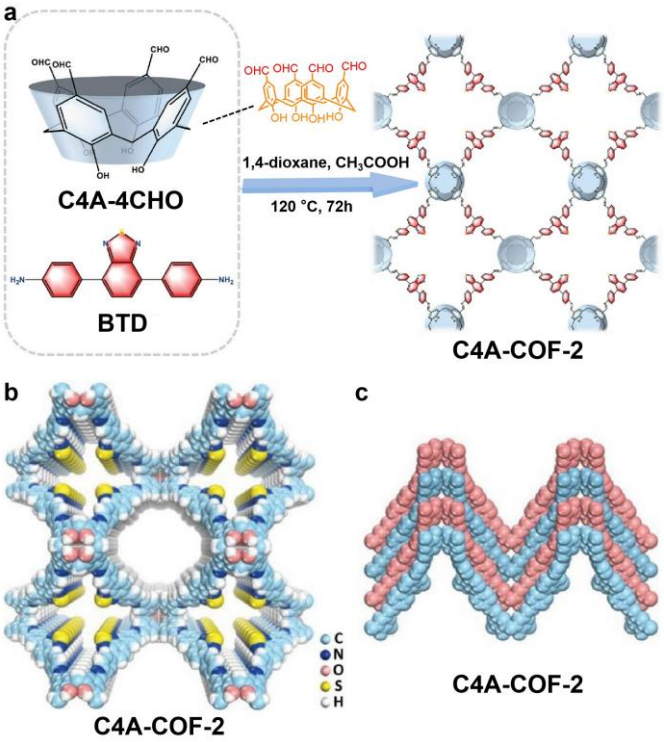

Fig. 38 (a) Structural representation of the construction of calix[4]arene-based **C4A-COF-2** using **CHO-C4A** and **BTD**. (b) Simulated structure of **C4A-COF-2** in spacefilling form. C atoms are light blue, N atoms are dark blue, O atoms are light pink, S atoms are yellow, and H atoms are white. (c) Spacefilling form model of **C4A-COF-2** networks. Reproduced from ref. 291 with permission from John Wiley & Sons, copyright 2023.[291]

6. Cucurbituril-based crystalline porous framework materials

This section outlines the reported results of cucurbituril (CB)-based framework materials, including molecular recognition and adsorption. Cucurbiturils are another kind of macrocyclic molecules like CAs (Fig. 39).[133,134,302-307] Because of the strong binding between cucurbiturils and many guest molecules, they have attracted extensive attention within the field.[306-308] However, the preparation and modification of CBs with high efficiency is still a main focus in CB chemistry. Thus, the development of CB-based framework materials remains a great challenge and only a small number of examples have been

reported in the literature. Herein we summarize the possible approaches for solving the technical problems in the preparation of CB-based crystalline porous framework materials.

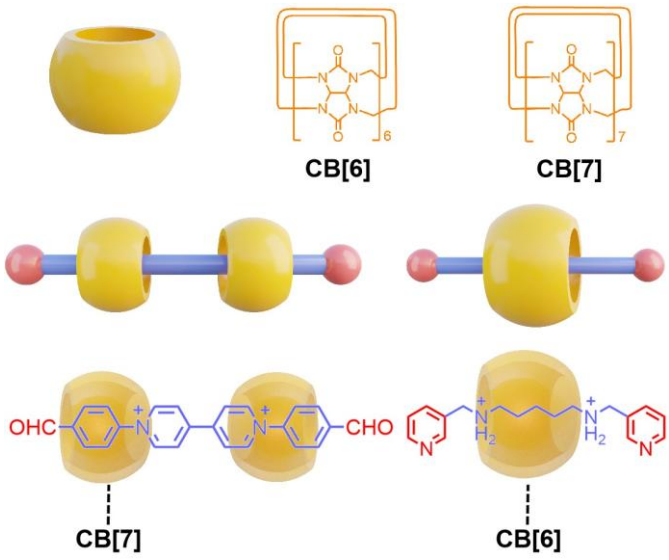

Fig. 39 Cartoon representations and chemical structures of CB-incorporated components involved in this review for preparing crystalline framework materials.

6.1. Cucurbituril-based MOFs

On account of the difficulty in modification of CBs, cases of CB-based MOFs have been rarely reported. Therefore, there is still a long way to go in the design and synthesis of CB-based MOFs. Here, two examples of CB-based MOFs and their applications in molecular recognition and gas adsorption are discussed.[143,309] These work guide the construction of CB-incorporated MOFs by using host–guest recognition of CBs.

6.1.1. Molecular recognition

Kim's group first reported CB-based MOFs in 2001.[143] They first synthesized a pseudorotaxane from a cucurbit[6]uril (CB[6]) and an alkyl chain with positive charges, and then used this pseudorotaxane to synthesize a novel MOF with large pores. The crystal structure of this MOF resembles to a two-dimensional polyrotaxane, where CB[6] is complexed on a two-dimensional coordination polymer network. This cationic MOF allows for selective anion exchange. More importantly, this work sets a precedent for the MOF synthesis with CBs.[143]

6.2. Cucurbituril-based COFs

CBs can also be integrated into COFs through forming host–guest complexes. Here, an example of CB-incorporated COFs is discussed below.[310]

6.2.1. Molecular recognition

Li's group prepared a three-dimensional flexible organic skeleton **FOF-1** by condensation of acylhydrazine with rigid 4,4 '-diphenyl-4,4'-bipyridinium dialdehyde in water through forming hydrazone bond.[310] They further utilized the dynamic properties of hydrazone bonds to construct a macrocycle-incorporated framework, **FOF-pc-1**, by complexing the diphenylpyridine structure with cucurbit[7]urils (**CB[7]-Rotaxane** in Fig. 40). The bipyridine units in both frameworks can be reduced to the dynamic organic frameworks **rc-FOF-1** or **rc-FOF-pc-1**. They found that the resulting polyrotaxane **rc-FOF-pc-1** can enhance the stability of the frameworks in water, while both **FOF-pc-1** and **rc-FOF-pc-1** can form more stable complexes with **CB[7]** through the use of ferrocene guests. Their new strategy can be used to construct neutral and mechanically interlocked structures (Fig. 40).[310] This case provides a strategy for constructing cucurbituril-based COFs. Therefore, considering the challenging modified property of CBs, the incorporation of CB components into crystalline frameworks could be in the form of rotaxane or catenane.

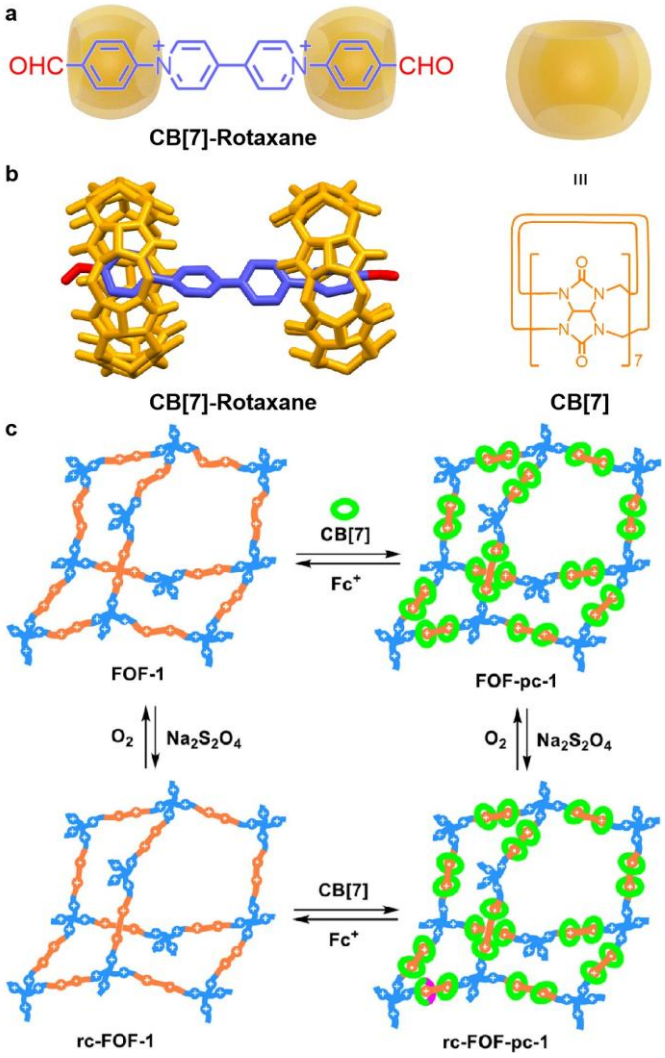

Fig. 40 Chemical structure (a) and single crystal structure (b) of **CB[7]-Rotaxane**. (c) Schematic illustration of the reversible

transformations of **FOF-1**, **FOF-pc-1**, **rc-FOF-pc-1** and **rc-FOF-1**.[310]

7. Pillararene-based crystalline porous framework materials

Pillararenes (PAs) can be synthesized from commercial chemicals in one step and in large quantities (gram scale).[87,311-321] In addition, the substituent groups on PAs can be easily modified into a variety of other substituents.[313] They have the advantages of simple synthesis, easy modification, and abundant host–guest properties like the recognition of alkyl chains and aromatic chemicals.[317,321-325] The reports of high-ordered and modified PAs have increased exponentially since the inception of PA studies.[127,315] Thus, various sized and functionalized PAs are readily available when attempting to create specific recognition of guests (Fig. 41).[326,327] However, constructing PA-based framework materials still remains a big challenge although with increased attention and versatility. Only a handful of reports have been published in the literature.[119,120,145,328] Finally, PAs have an important property, planar chirality, which allows them to be utilized in many applications.[324,329,330] The unique planar chirality of PAs will be highlighted as a future direction of developing PA-containing crystalline porous framework materials.

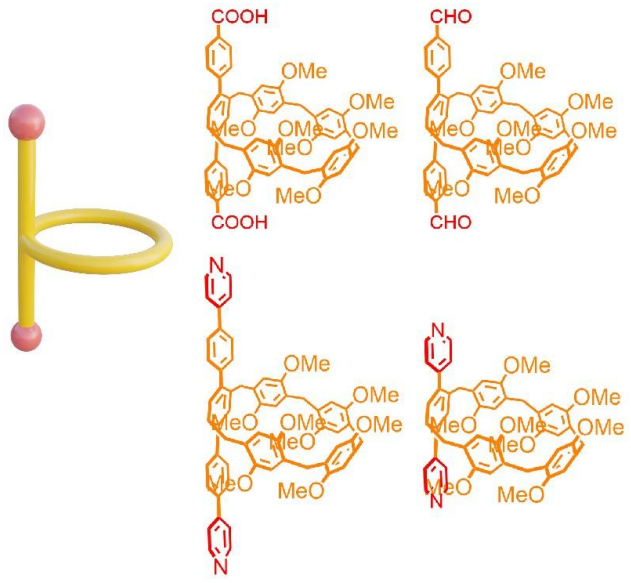

Fig. 41 Cartoon representations and chemical structures of PA-incorporated components involved in this review for preparing crystalline framework materials.

7.1. Pillararene-based MOFs

Due to the flexible nature, PA-based MOFs are difficult to synthesize and characterize.[119] Therefore, rationally designing the PA-containing ligands is the key to construct PA-based MOFs. Here, the reported cases of PA-based MOFs are discussed in the context of applications in molecular recognition, adsorption and separation.

7.1.1. Molecular recognition

Stoddart's group developed a functionalized pillar[5]arene modified MOF with planar chirality, named **P5A-MOF-1** (Fig. 42).[119] However, the crystal structure of **P5A-MOF-1** was unsolved on account of the high degree of motion and dynamics of pillar[5]arene units in the frameworks. They suggested through a confirmation by PXRD analysis that the framework had the same **pcu** topological structure as **MOF-5**.[119] The NLDFT surface area of 300 $m^2 g^{-1}$ was obtained by the activation of the **P5A-MOF-1** crystals with supercritical CO_2. This PA-based MOF has an active domain, which can adsorb neutral and positively charged aromatic guests with high selectivity. The crystal color of **P5A-MOF-1** after adsorbing the guest changed from light yellow to deep orange, which was caused by the charge transfer between the active domain of **P5A-MOF-1** and the guests.[119] Their work provides the first case of integrating PA components into MOFs, guiding the development of PA-based MOFs.[119] However, the resolution of the crystal structure determination of PA-based MOFs remains challenging and unsolved.

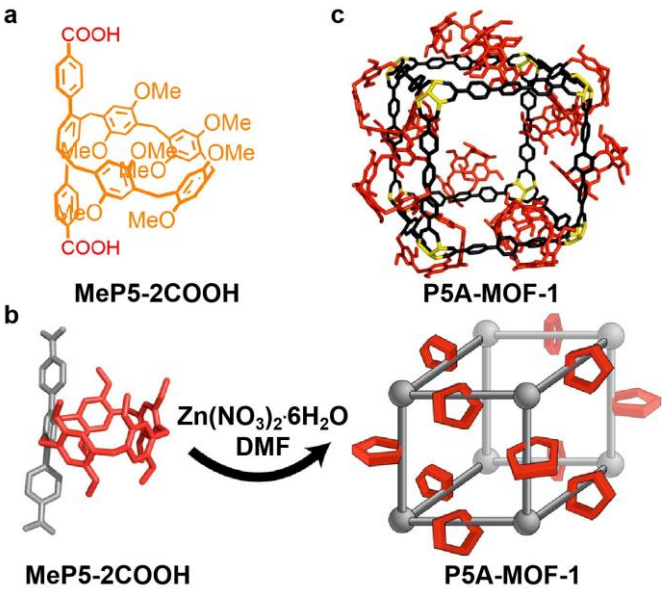

Fig. 42 (a) Chemical structure of **MeP5-2COOH**. (b) Schematic representation of the synthesis of **P5A-MOF-1** from PA-incorporated ligand **MeP5-2COOH**. (c) Simulated structure of **P5A-MOF-1**. Here pillar[5]arene units are red, organic struts are grey, and Zn nodes are yellow. Reproduced from ref. 119 with permission from American Chemical Society, copyright 2012.[119]

Stoddart's group further investigated the chiral MOFs using the same ligand.[328] Enantiopure struts containing planar chiral pillar[5]arenes (*pS*-**MeP5-2COOH** and *pR*-**MeP5-2COOH**) have been used to link zinc nodes to create MOFs containing

homochiral active domains and thus have the potential to uniquely serve as solid materials for chiral chromatography.[328] The PXRD patterns of *pS*-**P5A-MOF-1** and *pR*-**P5A-MOF-1** were almost identical, and almost matched the PXRD patterns of simulated *rac*-**P5A-MOF-1** in $P\bar{1}$ space group. However, further exploration in this aspect has not been conducted.

The crystalline framework materials containing the structure units of PAs can be used for molecular recognition and selective separation. However, as mentioned above, due to the flexibility of PAs, it is difficult to prepare and characterize MOFs with PA structural units, which limits the development of PA-incorporated MOFs. Despite these challenges Huang's group reported a series of MOFs containing pillar[5]arene units and successfully characterized pillar[5]arene units within the frameworks (Fig. 43).[120] The SCXRD analysis revealed that the interpenetrated networks appeared to impede the motion of the pillar[5]arene units in the frameworks, so the precise structures of the pillar[5]arene units within the MOFs were determined for the first time. The layers are connected together by **MeP5BPPy** to form a non-interpenetrated **fsc**-type framework structure **MeP5-MOF-2**. The BET surface area of **MeP5-MOF-2** was calculated to be 190 m^2/g. This MOF (**MeP5-MOF-2**) was able to recognize **PQT** and 1,2,4,5-tetracyanobenzene (**TCN**) in solution, and could be used for the separation of toluene (**Tol**) and pyridine (**Py**). This work provides a precedent for the applications of PA-incorporated MOFs in molecular recognition and selective separation.[120] Huang's work provides a reliable method to solve the structure characterization problems of PA-based MOFs, which could guide the development of PA-incorporated MOFs in the future.[120]

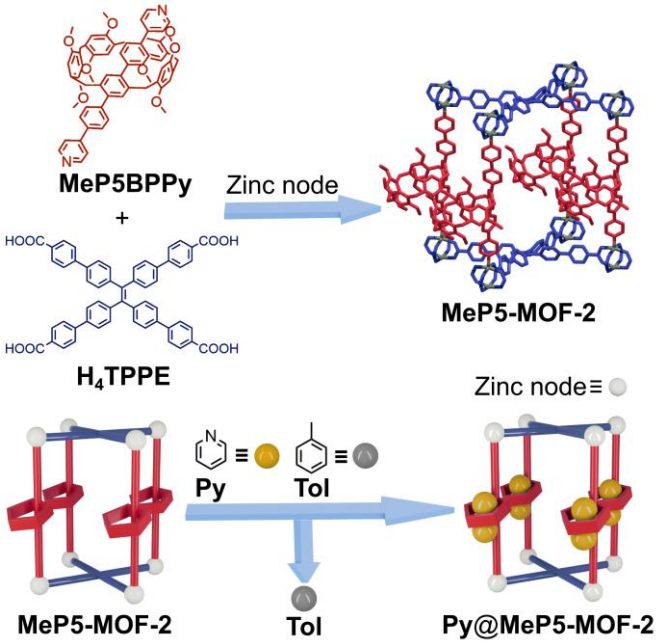

Fig. 43 Schematic illustrations of the synthesis of pillar[5]arene-based MOF **MeP5-MOF-2** from **MeP5BPPy** and **H_4TPPE**, and its application in the separation of **Tol** and **Py**. **Py** = pyridine; **Tol** = toluene.[120]

7.2. Pillararene-based COFs

Similar with PA-based MOFs, the integration of PAs into COFs also provides additional binding sites for molecular recognition.[145] A specific example is discussed as below in the context of gas separation.

7.2.1. Gas adsorption

As is known, it is important to maintain the selective molecular recognition ability of macrocycles in the solid state.[331,332] The integration of PAs into ordered COFs represents a promising strategy that could enable a wide range of practical applications, such as efficient molecular separation. However, as discussed in the MOF section, construction and characterization of COFs embedded with PAs remains a challenging task due to the flexible nature of PAs. Zhang's group designed and synthesized a COF based on a pillar[5]arene derivative (**MeP5-2NH$_2$**), referred to as **P5A-COF-1** (Fig. 44).[145] The N_2 adsorption experiments at 77 K showed that the adsorption isotherms of **P5A-COF-1** and **Model-COF-1** (without incorporation of pillar[5]arenes) showed the type IV adsorption. The BET surface areas of **P5A-COF-1** and **Model-COF-1** were 381 $m^2\ g^{-1}$ and 134 $m^2\ g^{-1}$, respectively. The aperture distribution of **Model-COF-1** was in the range of 2.0–3.2 nm. **P5A-COF-1** presented two pore sizes, 0.78 nm and 1.43 nm, which may be due to the pillar[5]arene units and the internal arrangement of pores in **P5A-COF-1**. The total pore volumes of **Model-COF-1** and **P5A-COF-1** are 0.53 $cm^3\ g^{-1}$ and 0.32 $cm^3\ g^{-1}$, respectively. Compared with **Model-COF-1**, the COF analogue without pillar[5]arene units incorporated, **P5A-COF-1** showed selective adsorption of C_2H_2, and its binding ability on **PQT** was also significantly enhanced. The adsorption capacities of **Model-COF-1** for C_2H_6, C_2H_4 and C_2H_2 were 22, 21 and 22 $cm^3\ g^{-1}$, respectively. At the same temperature and pressure, the adsorption capacities of **P5A-COF-1** for C_2H_6, C_2H_4 and C_2H_2 are 21, 18 and 43 $cm^3\ g^{-1}$, respectively. It was worth noting that compared with the **Model-COF-1**, the adsorption of C_2H_2 by **P5A-COF-1** increased approximately one fold, while the absorption of C_2H_6 and C_2H_4 was slightly decreased. This difference in C_2H_2 adsorption may be due to the stronger hydrogen bond interactions between pillar[5]arene units and C_2H_2 molecules. They established a strategy for PA-based COFs with customizable molecular recognition properties through a bottom-up "macrocycle to framework" design.[145]

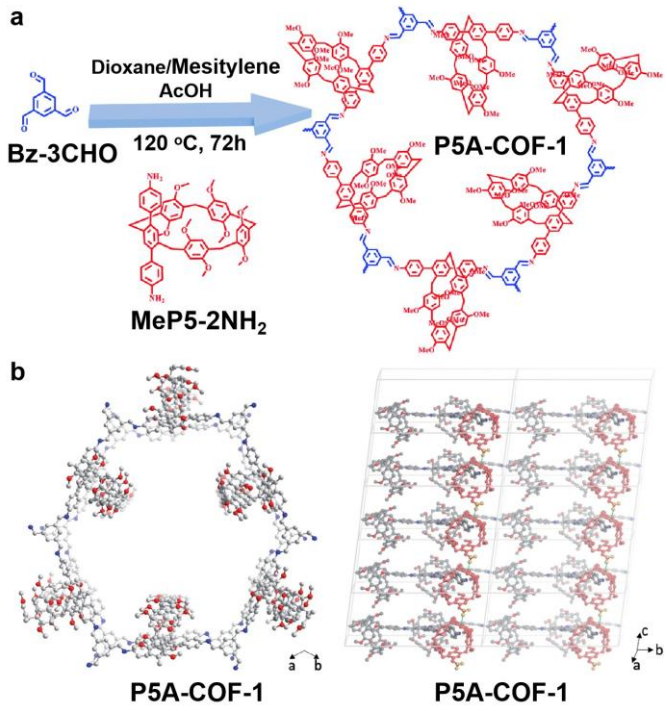

Fig. 44 (a) Chemical structure and synthesis of **P5A-COF-1**. (b) Simulated structure of **P5A-COF-1**. Here C atoms are grey, O atoms are red, N atoms are blue, and H atoms are omitted for clarity.[145]

8. Other macrocycle-based crystalline porous framework materials

We have summarized five typical macrocycle-based crystalline porous framework materials above. Additionally, there are also several nontypical macrocycles involved. Other synthetic macrocycles such as cyclophane cyclobis(paraquat-*p*-phenylene) [**CBPQT**], tetralactam macrocycle, amino linked macrocycle, arylene-ethynylene macrocycle and aza-bridged bis(phenanthroline) macrocycle also hold unlimited potential because of their unique design and applications in areas like sensing, water vapor sorption, and catalysis (Fig. 45).[111,333-336] Heterocyclic framework materials endow this area with unimaginable possibilities.

Several nontypical macrocycle-based MOFs have been explored due to their interesting properties. Their applications cover photo-catalysis, cargo delivery, and mechanically interlocked molecules.[333,334, 337] These studies are summarized below.

8.1. Macrocyclic hexamine-based MOFs

8.1.1. Photo-catalysis

It is well known that nanoscale confined spaces with clear functions have great potential of applications in controlling the efficiency and selectivity of catalytic reactions.[338-341] Shionoya's group reported the formation of intramolecular [2+2] cycloadduct of 1,6-diene under light irradiation.[337] Their results showed that the photo-induced olefin migration occurred first in porous crystalline metal-macrocyclic frameworks (MMFs) and inhibited the occurrence of [2+2] cycloaddition in confined spaces. Based on the calculations of UV-vis diffuse reflection spectroscopy and SCXRD, they proposed the reaction mechanism that photo-induced chemical bond dissociation led to olefin migration.[337] Their work poses a high potential for metal-catalyzed reactions like bond activation and cross-coupling in confined space of MMFs.

8.2. Tetralactam macrocycle-based MOFs

8.2.1. Cargo delivery

Berna's research group prepared a photosensitive MOF (**UMU-MOF-1**) using tetralactam macrocycle-based [2]rotaxanes (**UMU-1**) as the ligands and Cu ions as metal nodes (Fig. 46). They prepared the interlocked ligands by a hydrogen bonding guided method. SCXRD analysis of **UMU-MOF-1** showed that this MOF formed a stacked two-dimensional rhomboid grid structure, forming channels decorated by interlocked alkenyl axles. **UMU-MOF-1** crystallizes in a monoclinic *P*21/*n* space group with the structural formula of $[Cu_2(\mathbf{UMU\text{-}1})_2(H_2O)_2(DMF)_2]$. The topology is a non-interpenetrated **sql** network with Cu (II) paddle wheel clusters at the vertices connected by interlocked ligands and two coordinated water molecules in longitudinal positions. The dimensions of each grid are 20.7 × 20.7 Å^2. These metal grids are stacked into corrugated layers. Interestingly, this special arrangement between the layers forms channels along the *a*-axis, and it is estimated that the solvent accessible volume of **UMU-MOF-1** can reach 20% of the total volume. Using the deuterium-labeled MOF, they demonstrated that the geometry of the axles of interlocked structural units has a high strength due to the multiple non-covalent interactions between the various components. In addition, they demonstrated the potential of **UMU-MOF-1** as a molecular dose container by measuring the diffusion and photo-release properties of *p*-benzoquinone in different solvents and at different temperatures. Their work provides a new strategy for preparing novel rotaxane-containing crystalline framework materials.[342]

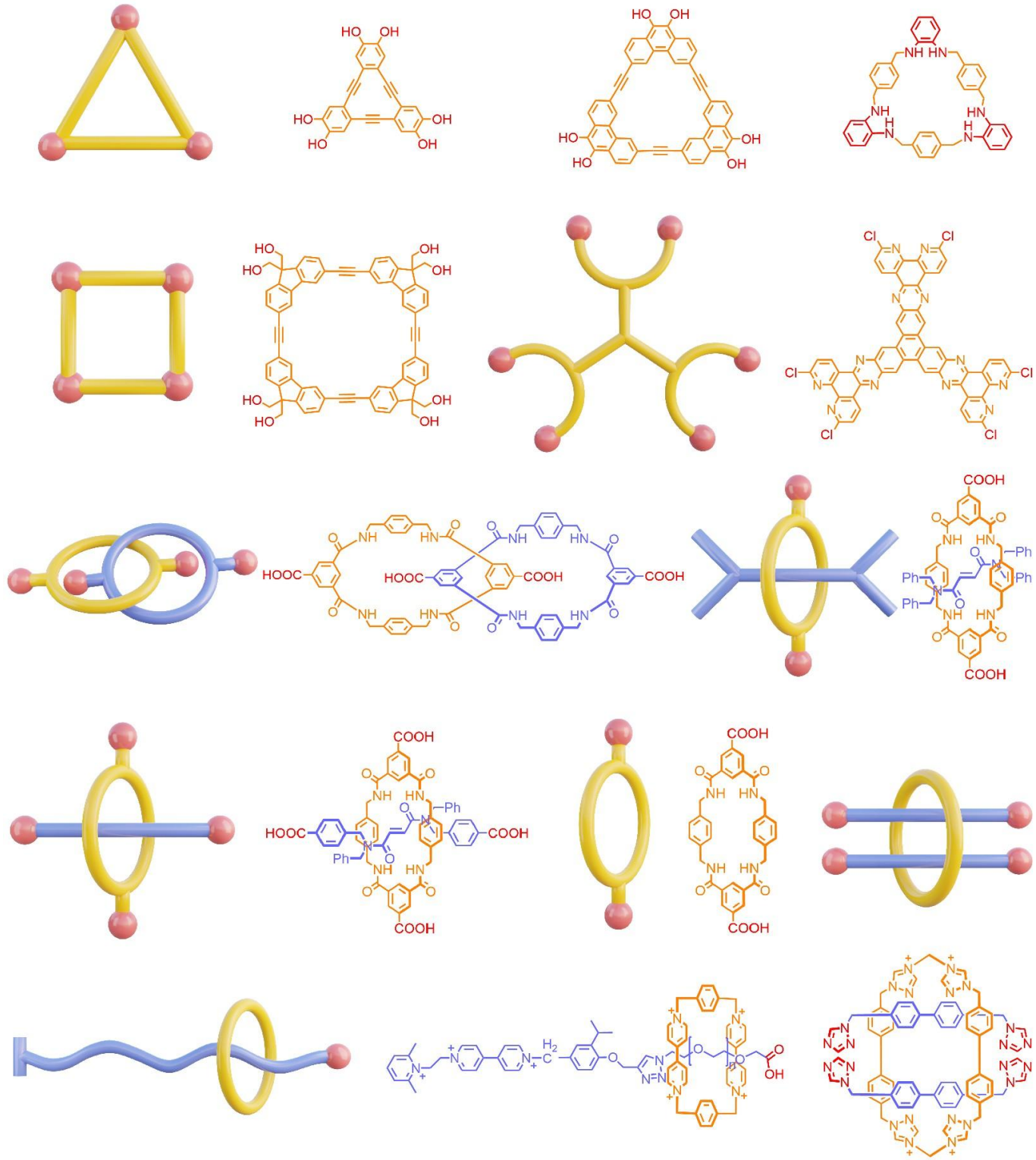

Fig. 45 Cartoon representations and chemical structures of other macrocycle-incorporated components involved in this review for preparing crystalline framework materials.

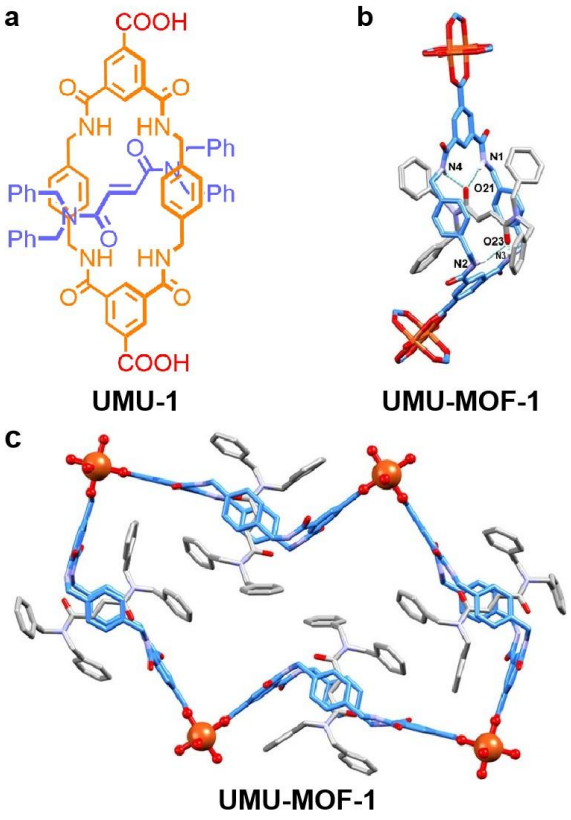

Fig. 46 (a) Chemical structure of **UMU-1**. (b and c) Single crystal structures of **UMU-MOF-1**. Here the organic struts are white, tetralactam macrocycles are light blue, O atoms are red, Cu clusters are brown, and H atoms are omitted for clarity. Reproduced from ref. 342 with permission from American Chemical Society, copyright 2020.[342]

The Berna group further prepared a more stable MOF (**UMU-MOF-2**) using a two-carboxyl functionalized flexible tetralactam macrocycle (**UMU-2**) as the organic ligand (Fig. 47). This MOF crystallizes in the *C*2/*m* space group of the monoclinic system with the molecular formula of $[Cu_2(\textbf{UMU-2})_2(H_2O)_2]\cdot nH_2O$, forms non-interpenetrated channels in the structure, and has a 46% solvent accessible volume. The crystal structure shows that this one-dimensional periodic MOF has curving macrocyclic ligands, which are connected to Cu paddle-wheel clusters by carboxylic groups. Each Cu cluster is coordinated with four **UMU-2** ligands, with two water molecules participating in the coordination at its axial position. The size of the channel formed between the two Cu clusters and the two **UMU-2** ligands is 19.47 Å × 10.96 Å. Interestingly, they have previously reported that in **UMU-MOF-1**, the presence of interlocked structures within tetralactam macrocycle cavities prevented the formation of 1D polymers, whereas in **UMU-MOF-2**, the overall structure would have better flexibility and larger pore size due to the absence of interlocked structures. This may be due to the larger conformational space of non-interlocked **UMU-2**, which require less space compared to **UMU-1** with the same macrocyclic structure. Unlike **UMU-MOF-1**, the absence of interlocked components in **UMU-MOF-2** results in a decrease in structure size, an increase in pore size and an increase in guest complexing ability. They studied the complexation of fullerene C_{60} in the MOF pores and calculated that C_{60} occupied 98% of the cavities in the adaptive pores. Using this MOF as the host, fullerenes of different sizes can be selectively complexed, for example, C_{60} can be selectively complexed from a mixture of C_{60} and C_{70}. This work provides a viable case of tetralactam macrocycle-based MOFs for cargo delivery.[343]

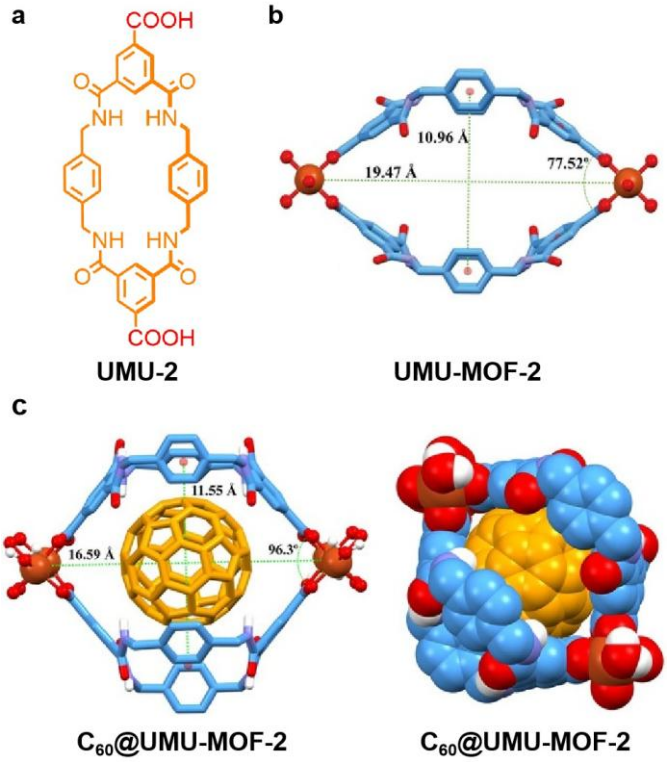

Fig. 47 (a) Chemical structure of **UMU-2**. (b) Single crystal structure of the structural unit of **UMU-MOF-2**. (c) Calculated structures of C_{60}**@UMU-MOF-1** in ball and stick form and spacefilling form. Here tetralactam macrocycles are light blue, O atoms are red, Cu clusters are brown, C_{60} molecules are orange, and H atoms on N and O atoms are white while the others are omitted for clarity.[343]

8.2.2. Mechanically interlocked molecules

The Berna group further reported the preparation of Co (II)- and Cu (II)-MOFs (**UMU-MOF-3** and **UMU-MOF-4**) using tetraclactam [2]rotaxane (**UMU-3**) as ligands (Fig.48). The interlocked ligands are functionalized with carboxylic groups. They successfully resolved the structure of the two MOFs using SCXRD. **UMU-MOF-3** crystallizes in a *C*2/*c* space group of the monoclinic system. The repeating structural unit shows that **UMU-3** is connected to four symmetrically related Cu paddlewheel clusters by four carboxylic groups. This structure has a periodic **sql** topology. **UMU-MOF-4** crystallizes in a *Pnma* space group of the orthorhombic system. The solid structure of **UMU-MOF-3** indicates that it has an internal channel structure, and the solvent within it can approach 28.9% of the total

volume (2179.0 Å^3). This value is 2184.0 Å^3 in **UMU-MOF-4** (27.5% of the total volume), and channels can also be formed within it. The CO_2 adsorption/desorption experiments showed that the BET surface area of **UMU-MOF-4** (334 m^2/g) was higher than that of **UMU-MOF-3** (296 m^2/g), although the pore volume was similar. Similarly, **UMU-MOF-4** also has the spatial topology of **sql**. The structures of these two MOFs exhibited different grid clustering patterns and great rigidity. Their results show that rigid MOFs with permanent pores can also be prepared using dynamic ligands.[344]

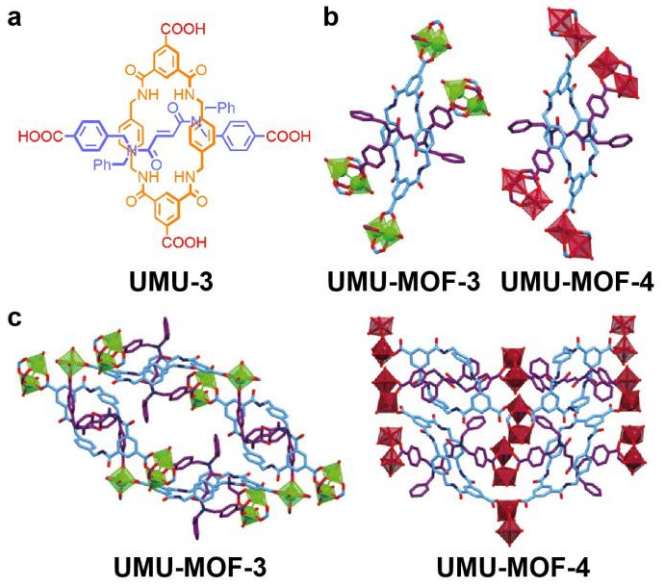

Fig. 48 (a) Chemical structure of **UMU-3**. (b and c) Single crystal structures of **UMU-MOF-3** and **UMU-MOF-4**. Here the organic struts are purple, tetralactam macrocycles are light blue, Cu clusters are green, Co clusters are red, and H atoms are omitted for clarity.[344]

The mechanical properties of materials consisting of interlocked structures have been a long-standing problem in materials science since the 1970s when polycatenanes and polyrotaxanes were first reported.[180,345] The Aida and Sato groups reported a tetraclactam [2]catenane-based MOF (denoted as **^{CTN}MOF**) from **H_4^{CTN}L** (Fig. 49).[334] This MOF consists of a tetragonal lattice and changes its geometry during the adsorption, exchange and release of guest molecules, and even its structure changes with temperature (at low temperatures). The results of SCXRD showed that the crystal structure has a chiral space group of $P4_122$, and its structure is formulated by $[Co_2(^{CTN}L)(H_2O)_7(DMF)_4]$, indicating that the symmetry was broken during the crystallization process. Therefore, the **^{CTN}L** units in **^{CTN}MOF** are arranged in a chiral topology, in a spiral arrangement along the quadruple helix axis. They measured a Young's modulus of 1.77 ± 0.16 GPa for *N*,*N*-dimethylformamide and 1.63 ± 0.13 GPa for tetrahydrofuran of **^{CTN}MOF**, which was the lowest in the reported MOFs. They also measured the hydrostatic compression and showed that this elastic MOF deformed the most along its *c*-axis, shrinking to 5% when compressed to 0.88 GPa. The crystal structure obtained at 0.46 GPa showed that the macrocycle portion migrated during the contraction. The MOF they developed was expected to solve the difficulty of achieving high absorption and release capacity of crystalline framework materials. Finally, they also provides a reliable method for constructing catenane-incorporated MOFs, which is significantly challenging during the last thirty years.[334]

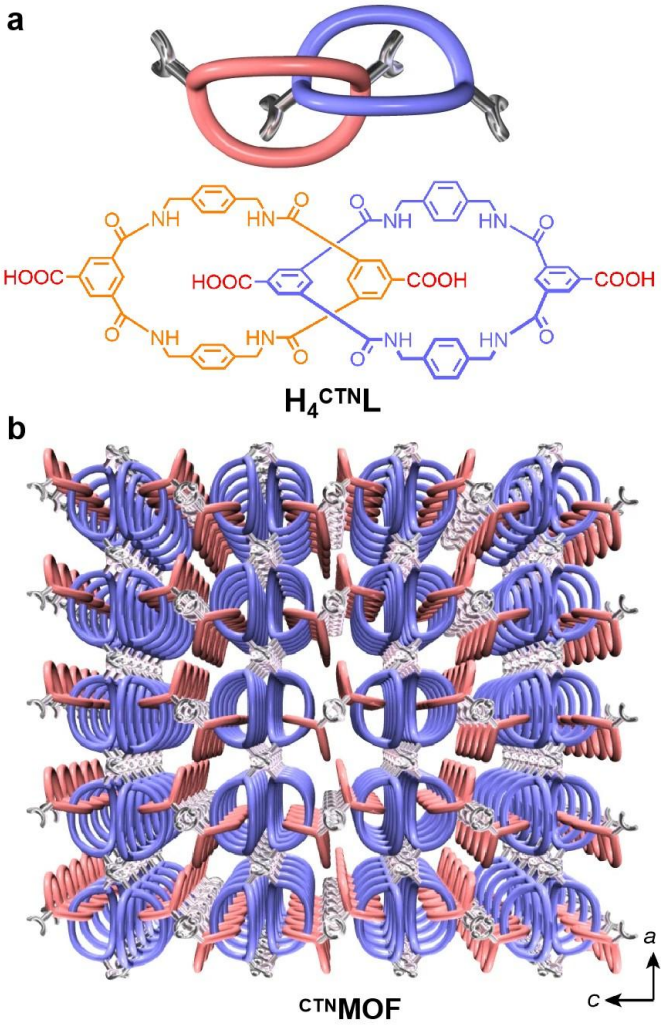

Fig. 49 (a) Cartoon representation and chemical structure of the [2]catenane-like ligand **H_4^{CTN}L**. (b) Cartoon representation of **^{CTN}MOF**. Reproduced from ref. 334 with permission from Springer Nature, copyright 2021.[334]

8.3. Cyclophane cyclobis(paraquat-*p*-phenylene) -based MOFs

8.3.1. Mechanically interlocked molecules

In addition, using the specific recognition of CEs and cyclophane cyclobis(paraquat-*p*-phenylene) (**CBPQT**), the Stoddart and Yaghi groups reported an example of the introduction of catenane structures into MOFs.[148] They introduced a [2]catenane into the MOF system (denoted as

MOF-1030), which formed an ordered three-dimensional entity. In **MOF-1030**, each Cu (I) coordinates to two carboxylate groups from the struts with a typical **nbo** network topology. The [2]catenane components in **MOF-1030** shows *S* and *R* chiralities. This orderly distributed structure has the potential to achieve mechanical motion and chiral property in crystalline framework materials.[148]

By using a post-synthetic modification strategy, Stoddart's group further introduced **CBPQT^{4+}**-containing bistable mechanically interlocked structures into the stable Zr-based MOF **NU-1000** (Fig. 50).[346] A [2]catenane (**FC^{4+}**) was modified to the interior of **NU-1000** *via* the SALE strategy, which consists of octahedral Zr_6 nodes and organic pyrene ligands. Each metal cluster is composed of eight bridging ligands, while the other coordinative sites are occupied by the OH and OH_2 sites. They tried to realize the application of the **FC^{4+}**-incorporated MOF. Each repeated hexagonal channel of **NU-1000** can bind two bistable [2]catenane units and form **NU-1000-FC^{n+}**. Solid state UV-vis-near infrared (NIR) spectroscopy and cyclic voltammetry experiments showed that the reversible redox properties of bistable [2]catenanes could be preserved in **NU-1000-FC^{n+}**. This work shows that bistable mechanically interlocked structures can exhibit excellent dynamics within the pores of MOFs, and is expected to introduce molecular electronics into framework materials.[346]

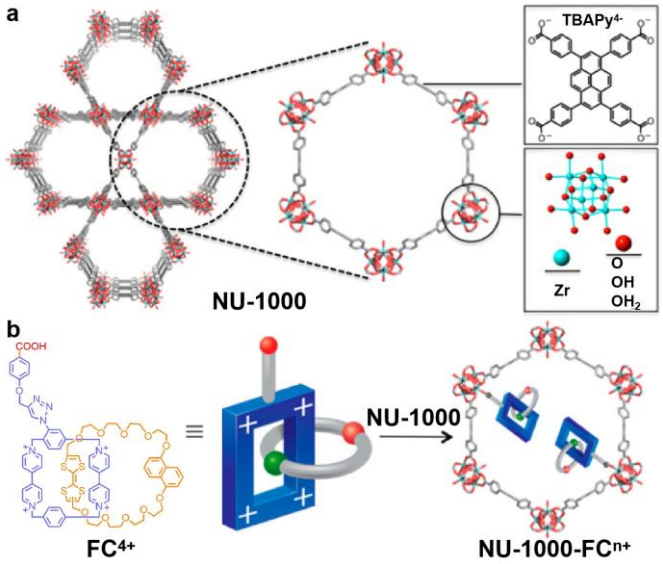

Fig. 50 (a) Crystal structure of **NU-1000**. C atoms are grey, O atoms are red, Zr atoms are blue, and H atoms are omitted for clarity. (b) Schematic illustration of the bistable [2]catenane **FC^{4+}**-incorporated MOF **NU-1000-FC^{n+}**. Reproduced from ref. 346 with permission from American Chemical Society, copyright 2016.[346]

In the last century, adsorption in equilibrium systems has been widely studied by scientists. The common adsorption mechanisms are physical adsorption and chemical adsorption.[347] Stoddart's research group proposed and reported a new adsorption mechanism, mechanical adsorption.[347] They used molecular pump grafted MOFs to enable repeated adsorption of **CBPQT^{4+}** from solution under redox control. **CBPQT^{4+}** contain redox switching bipyridine units, and the adsorbed **CBPQT^{4+}** under reduction conditions can be separated from the solution and transferred to the collecting chain in a precise manner *via* a molecular pump. This redox controlled active adsorption transferred the macrocycles from a solution to a higher concentration solution, thus repeated mechanical adsorption can be achieved. They chose a MOF substrate composed of Zr-BTB as the carrier of the grafted molecular pumps.[347] Due to the mechanical bonds formed between the adsorbent and the adsorbate, the active adsorption mode they reported can be achieved on the surface of the MOFs grafted by the molecular pumps. The adsorbate can be transported from one compartment to another. The introduction of mechanical adsorption expands the scope and potential of adsorption phenomena and provides a revolutionary method for controlling interfacial chemical reactions.[347]

Fu's group reported another variational **CBPQT-1** system. According to the SCXRD analysis, in the asymmetric structure unit, **CBPQT-MOF-1** consists of a [Cu(**CBPQT-1**)$_2$]$^{2+}$ fragment and a free [(CH_2 **CBPQT-1**)$_2$]$^{4+}$ fragment (Fig. 51). Each Cu node is in a six-coordination environment, coordinated by four N atoms from four organic ligands, forming a Z-shaped structure. The two dimensional structure is an infinitely interpenetrated polyrotaxane structure. The layers are arranged in an overlapped geometry, with a distance of 14.3 Å between adjacent layers. Their work proposes a novel strategy for the synthesis of macrocyclic MOFs with entanglement and two-dimensional layered structures with high proton conductivity and photocatalytic activity by an ion-thermal method.[348]

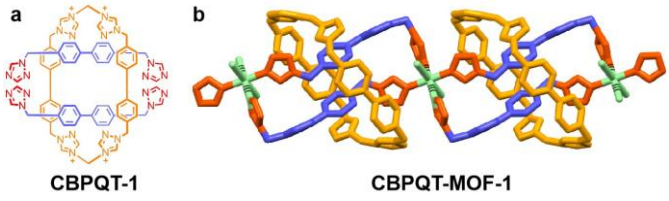

Fig. 51 (a) Chemical structure of **CBPQT-1**. (b) Single crystal structure of **CBPQT-MOF-1**. Macrocyclic units are orange, organic struts are blue, coordinative groups are red, and Cu nodes are green. Reproduced from ref. 348 with permission from American Chemical Society, copyright 2019.[348]

The nontypical macrocycle components also have their potential in constructing COFs. They can be applied in gas storage, Li^+ conduction and electrical device.[111, 335, 336, 349]

8.4. D_4-symmetric macrocycle-based COFs

8.4.1. Gas adsorption and Li^+ conduction

By forming spiroborate ester bonds, Zhang's group prepared two ionic COFs (denoted as **ICOF-1** and **ICOF-2**) containing boron anion centers and tunable cations.[336] They tried soaking **ICOF-1** in a 1 M LiOH solution to exchange cations and convert **ICOF-1** into the more crystalline **ICOF-2**. However, compared to **ICOF-1**, the crystallinity was not improved. Due to the limited quality of the crystal data, they were unable to simulate the crystal stacking structure. They further tested the adsorption behavior of **ICOF-1** and **ICOF-2** of N_2 at 77 K. **ICOF-1** exhibited a typical type I adsorption behavior and rapidly adsorbed N_2 at low pressure (P/P_0 < 0.01), indicating its permanent microporous properties. The adsorption isotherms of **ICOF-2** were the intermediate lines of type I and type IV, with obvious hysteria under low pressure. The specific surface areas of **ICOF-1** and **ICOF-2** were calculated to be 1022 and 1259 $m^2\ g^{-1}$, respectively. The NLDFT pore size distribution analysis showed that **ICOF-1** had a 1.1 nm pore, while **ICOF-2** had a 2.2 nm pore. **ICOF-2** could adsorb H_2 (up to 3.11 wt%, 77 K, 1 bar) and CH_4 (up to 4.62 wt%, 273 K, 1 bar). The material also showed excellent stability, maintaining its crystallinity after soaking in water or alkaline solutions for two days. The presence of ion centers in ICOFs gave it a room temperature Li^+ conductivity of 3.05 x 10^{-5} S cm^{-1} and an average Li^+ transfer value of 0.80 ± 0.02. Thus, their method provides a simple pathway to obtain highly stable COFs with ion recognition sites, which can be used to adsorb H_2 and CH_4, as well as solid electrolytes for next-generation lithium batteries.[336]

8.5. Arylene-ethynylene macrocycle-based COFs

8.5.1. Gas storage

Zhang's group also prepared two two-dimensional COFs (**AEM-COF-1** and **AEM-COF-2**) composed of arylene-ethynylene macrocycles.[349] PXRD patterns confirmed the long-range molecular order of the two COFs. They also calculated the PXRD patterns of the structural models and compared them with the experimental results. They found that the simulated **AEM-COF-1** and **AEM-COF-2** patterns were in good agreement with the experimental results. **AEM-COF-1** and **AEM-COF-2** packed in overlapped layers to form one-dimensional mesopores with theoretical diameters of 34 Å and 39 Å, respectively. They studied the porosity of **AEM-COF-1** and **AEM-COF-2** by N_2 adsorption/desorption isotherms at 77 K, and the BET surface areas of **AEM-COF-1** (1445 $m^2\ g^{-1}$) and **AEM-COF-2** (1489 $m^2\ g^{-1}$) were similar. The calculated structures of NLDFT showed that **AEM-COF-1** and **AEM-COF-2** have pore size distributions (PSD) of 3.2 nm and 3.8 nm, respectively. These structures were consistent with the theoretical pore sizes of **AEM-COF-1** and **AEM-COF-2** (3.4 nm and 3.9 nm, respectively). Accordingly, they observed pore volumes of 1.15 $cm^3\ g^{-1}$ (**AEM-COF-1**) and 1.38 $cm^3\ g^{-1}$ (**AEM-COF-2**), respectively. Their study found that the use of arylene-ethynylene macrocycles could also expand the aperture of COFs. They used macrocycles with different sizes, shapes and cavities, and constructed COFs using the macrocycle-framework strategy to expand the structure diversity of COFs with hierarchal pore structures in the frameworks.[349]

8.6. Aza-bridged bis(phenanthroline) macrocycle-based COFs

8.6.1. Conductive COFs

At present, COFs are still not suitable for energy storage and electrochemical catalysis, because COFs are generally insulators.[350-354] Therefore, the construction of chemically stable conductive COFs remains challenging. Despite this, Baek's group reported the preparation of 2D aza-bridged bis(phenanthroline) macrocyclic COF (denoted as **ABBPM-COF**) by heat-induced poly-condensation of tri-chelate monomers and ammonia in the solvent-free and catalyst-free conditions (Fig. 52).[111] They confirmed the structure of **ABBPM-COF** using SCXRD analysis and structure simulation. The experimental PXRD pattern matched well with the simulated PXRD pattern of the structure in an ABC packing mode. Therefore, the guest molecules in the hexagonal holes block the connections between the triphenyl nodes, and thus the planar structure was maintained. The theoretical BET specific surface area of the **ABBPM-COF** model structure with the ABC packing pattern containing guest molecules was 893 $m^2\ g^{-1}$. The pore size (0.34 nm) of the ABC packing model of **ABBPM-COF** containing guest molecules was beyond the kinetic diameter (0.36 nm) of N_2. Therefore, N_2 cannot enter the pores, and the experimental BET surface areas calculated by N_2 adsorption was only 8.7 $m^2\ g^{-1}$, which was not consistent with the theoretical calculation value. Considering that the pore size (0.34 nm) of the **ABBM-COF** model containing guest molecules was larger than the kinetic diameter of CO_2 (0.33 nm), they conducted adsorption experiments for CO_2 at low pressures of 273 and 298 K. At 273 K and 1 bar, the CO_2 adsorption capacity of **ABBPM-COF** was as high as 23.3 $cm^3\ g^{-1}$. They further found that **ABBPM-COF** had good chemical stability in acid-base solutions. Interestingly, the conductivity measurements showed that the originally insulated **ABBPM-COF** could become a semiconductor with a 2.6×10^{-4} S/cm electrical conductivity after being exposed to iodine vapor. This study proves that **ABBPM-COF** has potential in electrochemical applications and the barriers to conductive COFs are beginning to be overcome.[111]

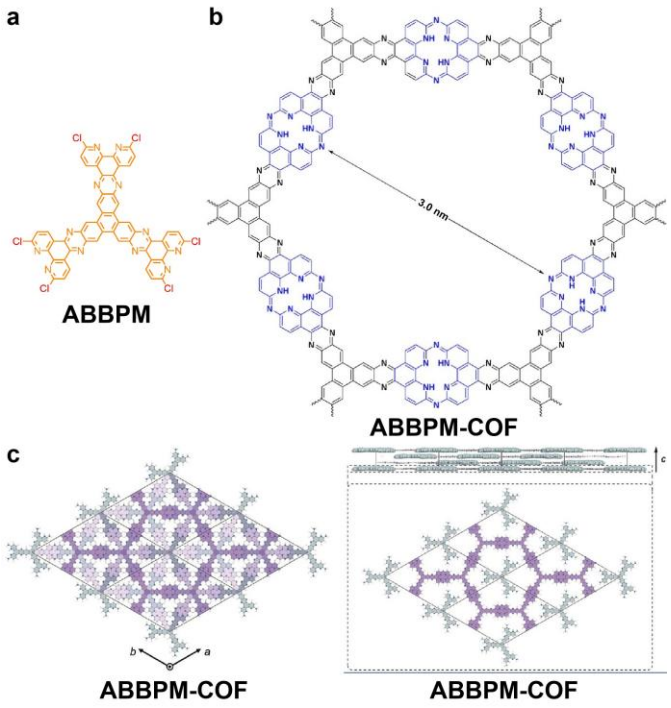

Fig. 52 (a) Chemical structure of **ABBPM**. (b) Chemical structure of **ABBPM-COF**. (c) Simulated structure of **ABBPM-COF** with an ABC packing mode.[111]

9. Conclusions

In our review, we delve into macrocycle-based crystalline porous framework materials, explore their development history, address current challenges, and examine future opportunities. Additionally, we also discuss the techniques for accurately sizing macrocycles within these frameworks, enhancing their molecular recognition capabilities, and increasing their potential for future commercial applications. Challenges faced by these materials and potential workarounds to overcome these issues are also discussed. For example, the design and synthesis of macrocycle-incorporated frameworks commonly need multiple steps. Thus, simplifying the synthetic route to the final products is the key to solve these problems. We intend for this review to be conducive for guiding the future directions of this field and help new scientists thoroughly understand this area. Furthermore, we hope to promote the development of functional crystalline porous framework materials which can solve energy and environmental problems globally. Three aspects stimulating the development of this area in the fields of chemistry, engineering, and commercialization are discussed below.

9.1. Chemistry

Various synthetic macrocycles can be incorporated into crystalline porous framework materials, depending on the sizes of binding sites for the guest species. Macrocycles have the capability for specific recognition and can be customized into frameworks that satisfy specific design requirements. Finally advances in macrocycle chemistry will contribute to the development of a new generation of functional crystalline porous frameworks.

Different from traditional structural units for preparing MOFs and COFs, macrocyclic units for preparing MOFs and COFs are usually not commercially available. These motifs need rational design and multiple synthetic steps. By rational design, the macrocyclic units could be modified to MOFs/COFs in the forms of side chain, main backbone, pseudorotaxane, rotaxane and catenane units. The typical macrocycles for preparing macrocycle-based side chains and main backbones in MOFs/COFs are crown ethers, cyclodextrins, calixarenes and pillararenes. In these cases, the carboxyl, hydroxyl, pyridine, aldehyde and amino groups could be modified to these macrocyclic units *via* reactions such as Suzuki coupling reaction and Sonogashira-Hagihara coupling reaction. The macrocyclic moieties could also be incorporated into MOFs/COFs in the forms of rotaxane and catenane units by host–guest recognition. The rotaxane and catenane units could be established in MOFs/COFs in two approaches: 1) preparing pre-organized rotaxane and catenane units and then using them to construct MOFs/COFs; 2) constructing the frameworks first and then using them to incorporate macrocyclic units, typically suitable for pseudorotaxane units. Typically, with the macrocycle-containing motifs in hand, the crystalline frameworks could be prepared by reacting with various metal nodes (for MOFs) or organic components (for COFs). It is undeniable that the synthetic steps of macrocycles are unavoidable and might be challenging for material scientists. One feasible approach to overcome this challenge is to collaborate with supramolecular chemists who are able to expertly prepare the macrocyclic motifs. Moreover, one thing that worth noting is that the applications of macrocycle-based crystalline porous frameworks should be better focused on terse but forceful aspects such as the adsorption and separation of fine chemicals and avoid to apply them on bulk chemicals. Since it is significantly challenging to do volume production for these materials, which would be uncompetitive to commercial-available MOFs/COFs in these aspects.

9.2. Engineering

With chemical limitations aside, it is essential to develop shaping techniques such as 3D printing to integrate powders of crystalline porous framework materials into viable devices. In order to process these materials, thermal, mechanical, and chemical stability need to be considered. Therefore, we encourage the development of processing strategies that take advantage of the host–guest interactions between macrocycle-based building blocks of crystalline porous frameworks and the functional monomers of binder polymers.

9.3. Commercialization

Future directions for commercialization should be targeted to specific applications. Most promising applications discussed within this review include efficient chiral separation, structure determination of molecules, and targeted drug delivery. While cost is an important factor, finding the suitable applications of the developed materials is more important. Some of the macrocycle-based crystalline frameworks have been applied for patents due to their potential commercial applications.[355-362] To date the commercialization of crown ethers and cyclodextrins have been realized, thus making the preparation of their crystalline frameworks relative convenient. However, the preparation of cucurbiturils, calixarenes and pillararenes is still under development, reducing the cost of these macrocycles is of great significance for preparing macrocycle-based MOFs and COFs. Moreover, the commercialization of CD-MOFs has been realized on account of their simple synthesis and easy-acquired raw materials. The commercialization of other mentioned macrocycle-based crystalline frameworks still needs to be further studied.

Author contributions

Y.W. wrote the review. Y.W., M.T., M.L.B., Z.C. and F.H. discussed and revised the review.

Conflicts of interest

The authors declare no competing interest.

Acknowledgements

Y.W. is supported by the National Postdoctoral Program for Innovative Talents (BX20240316) and China Postdoctoral Science Foundation for General Program (2024M762793). M.L.B. would like to acknowledge Vinayak P. Dravid and Omar K. Farha for their advising support and M.L.B. is supported by the Department of Energy under grant number DOE-BES DE-SC0022332. Z.C. gratefully acknowledges support from the National Natural Science Foundation of China (grant No. 22471237, 22201247). F.H. is supported by the National Key Research and Development Program of China (2021YFA0910100), the National Natural Science Foundation of China (22035006, 22320102001, 22350007), the Starry Night Science Fund of Zhejiang University Shanghai Institute for Advanced Study (SN-ZJU-SIAS-006), and the Leading Innovation Team grant from the Department of Science and Technology of Zhejiang Province (2022R01005). We thank the staff at BL17B1 beamline of the National Facility for Protein Science in Shanghai (NFPS), Shanghai Advanced Research Institute, CAS, for providing technical support in X-ray diffraction data collection and analysis. We thank the Chemistry Instrumentation Centre of Zhejiang University for the technical support.

Notes and references

1. C. Qian, L.-L. Feng, W.-L. Teo, J.-W. Liu, W. Zhou, D.-D. Wang and Y.-L. Zhao, *Nat. Rev. Chem.*, 2022, **6**, 881-898.
2. X. Meng, H. Wang, S. Song and H. Zhang, *Chem. Soc. Rev.*, 2017, **46**, 464-480.
3. S. Y. Ding and W. Wang, *Chem. Soc. Rev.*, 2013, **42**, 548-568.
4. L. Kong, M. Zhong, W. Shuang, Y. Xu and X. Bu, *Chem. Soc. Rev.*, 2020, **49**, 2378-2407.
5. Z. Hu, B. J. Deibert and J. Li, *Chem. Soc. Rev.*, 2014, **43**, 5815-5840.
6. N. Hanikel, X. Pei, S. Chheda, H. Lyu, W. Jeong, J. Sauer, L. Gagliardi and O. M. Yaghi, *Science*, 2021, **374**, 454.
7. J. Jiang and O. M. Yaghi, *Chem. Rev.*, 2015, **115**, 6966-6997.
8. C. A. Trickett, A. Helal, B. A. Al-Maythalony, Z. H. Yamani, K. E. Cordova and O. M. Yaghi, *Nat. Rev. Mater.*, 2017, **2**, 17045.
9. C. S. Diercks and O. M. Yaghi, *Science*, 2017, **355**, aal1585.
10. S. Lin, C. S. Diercks, Y. B. Zhang, N. Kornienko, E. M. Nichols, Y. B. Zhao, A. R. Paris, D. Kim, P. Yang, O. M. Yaghi and C. J. Chang, *Science*, 2015, **349**, 1208-1213.
11. L. Shi, K. O. Kirlikovali, Z. J. Chen and O. K. Farha, *Chem*, 2024, **10**, 484-503.
12. L. Shi, Z. Xiong, H. Wang, H. Cao and Z. Chen, *Chem*, 2024, **10**, 10.
13. H. Furukawa, K. E. Cordova, M. O'Keeffe and O. M. Yaghi, *Science*, 2013, **341**, 974.
14. S. Horike and S. Kitagawa, *Nat. Mater.*, 2022, **21**, 983-985.
15. Z. Chen, H. Jiang, M. Li, M. O'Keeffe and M. Eddaoudi, *Chem. Rev.*, 2020, **120**, 8039-8065.
16. C. Gu, N. Hosono, J. J. Zheng, Y. Sato, S. Kusaka, S. Sakaki and S. Kitagawa, *Science*, 2019, **363**, 387.
17. V. I. Nikolayenko, D. C. Castell, D. Sensharma, M. Shivanna, L. Loots, K. A. Forrest, C. J. Solanilla-Salinas, K. I. Otake, S. Kitagawa, L. J. Barbour, B. Space and M. J. Zaworotko, *Nat. Chem.*, 2023, **15**, 542.
18. M. Shivanna, K. I. Otake, B. Q. Song, L. M. van Wyk, Q. Y. Yang, N. Kumar, W. K. Feldmann, T. Pham, S. Suepaul, B. Space, L. J. Barbour, S. Kitagawa and M. J. Zaworotko, *Angew. Chem. Int. Ed.*, 2021, **60**, 20383-20390.
19. H. Li, X. Kong, S. Han, J. Pang, T. He, G. Wang and X. Bu, *Chem. Soc. Rev.*, 2024, **53**, 5626-5676.
20. W. Wang, H. Yang, Y. Chen, X. Bu and P. Feng, *J. Am. Chem. Soc.*, 2023, **145**, 17551-17556.
21. K. Hou, J. Börgel, H. Jiang, D. J. SantaLucia, H. Kwon, H. Zhuang, K. Chakarawet, R. C. Rohde, J. W. Taylor, C. Dun, M. V. Paley, A. B. Turkiewicz, J. G. Park, H. Mao, Z. Zhu, E. E. Alp, J. Zhao, M. Hu, B. Lavina, S. Peredkov, X. Lv, J. Oktawiec, K. R. Meihaus, D. A. Pantazis, M. Vandone, V. Colombo, E. Bill, J. J. Urban, R. D. Britt, F. Grandjean, G. J. Long, S. DeBeer, F. Neese, J. A. Reimer and J. R. Long, *Science*, 2023, **382**, 547-553.
22. B. E. R. Snyder, A. B. Turkiewicz, H. Furukawa, M. V. Paley, E. O. Velasquez, M. N. Dods and J. R. Long, *Nature*, 2023, **613**, 287.
23. K. C. Park, P. Kittikhunnatham, J. Lim, G. C. Thaggard, Y. Liu, C. R. Martin, G. A. Leith, D. J. Toler, A. T. Ta, N. Birkner, I. Lehman-Andino, A. Hernandez-Jimenez, G. Morrison, J. W. Amoroso, H. C. zur Loye, D. P. DiPrete, M. D. Smith, K. S. Brinkman, S. R. Phillpot and N. B. Shustova, *Angew. Chem. Int. Ed.*, 2023, **62**, e202216349.
24. K. C. Park, C. R. Martin, G. A. Leith, G. C. Thaggard, G. R. Wilson, B. J. Yarbrough, B. K. M. Kankanamalage, P. Kittikhunnatham, A. Mathur, I. Jatoi, M. A. Manzi, J. Lim, I. Lehman-Andino, A. Hernandez-Jimenez, J. W. Amoroso, D. P. DiPrete, Y. Liu, J. Schaeperkoetter, S. T. T. Misture, S. R. Phillpot, S. Hu, Y. Li, A.

Leydier, V. Proust, A. Grandjean, M. D. Smith and N. B. Shustova, *J. Am. Chem. Soc.*, 2022, **144**, 16139-16149.
25. L. Shi, Y. L. Zhong, H. H. Cao, H. Wang, Z. Y. Xiong, K. Wang, H. Y. Shen and Z. J. Chen, *Nat. Synth.*, 2024, **3**, 1560-1566.
26. Q. Zhu and Q. Xu, *Chem. Soc. Rev.*, 2014, **43**, 5468-5512.
27. W. P. Lustig, S. Mukherjee, N. D. Rudd, A. V. Desai, J. Li and S. K. Ghosh, *Chem. Soc. Rev.*, 2017, **46**, 3242-3285.
28. S. Horike, S. Shimomura and S. Kitagawa, *Nat. Chem.*, 2009, **1**, 695-704.
29. X. Feng, X. Ding and D. Jiang, *Chem. Soc. Rev.*, 2012, **41**, 6010-6022.
30. P. J. Waller, F. Gándara and O. M. Yaghi, *Acc. Chem. Res.*, 2015, **48**, 3053-3063.
31. A. Schneemann, V. Bon, I. Schwedler, I. Senkovska, S. Kaskel and R. A. Fischer, *Chem. Soc. Rev.*, 2014, **43**, 6062-6096.
32. N. Hanikel, M. S. Prévot and O. M. Yaghi, *Nat. Nanotechnol.*, 2020, **15**, 348-355.
33. A. Schoedel, Z. Ji and O. M. Yaghi, *Nat. Energy*, 2016, **1**, 16034 .
34. M. Li, D. Li, M. O'Keeffe and O. M. Yaghi, *Chem. Rev.*, 2014, **114**, 1343-1370.
35. A. Schoedel, M. Li, D. Li, M. O'Keeffe and O. M. Yaghi, *Chem. Rev.*, 2016, **116**, 12466-12535.
36. L. Shi, Z. N. Yang, F. R. Sha and Z. J. Chen, *Sci. China. Chem.*, 2023, **66**, 3383-3397.
37. Z. Chen, P. H. Li, R. Anderson, X. Wang, X. Zhang, L. Robison, L. R. Redfern, S. Moribe, T. Islamoglu, D. A. Gómez-Gualdrón, T. Yildirim, J. F. Stoddart and O. K. Farha, *Science*, 2020, **368**, 297.
38. O. M. Yaghi, M. O'Keeffe, N. W. Ockwig, H. K. Chae, M. Eddaoudi and J. Kim, *Nature*, 2003, **423**, 705-714.
39. V. Nagarajan, S. Kizhaeral, M. Subramanian, S. Rajendran and J. Ranjan, *ACS Food Sci. Technol.*, 2021, **1**, 1936-1944.
40. L. Huang, L. Yu, B. Li, B. Li, H. Wang and J. Li, *ACS Mater. Lett.*, 2022, **4**, 1053-1057.
41. S. Li, X. Hu, S. Chen, X. Wang, H. Shang, Y. Zhou, J. Dai, L. Xiao, W. Qin and Y. Liu, *Food Hydrocolloid.*, 2023, **136**, 108294.
42. M. P. Suh, H. J. Park, T. K. Prasad and D. W. Lim, *Chem. Rev.*, 2012, **112**, 782-835.
43. T. A. Makal, J. R. Li, W. G. Lu and H. C. Zhou, *Chem. Soc. Rev.*, 2012, **41**, 7761-7779.
44. J. Arnó, O. K. Farha, W. Morris, P. W. Siu, G. M. Tom, M. H. Weston and P. E. Fuller, *MRS Adv.*, 2022, **7**, 1426-1430.
45. J. Arnó, O. K. Farha, W. Morris, P. W. Siu, G. M. Tom, M. H. Weston and P. E. Fuller, Wurzburg, GERMANY, 2018.
46. J. L. C. Rowsell and O. M. Yaghi, *Micropor. Mesopor. Mat.*, 2004, **73**, 3-14.
47. L. J. Murray, M. Dinca and J. R. Long, *Chem. Soc. Rev.*, 2009, **38**, 1294-1314.
48. T. Islamoglu, Z. J. Chen, M. C. Wasson, C. T. Buru, K. O. Kirlikovali, U. Afrin, M. R. Mian and O. K. Farha, *Chem. Rev.*, 2020, **120**, 8130-8160.
49. S. Bose, D. Sengupta, C. D. Malliakas, K. B. Idrees, H. M. Xie, X. L. Wang, M. L. Barsoum, N. M. Barker, V. P. Dravid, T. Islamoglu and O. K. Farha, *Chem. Sci.*, 2023, **14**, 9380-9388.
50. M. L. Barsoum, J. Hofmann, H. Xie, Z. Chen, S. M. Vornholt, R. dos Reis, N. Burns, S. Kycia, K. W. Chapman, V. P. Dravid and O. K. Farha, *J. Am. Chem. Soc.*, 2024, **146**, 6557-6565.
51. T. M. McDonald, J. A. Mason, X. Q. Kong, E. D. Bloch, D. Gygi, A. Dani, V. Crocellà, F. Giordanino, S. O. Odoh, W. S. Drisdell, B. Vlaisavljevich, A. L. Dzubak, R. Poloni, S. K. Schnell, N. Planas, K. Lee, T. Pascal, L. W. F. Wan, D. Prendergast, J. B. Neaton, B. Smit, J. B. Kortright, L. Gagliardi, S. Bordiga, J. A. Reimer and J. R. Long, *Nature*, 2015, **519**, 303.
52. J. Yang, G. Yang and Z. Chen, *Chin. J. Struct. Chem.*, 2024, **43**, 100267.
53. Y. Liang, E. Li, K. Wang, Z. Guan, H. He, L. Zhang, H.-C. Zhou, F. Huang and Y. Fang, *Chem. Soc. Rev.*, 2022, **51**, 8378-8405.
54. H. Zhang, R. Zou and Y.-L. Zhao, *Coord. Chem. Rev.*, 2015, **292**, 74-90.
55. J.-R. Wu and Y.-W. Yang, *Angew. Chem. Int. Ed.*, 2021, **60**, 1690-1701.
56. Y. Song, Q. Sun, B. Aguila and S. Ma, *Adv. Sci.*, 2019, **6**, 1801410 .
57. A. G. Slater and A. I. Cooper, *Science*, 2015, **348**, 11.
58. A. D. Roberts, X. Li and H. Zhang, *Chem. Soc. Rev.*, 2014, **43**, 4341-4356.
59. R. Lin, L. Li, H. Zhou, H. Wu, C. He, S. Li, R. Krishna, J. Li, W. Zhou and B. Chen, *Nat. Mater.*, 2018, **17**, 1128.
60. X. Cui, K. Chen, H. Xing, Q. Yang, R. Krishna, Z. Bao, H. Wu, W. Zhou, X. Dong, Y. Han, B. Li, Q. Ren, M. J. Zaworotko and B. Chen, *Science*, 2016, **353**, 141-144.
61. Q. Fang, Z. Zhuang, S. Gu, R. B. Kaspar, J. Zheng, J. Wang, S. Qiu and Y. Yan, *Nat. Commun.*, 2014, **5**, 4503.
62. H. Zhu, L. Chen, B. Sun, M. Wang, H. Li, J. F. Stoddart and F. Huang, *Nat. Rev. Chem.*, 2023, **7**, 768-782.
63. M. Ding, R. Flaig, H. Jiang and O. M. Yaghi, *Chem. Soc. Rev.*, 2019, **48**, 2783-2828.
64. H. Furukawa, F. Gándara, Y. B. Zhang, J. C. Jiang, W. L. Queen, M. R. Hudson and O. M. Yaghi, *J. Am. Chem. Soc.*, 2014, **136**, 4369-4381.
65. G. Cai, P. Yan, L. Zhang, H.-C. Zhou and H.-L. Jiang, *Chem. Rev.*, 2021, **121**, 12278-12326.
66. L. Feng, K. Wang, X. Lv, T. H. Yan and H.-C. Zhou, *Natl. Sci. Rev.*, 2020, **7**, 1743-1758.
67. S. Yuan, L. Feng, K. Wang, J. Pang, M. Bosch, C. Lollar, Y. Sun, J. Qin, X. Yang, P. Zhang, Q. Wang, L. Zou, Y. Zhang, L. Zhang, Y. Fang, J. Li and H.-C. Zhou, *Adv. Mater.*, 2018, **30**, 1704303.
68. S. Yuan, L. Zou, J. Qin, J. Li, L. Huang, L. Feng, X. Wang, M. Bosch, A. Alsalme, T. Cagin and H.-C. Zhou, *Nat. Commun.*, 2017, **8**, 15356.
69. R. Lin, Y. He, P. Li, H. Wang, W. Zhou and B. Chen, *Chem. Soc. Rev.*, 2019, **48**, 1362-1389.
70. Y. He, W. Zhou, G. Qian and B. Chen, *Chem. Soc. Rev.*, 2014, **43**, 5657-5678.
71. Y. He, F. Chen, B. Li, G. Qian, W. Zhou and B. Chen, *Coord. Chem. Rev.*, 2018, **373**, 167-198.
72. L. Yang, J. Hu, M.-C. Li, M. Xu, Z.-Y. Gu, *Chem Asian J.* 2022, **17**, e202200775.
73. Z. Sun, J. Hou, L. Li and Z. Tang, *Coord. Chem. Rev.*, 2020, **425**, 213481.
74. B. Chen, S. Xiang and G. Qian, *Acc. Chem. Res.*, 2010, **43**, 1115-1124.
75. I. M. Hönicke, I. Senkovska, V. Bon, I. A. Baburin, N. Bönisch, S. Raschke, J. D. Evans and S. Kaskel, *Angew. Chem. Int. Ed.*, 2018, **57**, 13780-13783.
76. M. E. Carrington, N. Rampal, D. G. Madden, D. O'Nolan, N. P. M. Casati, G. Divitini, J. A. Martín-Illán, M. Tricarico, R. Cepitis, C. Çamur, T. Curtin, J. Silvestre-Albero, J. C. Tan, F. Zamora, S. Taraskin, K. W. Chapman and D. Fairen-Jimenez, *Chem*, 2022, **8**, 2961-2977.
77. P. Chen, X. He, M. Pang, X. Dong, S. Zhao and W. Zhang, *ACS Appl. Mater. Interfaces*, 2020, **12**, 20429-20439.
78. Y. Xu, S. Jin, H. Xu, A. Nagai and D. Jiang, *Chem. Soc. Rev.*, 2013, **42**, 8012-8031.
79. Z. Zhang, Y. Ye, S. Xiang and B. Chen, *Acc. Chem. Res.*, 2022, **55**, 3752-3766.

80. Y. Zou, Y. Huang, D. Si, Q. Yin, Q. Wu, Z. Weng and R. Cao, *Angew. Chem. Int. Ed.*, 2021, **60**, 20915-20920.
81. Z. Mu, Y. Zhu, B. Li, A. Dong, B. Wang and X. Feng, *J. Am. Chem. Soc.*, 2022, **144**, 5145-5154.
82. H. Wang, D. Wang, Y. Wu and Y. Zhao, *Chem.-Eur. J.*, 2024, **30**, 14.
83. J.-R. Wu, G. Wu, D. Li and Y.-W. Yang, *Angew. Chem. Int. Ed.*, 2023, **62**, e202218142.
84. T. Ogoshi, T. Kakuta and T. Yamagishi, *Angew. Chem. Int. Ed.*, 2019, **58**, 2197-2206.
85. W.-L. Guan, J.-F. Chen, J. Liu, B. Shi, H. Yao, Y.-M. Zhang, T.-B. Wei, Q. Lin, *Coord. Chem. Rev.* 2024, **507**, 215717.
86. H. Feng, Y. Yuan, J. Xiong, Y. Zheng and B.-Z. Tang, *Chem. Soc. Rev.*, 2018, **47**, 7452-7476.
87. H. Zhang, Z. Liu and Y.-L. Zhao, *Chem. Soc. Rev.*, 2018, **47**, 5491-5528.
88. S. Dong, B. Zheng, F. Wang and F. Huang, *Acc. Chem. Res.*, 2014, **47**, 1982-1994.
89. T. Kakuta, T. Yamagishi and T. Ogoshi, *Acc. Chem. Res.*, 2018, **51**, 1656-1666.
90. R. Kumar, A. Sharma, H. Singh, P. Suating, H. S. Kim, K. Sunwoo, I. Shim, B. C. Gibb and J. S. Kim, *Chem. Rev.*, 2019, **119**, 9657-9721.
91. Z. Zhang and C. Li, *Acc. Chem. Res.*, 2022, **55**, 916-929.
92. Z. Liu, S. K. M. Nalluri and J. F. Stoddart, *Chem. Soc. Rev.*, 2017, **46**, 2459-2478.
93. M. Xue, Y. Yang, X. Chi, Z. Zhang and F. Huang, *Acc. Chem. Res.*, 2012, **45**, 1294-1308.
94. X. Ji, M. Ahmed, L. Long, N. M. Khashab, F. Huang and J. L. Sessler, *Chem. Soc. Rev.*, 2019, **48**, 2682-2697.
95. Q. He, G. I. Vargas-Zúñiga, S. H. Kim, S. K. Kim and J. L. Sessler, *Chem. Rev.*, 2019, **119**, 9753-9835.
96. N. L. Strutt, H. Zhang, S. T. Schneebeli and J. F. Stoddart, *Acc. Chem. Res.*, 2014, **47**, 2631-2642.
97. Y. Zhou, K. Jie, R. Zhao and F. Huang, *Adv. Mater.*, 2020, **32**, 1904824.
98. Z. Li and Y.-W. Yang, *Adv. Mater.*, 2022, **34**, 2107401.
99. Y. Yuan, K. Bang, R. Wang and Y. Kim, *Adv. Mater.*, 2023, **35**, 2210952.
100. M. H. Gu, S. Suleman and Y. Kim, *ChemPlusChem*, 2024, DOI: 10.1002/cplu.202400597, 13.
101. A. Saura-Sanmartin, A. Pastor, A. Martinez-Cuezva, G. Cutillas-Font, M. Alajarin and J. Berna, *Chem. Soc. Rev.*, 2022, **51**, 4949-4976.
102. M. Shen, X. Lin, J. Luo, W. Li, Y. Ye and X. Wang, *Mol. Syst. Des. Eng.*, 2022, **7**, 1570-1587.
103. Q. Wu, J. Liang, D. Wang, R. Wang and C. Janiak, *Chem. Soc. Rev.*, 2024, DOI: 10.1039/d4cs00371c, 22.
104. B. H. Wilson and S. J. Loeb, *Chem*, 2020, **6**, 1604-1612.
105. S. Huang, J. Y. Choi, Q. C. Xu, Y. H. Jin, J. Park and W. Zhang, *Angew. Chem. Int. Ed.*, 2023, **62**, e202303538.
106. M. Chen, H. Li, C. Liu, J. Liu, Y. Feng, A. G. H. Wee and B. Zhang, *Coord. Chem. Rev.*, 2021, **435**, 213778.
107. S. Tashiro and M. Shionoya, *Acc. Chem. Res.*, 2020, **53**, 632-643.
108. Y. Zhang, J. Duan, D. Ma, P. Li, S. Li, H. Li, J. Zhou, X. Ma, X. Feng and B. Wang, *Angew. Chem. Int. Ed.*, 2017, **56**, 16313-16317.
109. M. Li, C. Xu and Y.-W. Yang, *Coord. Chem. Rev.*, 2024, **512**, 24.
110. T. Skorjanc, D. Shetty and A. Trabolsi, *Chem*, 2021, **7**, 882-918.
111. Y. Jiang, H. Jung, S. H. Joo, Q. K. Sun, C. Li, H. J. Noh, I. Oh, Y. J. Kim, S. K. Kwak, J. W. Yoo and J. B. Baek, *Angew. Chem. Int. Ed.*, 2021, **60**, 17191-17197.
112. M. Li, Z. Yang, Z. Li, J.-R. Wu, B. Yang and Y.-W. Yang, *Chem. Mat.*, 2022, **34**, 5726-5739.
113. T. D. Bennett and A. K. Cheetham, *Acc. Chem. Res.*, 2014, **47**, 1555-1562.
114. Q. Li, W. Zhang, O. Miljanic, C.-H. Sue, Y.-L. Zhao, L. Liu, C. B. Knobler, J. F. Stoddart and O. M. Yaghi, *Science*, 2009, **325**, 855-859.
115. K. Wang, J. Zhang, Y. C. Hsu, H. Lin, Z. Han, J. Pang, Z. Yang, R. R. Liang, W. Shi and H.-C. Zhou, *Chem. Rev.*, 2023, **123**, 5347-5420.
116. I. Nath, J. Chakraborty and F. Verpoort, *Chem. Soc. Rev.*, 2016, **45**, 4127-4170.
117. J. Xu, Y. Zhang, X. Zhu, G. Ling and P. Zhang, *J. Hazard. Mater.*, 2024, **465**, 11.
118. M. Zhao, S. Ou and C. Wu, *Acc. Chem. Res.*, 2014, **47**, 1199-1207.
119. N. L. Strutt, D. Fairen-Jimenez, J. Iehl, M. B. Lalonde, R. Q. Snurr, O. K. Farha, J. T. Hupp and J. F. Stoddart, *J. Am. Chem. Soc.*, 2012, **134**, 17436-17439.
120. Y. Wu, M. Tang, Z. Wang, L. Shi, Z. Xiong, Z. Chen, J. L. Sessler and F. Huang, *Nat. Commun.*, 2023, **14**, 4927.
121. A. Coskun, M. Hmadeh, G. Barin, F. Gándara, Q. W. Li, E. Choi, N. L. Strutt, D. B. Cordes, A. M. Z. Slawin, J. F. Stoddart, J. P. Sauvage and O. M. Yaghi, *Angew. Chem. Int. Ed.*, 2012, **51**, 2160-2163.
122. X. Li, J. Xie, Z. Du, L. Jiang, G. Li, S. Ling and K. Zhu, *Chem. Sci.*, 2022, **13**, 6291-6296.
123. L. Liu, X. Wang, Q. Zhang, Q. Li and Y.-L. Zhao, *Crystengcomm*, 2013, **15**, 841-844.
124. H.-Y. Gong, B. M. Rambo, W. Cho, V. M. Lynch, M. Oh, J. L. Sessler, *Chem. Commun.*, 2011, **47**, 5973-5975.
125. S. J. Loeb, *Chem. Soc. Rev.*, 2007, **36**, 226-235.
126. D. J. Hoffart and S. J. Loeb, *Angew. Chem. Int. Ed.*, 2005, **44**, 901-904.
127. Q. Li, H. Zhu and F. Huang, *Trends Chem.*, 2020, **2**, 850-864.
128. H. Zhang, J. Han and C. Li, *Polym. Chem.*, 2021, **12**, 2808-2824.
129. A. Harada, *Acc. Chem. Res.*, 2001, **34**, 456-464.
130. I. Roy and J. F. Stoddart, *Acc. Chem. Res.*, 2021, **54**, 1440-1453.
131. C. D. Gutsche, *Acc. Chem. Res.*, 1983, **16**, 161-170.
132. S. B. Nimse and T. Kim, *Chem. Soc. Rev.*, 2013, **42**, 366-386.
133. J. Murray, K. Kim, T. Ogoshi, W. Yao and B. C. Gibb, *Chem. Soc. Rev.*, 2017, **46**, 2479-2496.
134. X. Ni, X. Xiao, H. Cong, L. Liang, K. Cheng, X. Cheng, N. Ji, Q. Zhu, S. Xue and Z. Tao, *Chem. Soc. Rev.*, 2013, **42**, 9480-9508.
135. Y. Inokuma, T. Arai and M. Fujita, *Nat. Chem.*, 2010, **2**, 780-783.
136. Y. Inokuma, S. Yoshioka, J. Ariyoshi, T. Arai, Y. Hitora, K. Takada, S. Matsunaga, K. Rissanen and M. Fujita, *Nature*, 2013, **495**, 461.
137. S. Lee, E. A. Kapustin and O. M. Yaghi, *Science*, 2016, **353**, 808-811.
138. X. Pei, H. B. Bürgi, E. A. Kapustin, Y. Liu and O. M. Yaghi, *J. Am. Chem. Soc.*, 2019, **141**, 18862-18869.
139. R. Gao, Y. Huang, K. Chen and Z. Tao, *Coord. Chem. Rev.*, 2021, **437**, 213741.
140. J. T. Li, P. M. Bhatt, J. Y. Li, M. Eddaoudi and Y. L. Liu, *Adv. Mater.*, 2020, **32**, 2002563 .
141. R. A. Smaldone, R. S. Forgan, H. Furukawa, J. J. Gassensmith, A. M. Z. Slawin, O. M. Yaghi and J. F. Stoddart, *Angew. Chem. Int. Ed.*, 2010, **49**, 8630-8634.
142. S. P. Bew, A. D. Burrows, T. Düren, M. F. Mahon, P. Z. Moghadam, V. M. Sebestyen and S. Thurston, *Chem. Commun.*, 2012, **48**, 4824-4826.
143. E. Lee, J. Kim, J. Heo, D. Whang and K. Kim, *Angew. Chem. Int. Ed.*, 2001, **40**, 399-402.

144. S. An, Q. Xu, Z. Ni, J. Hu, C. Peng, L. Zhai, Y. Guo and H. Liu, *Angew. Chem. Int. Ed.*, 2021, **60**, 9959-9963.
145. L. Liu, Y. M. Hu, S. F. Huang, Y. Jin, J. Cui, W. Gong and W. Zhang, *Chem. Sci.*, 2021, **12**, 13316-13320.
146. V. N. Vukotic, K. J. Harris, K. L. Zhu, R. W. Schurko and S. J. Loeb, *Nat. Chem.*, 2012, **4**, 456-460.
147. K. Zhu, V. N. Vukotic, C. A. O'Keefe, R. W. Schurko and S. J. Loeb, *J. Am. Chem. Soc.*, 2014, **136**, 7403-7409.
148. Q. Li, C. Sue, S. Basu, A. Shveyd, W. Zhang, G. Barin, L. Fang, A. A. Sarjeant, J. F. Stoddart and O. M. Yaghi, *Angew. Chem. Int. Ed.*, 2010, **49**, 6751-6755.
149. V. N. Vukotic and S. J. Loeb, *Chem. Soc. Rev.*, 2012, **41**, 5896-5906.
150. L. J. Feng, X. R. Chen, M. Cao, S. L. Zhao, H. Wang, D. Chen, Y. Ma, T. Liu, N. Wang and Y. H. Yuan, *Angew. Chem. Int. Ed.*, 2023, **62**, e202312894.
151. H. An, M. Li, J. Ga, Z. Zhang, S. Ma and Y. Chen, *Coord. Chem. Rev.*, 2019, **384**, 90-106.
152. T. Chen, J. Yi, Y. Zhao and X. Chu, *J. Am. Chem. Soc.*, 2018, **140**, 9912-9920.
153. I. A. Lázaro, C. J. R. Wells and R. S. Forgan, *Angew. Chem. Int. Ed.*, 2020, **59**, 5211-5217.
154. G. Chen, S. Huang, X. Kou, S. Wei, S. Huang, S. Jiang, J. Shen, F. Zhu and G. Ouyang, *Angew. Chem. Int. Ed.*, 2019, **58**, 1463-1467.
155. M. J. Katz, J. E. Mondloch, R. K. Totten, J. K. Park, S. T. Nguyen, O. K. Farha and J. T. Hupp, *Angew. Chem. Int. Ed.*, 2014, **53**, 497-501.
156. Y. Huang, M. Zhao, S. Han, Z. Lai, J. Yang, C. Tan, Q. Ma, Q. Lu, J. Chen, X. Zhang, Z. Zhang, B. Li, B. Chen, Y. Zong and H. Zhang, *Adv. Mater.*, 2017, **29**, 1700102.
157. Y. Wu, L. Shangguan, Q. Li, J. Cao, Y. Liu, Z. Wang, H. Zhu, F. Wang and F. Huang, *Angew. Chem. Int. Ed.*, 2021, **60**, 19997-20002.
158. J. Li, D. Yim, W. D. Jang and J. Yoon, *Chem. Soc. Rev.*, 2017, **46**, 2437-2458.
159. Y. Han, Z. Meng, Y. Ma and C. Chen, *Acc. Chem. Res.*, 2014, **47**, 2026-2040.
160. Y.-L. Zhao, L. Liu, W. Zhang, C.-H. Sue, Q. Li, O. S. Miljanic, O. M. Yaghi and J. F. Stoddart, *Chem.-Eur. J.*, 2009, **15**, 13356-13380.
161. D. W. Lim, S. A. Chyun and M. P. Suh, *Angew. Chem. Int. Ed.*, 2014, **53**, 7819-7822.
162. H. Jiang, K. Yang, X. Zhao, W. Zhang, Y. Liu, J. Jiang and Y. Cui, *J. Am. Chem. Soc.*, 2021, **143**, 390-398.
163. S. An, C. Lu, Q. Xu, C. Lian, C. Peng, J. Hu, X. Zhuang and H. Liu, *ACS Energy Lett.*, 2021, **6**, 3496-3502.
164. M. B. Andrews and C. L. Cahill, *Chem. Rev.*, 2013, **113**, 1121-1136.
165. J. Liang, X. Wang, Y. Jiao, C. Qin, K. Shao, Z. Su and Q. Wu, *Chem. Commun.*, 2013, **49**, 8555-8557.
166. T. Mehtab, G. Yasin, M. Arif, M. Shakeel, R. M. Korai, M. Nadeem, N. Muhammad and X. Lu, *J. Energy Storage*, 2019, **21**, 632-646.
167. J. A. Mason, J. Oktawiec, M. K. Taylor, M. R. Hudson, J. Rodriguez, J. E. Bachman, M. I. Gonzalez, A. Cervellino, A. Guagliardi, C. M. Brown, P. L. Llewellyn, N. Masciocchi and J. R. Long, *Nature*, 2015, **527**, 357.
168. Z. Ji, H. Z. Wang, S. Canossa, S. Wuttke and O. M. Yaghi, *Adv. Funct. Mater.*, 2020, **30**, 2000238.
169. B. Wang, Q. Yang, C. Guo, Y. Sun, L. Xie and J. Li, *ACS Appl. Mater. Interfaces*, 2017, **9**, 10286-10295.
170. Y. Xia, Y. Sun, Y. Cheng, Y. Xia and X. Yin, *Anal. Chim. Acta*, 2022, **1204**, 339731.
171. I. Mironyuk, T. Tatarchuk, M. Naushad, H. Vasylyeva and I. Mykytyn, *J. Mol. Liq.*, 2019, **285**, 742-753.
172. T. Zhang, P. Li, L. L. Li and W. K. Dong, *Transit. Met. Chem.*, 2022, **47**, 53-65.
173. L. Li, K. Kang, T. S. Chee, Z. Tian, Q. Sun and C. Xiao, *Adv. Sci.*, 2024, **11**, 2308663.
174. H. Qian, C. Yang and X. Yan, *Nat. Commun.*, 2016, **7**, 12104 .
175. L. Chen, P. S. Reiss, S. Y. Chong, D. Holden, K. E. Jelfs, T. Hasell, M. A. Little, A. Kewley, M. E. Briggs, A. Stephenson, K. M. Thomas, J. A. Armstrong, J. Bell, J. Busto, R. Noel, J. Liu, D. M. Strachan, P. K. Thallapally and A. I. Cooper, *Nat. Mater.*, 2014, **13**, 954-960.
176. Z. Gu, C. Zhan, J. Zhang and X. Bu, *Chem. Soc. Rev.*, 2016, **45**, 3122-3144.
177. J. Navarro-Sánchez, A. I. Argente-García, Y. Moliner-Martínez, D. Roca-Sanjuán, D. Antypov, P. Campíns-Falcó, M. J. Rosseinsky and C. Martí-Gastaldo, *J. Am. Chem. Soc.*, 2017, **139**, 4294-4297.
178. H. Dou, M. Xu, B. Wang, Z. Zhang, G. Wen, Y. Zheng, D. Luo, L. Zhao, A. Yu, L. Zhang, Z. Jiang and Z. Chen, *Chem. Soc. Rev.*, 2021, **50**, 986-1029.
179. L. Chen, X. Sheng, G. Li and F. Huang, *Chem. Soc. Rev.*, 2022, **51**, 7046-7065.
180. L. F. Hart, J. E. Hertzog, P. M. Rauscher, B. W. Rawe, M. M. Tranquilli and S. J. Rowan, *Nat. Rev. Mater.*, 2021, **6**, 508-530.
181. J. X. Liu, K. Chen and C. Redshaw, *Chem. Soc. Rev.*, 2023, **52**, 1428-1455.
182. V. N. Vukotic, C. A. O'Keefe, K. L. Zhu, K. J. Harris, C. To, R. W. Schurko and S. J. Loeb, *J. Am. Chem. Soc.*, 2015, **137**, 9643-9651.
183. H. Liu, W. Ye, Y. Mu, H. Ma, A. Lv, S. Han, H. Shi, J. Li, Z. An, G. M. Wang and W. Huang, *Adv. Mater.*, 2022, **34**, 2107612.
184. P. Gao, Y. Jiang, H. Liu, M. Zhou, T. Li, H. Fu, L. Ma and D. Li, *ACS Appl. Mater. Interfaces*, 2022, **14**, 16435-16444.
185. E. R. Kay and D. A. Leigh, *Angew. Chem. Int. Ed.*, 2015, **54**, 10080-10088.
186. J. F. Stoddart, *Angew. Chem. Int. Ed.*, 2017, **56**, 11094-11125.
187. D. Qu, Q. Wang, Q. Zhang, X. Ma and H. Tian, *Chem. Rev.*, 2015, **115**, 7543-7588.
188. K. Zhu, C. A. O'Keefe, V. N. Vukotic, R. W. Schurko and S. J. Loeb, *Nat. Chem.*, 2015, **7**, 514-519.
189. N. Farahani, K. L. Zhu, C. A. O'Keefe, R. W. Schurko and S. J. Loeb, *ChemPlusChem*, 2016, **81**, 836-841.
190. P. Martinez-Bulit, C. A. O'Keefe, K. L. Zhu, R. W. Schurko and S. J. Loeb, *Cryst. Growth Des.*, 2019, **19**, 5679-5685.
191. B. H. Wilson, C. S. Vojvodin, G. Gholami, L. M. Abdulla, C. A. O'Keefe, R. W. Schurko and S. J. Loeb, *Chem*, 2021, **7**, 202-211.
192. B. H. Wilson, L. M. Abdulla, R. W. Schurko and S. J. Loeb, *Chem. Sci.*, 2021, **12**, 3944-3951.
193. T. Dudev and C. Lim, *Chem. Rev.*, 2014, **114**, 538-556.
194. A. Tsirigotaki, J. De Geyter, N. Sostaric, A. Economou and S. Karamanou, *Nat. Rev. Microbiol.*, 2017, **15**, 21-36.
195. J. L. Nieto-Torres, C. Verdiá-Báguena, J. M. Jimenez-Guardeño, J. A. Regla-Nava, C. Castaño-Rodriguez, R. Fernandez-Delgado, J. Torres, V. M. Aguilella and L. Enjuanes, *Virology*, 2015, **485**, 330-339.
196. J. Li, Y. Shi, C. Qi, B. Zhang, X. Xing, Y. Li, T. Chen, X. Mao, Z. Zuo, X. Zhao, Z. Pan, L. Li, X. Yang and C. Li, *Angew. Chem. Int. Ed.*, 2023, **62**, e202309918.
197. J. Shen, W. Jiang, W. Guo, Q. Qi, D. Ma, X. Lou, M. Shen, B. Hu, H. Yang and X. Zhao, *Chem. Commun.*, 2020, **56**, 595-598.
198. J. Li, J. Lan, R. Cao, J. Sun, X. Ding, X. Liu, L. Yuan and W. Shi, *ACS Appl. Mater. Interfaces*, 2023, **15**, 59544-59551.

199. A. Manna, A. K. Maharana, G. Rambabu, S. Nayak, S. Basu and S. Das, *ACS Appl. Polym. Mater.*, 2021, **3**, 5527-5535.
200. J. Kim, S. Kim, J. Park, S. Kang, D. J. Seo, N. Park, S. Lee, J. J. Kim, W. B. Lee, J. Park and J. C. Lee, *J. Am. Chem. Soc.*, 2024, **146**, 4532-4541.
201. C. Yuan, W. Jia, Z. Yu, Y. Li, M. Zi, L. Yuan and Y. Cui, *J. Am. Chem. Soc.*, 2022, **144**, 891-900.
202. X. Li, H. Xu, K. Leng, S. W. Chee, X. Zhao, N. Jain, H. Xu, J. Qiao, Q. Gao, I. H. Park, S. Y. Quek, U. Mirsaidov and K. P. Loh, *Nat. Chem.*, 2020, **12**, 1115.
203. S. Zheng, S. Bi, Y. Fu, Y. Wu, M. Liu, Q. Xu and G. Zeng, *Adv. Mater.*, 2024, **36**, 2313076.
204. J. Wang, C. Wang, S. Liu, Y. Zhang, J. Zhang, W. Dang, W. Wu and J. Wang, *ACS Appl. Nano Mater.*, 2024, **7**, 3774-3781.
205. X. Ruan, Y. Yang, W. Liu, X. Ma, C. Zhang, Q. Meng, Z. Wang, F. Cui, J. Feng, F. Cai, Y. Yuan and G. Zhu, *ACS Central Sci.*, 2021, **7**, 1698-1706.
206. S. Zhong, Y. Wang, J. Lan, M. Xie, Y. Wu, J. Li, F. J. Liu, L. Jiang, J. Peng, L. Yuan, M. Zhai and W. Shi, *CCS Chem.*, 2024, **6**, 2594–2606 .
207. S. Xu and E. A. Carter, *Chem. Rev.*, 2019, **119**, 6631-6669.
208. X. Han, C. Yuan, B. Hou, L. Liu, H. Li, Y. Liu and Y. Cui, *Chem. Soc. Rev.*, 2020, **49**, 6248-6272.
209. X. Luo, W. Li, H. Liang, H. Zhang, K. Du, X. Wang, X. Liu, J. Zhang and X. Wu, *Angew. Chem. Int. Ed.*, 2022, **61**, 8.
210. D. Y. Zhu, G. Y. Xu, M. Barnes, Y. L. Li, C. P. Tseng, Z. Q. Zhang, J. J. Zhang, Y. F. Zhu, S. Y. Khalil, M. M. Rahman, R. Verduzco and P. M. Ajayan, *Adv. Funct. Mater.*, 2021, **31**, 2100505.
211. F. Xu, S. Jin, H. Zhong, D. Wu, X. Yang, X. Chen, H. Wei, R. Fu and D. Jiang, *Sci. Rep.*, 2015, **5**, 8225.
212. J. Xiao, Q. Li, Y. Bi, M. Cai, B. Dunn, T. Glossmann, J. Liu, T. Osaka, R. Sugiura, B. Wu, J. Yang, J. Zhang and M. S. Whittingham, *Nat. Energy*, 2020, **5**, 561-568.
213. M. V. Reddy, A. Mauger, C. M. Julien, A. Paolella and K. Zaghib, *Materials*, 2020, **13**, 1884.
214. R. Fang, K. Chen, L. Yin, Z. Sun, F. Li and H. Cheng, *Adv. Mater.*, 2019, **31**, 1800863.
215. Y. Jie, X. Liu, Z. Lei, S. Wang, Y. Chen, F. Huang, R. Cao, G. Zhang and S. Jiao, *Angew. Chem. Int. Ed.*, 2020, **59**, 3505-3510.
216. R. Younesi, G. M. Veith, P. Johansson, K. Edstrom and T. Vegge, *Energy Environ. Sci.*, 2015, **8**, 1905-1922.
217. W. Huang, C. Zhao, P. Wu, H. Yuan, W. Feng, Z. Liu, Y. Lu, S. Sun, Z. Fu, J. Hu, S. Yang, J. Huang and Q. Zhang, *Adv. Energy Mater.*, 2022, **12**, 2201044.
218. Y. Cai, Y. Jiang, L. Feng, Y. Hua, H. Liu, C. Fan, M. Yin, S. Li, X. Lv and H. Wang, *Anal. Chim. Acta*, 2019, **1057**, 88-97.
219. Q. Yang and C. Zhong, *Langmuir*, 2009, **25**, 2302-2308.
220. H. Sahabudeen, H. Y. Qi, M. Ballabio, M. Polozij, S. Olthof, R. Shivhare, Y. Jing, S. Park, K. J. Liu, T. Zhang, J. Ma, B. Rellinghaus, S. Mannsfeld, T. Heine, M. Bonn, E. Canovas, Z. K. Zheng, U. Kaiser, R. H. Dong and X. L. Feng, *Angew. Chem. Int. Ed.*, 2020, **59**, 6028-6036.
221. F. Bellia, D. La Mendola, C. Pedone, E. Rizzarelli, M. Saviano and G. Vecchio, *Chem. Soc. Rev.*, 2009, **38**, 2756-2781.
222. A. Harada, Y. Takashima and H. Yamaguchi, *Chem. Soc. Rev.*, 2009, **38**, 875-882.
223. G. Crini, *Chem. Rev.*, 2014, **114**, 10940-10975.
224. B. Schmidt and C. Barner-Kowollik, *Angew. Chem. Int. Ed.*, 2017, **56**, 8350-8369.
225. P. Saokham, C. Muankaew, P. Jansook and T. Loftsson, *Molecules*, 2018, **23**, 1161.
226. A. Cid-Samamed, J. Rakmai, J. C. Mejuto, J. Simal-Gandara and G. Astray, *Food Chem.*, 2022, **384**, 132467.
227. S. S. Jambhekar and P. Breen, *Drug Discov. Today*, 2016, **21**, 356-362.
228. E. Pinho, M. Grootveld, G. Soares and M. Henriques, *Carbohydr. Polym.*, 2014, **101**, 121-135.
229. R. S. Forgan, R. A. Smaldone, J. J. Gassensmith, H. Furukawa, D. B. Cordes, Q. W. Li, C. E. Wilmer, Y. Y. Botros, R. Q. Snurr, A. M. Z. Slawin and J. F. Stoddart, *J. Am. Chem. Soc.*, 2012, **134**, 406-417.
230. S. M. Yoon, S. C. Warren and B. A. Grzybowski, *Angew. Chem. Int. Ed.*, 2014, **53**, 4437-4441.
231. L. Y. Hu, K. Li, W. L. Shang, X. F. Zhu and M. H. Liu, *Angew. Chem. Int. Ed.*, 2020, **59**, 4953-4958.
232. T. D. Bennett and S. Horike, *Nat. Rev. Mater.*, 2018, **3**, 431-440.
233. P. Li, S. Y. Moon, M. A. Guelta, S. P. Harvey, J. T. Hupp and O. K. Farha, *J. Am. Chem. Soc.*, 2016, **138**, 8052-8055.
234. D. Feng, K. Wang, Z. Wei, Y. Chen, C. M. Simon, R. K. Arvapally, R. L. Martin, M. Bosch, T. Liu, S. Fordham, D. Yuan, M. A. Omary, M. Haranczyk, B. Smit and H.-C. Zhou, *Nat. Commun.*, 2014, **5**, 5723.
235. S. Zhou, O. Shekhah, J. T. Jia, J. Czaban-Józwiak, P. M. Bhatt, A. Ramírez, J. Gascon and M. Eddaoudi, *Nat. Energy*, 2021, **6**, 882-891.
236. N. S. Bobbitt, M. L. Mendonca, A. J. Howarth, T. Islamoglu, J. T. Hupp, O. K. Farha and R. Q. Snurr, *Chem. Soc. Rev.*, 2017, **46**, 3357-3385.
237. M. Ali, N. K. Jha, N. Pal, A. Keshavarz, H. Hoteit and M. Sarmadivaleh, *Earth-Sci. Rev.*, 2022, **225**, 27.
238. Z. Zhang, T. Wang, M. J. Blunt, E. J. Anthony, A. H. A. Park, R. W. Hughes, P. A. Webley and J. Yan, *Appl. Energy*, 2020, **278**, 115627.
239. A. Cadiau, K. Adil, P. M. Bhatt, Y. Belmabkhout and M. Eddaoudi, *Science*, 2016, **353**, 137-140.
240. H. Li, K. Wang, Y. Sun, C. T. Lollar, J. Li and H.-C. Zhou, *Mater. Today*, 2018, **21**, 108-121.
241. J. J. Gassensmith, H. Furukawa, R. A. Smaldone, R. S. Forgan, Y. Y. Botros, O. M. Yaghi and J. F. Stoddart, *J. Am. Chem. Soc.*, 2011, **133**, 15312-15315.
242. J. J. Gassensmith, J. Y. Kim, J. M. Holcroft, O. K. Farha, J. F. Stoddart, J. T. Hupp and N. C. Jeong, *J. Am. Chem. Soc.*, 2014, **136**, 8277-8282.
243. D. Wu, J. J. Gassensmith, D. Gouvêa, S. Ushakov, J. F. Stoddart and A. Navrotsky, *J. Am. Chem. Soc.*, 2013, **135**, 6790-6793.
244. C. A. Schalley, *Mass Spectrom. Rev.*, 2001, **20**, 253-309.
245. H. A. Patel, T. Islamoglu, Z. C. Liu, S. K. M. Nalluri, A. Samanta, O. Anamimoghadam, C. D. Malliakas, O. K. Farha and J. F. Stoddart, *J. Am. Chem. Soc.*, 2017, **139**, 11020-11023.
246. X. R. Wang, C. L. Chi, K. Zhang, Y. H. Qian, K. M. Gupta, Z. X. Kang, J. W. Jiang and D. Zhao, *Nat. Commun.*, 2017, **8**, 14460.
247. N. A. Khan and S. H. Jhung, *J. Hazard. Mater.*, 2017, **325**, 198-213.
248. B. Van de Voorde, B. Bueken, J. Denayer and D. De Vos, *Chem. Soc. Rev.*, 2014, **43**, 5766-5788.
249. D. Banerjee, C. M. Simon, A. M. Plonka, R. K. Motkuri, J. Liu, X. Y. Chen, B. Smit, J. B. Parise, M. Haranczyk and P. K. Thallapally, *Nat. Commun.*, 2016, **7**, 11831.
250. J. M. Holcroft, K. J. Hartlieb, P. Z. Moghadam, J. G. Bell, G. Barin, D. P. Ferris, E. D. Bloch, M. M. Algaradah, M. S. Nassar, Y. Y. Botros, K. M. Thomas, J. R. Long, R. Q. Snurr and J. F. Stoddart, *J. Am. Chem. Soc.*, 2015, **137**, 5706-5719.

251. K. J. Hartlieb, J. M. Holcroft, P. Z. Moghadam, N. A. Vermeulen, M. M. Algaradah, M. S. Nassar, Y. Y. Botros, R. Q. Snurr and J. F. Stoddart, *J. Am. Chem. Soc.*, 2016, **138**, 2292-2301.
252. X. Z. Lian, Y. Fang, E. Joseph, Q. Wang, J. Li, S. Banerjee, C. Lollar, X. Wang and H.-C. Zhou, *Chem. Soc. Rev.*, 2017, **46**, 3386-3401.
253. D. Feng, T. Liu, J. Su, M. Bosch, Z. Wei, W. Wan, D. Yuan, Y. Chen, X. Wang, K. Wang, X. Lian, Z. Gu, J. Park, X. Zou and H. C. Zhou, *Nat. Commun.*, 2015, **6**, 5979.
254. Y. Zhang, J. Ge and Z. Liu, *ACS Catal.*, 2015, **5**, 4503-4513.
255. X. Chen, H. Chen, L. Dordevic, Q. Guo, H. Wu, Y. Wang, L. Zhang, Y. Jiao, K. Cai, H. Chen, C. L. Stern, S. I. Stupp, R. Q. Snurr, D. K. Shen and J. F. Stoddart, *J. Am. Chem. Soc.*, 2021, **143**, 9129-9139.
256. D. Shen, G. Wang, Z. Liu, P. Li, K. Cai, C. Cheng, Y. Shi, J. Han, C. W. Kung, X. Gong, Q. Guo, H. Chen, A. C. H. Sue, Y. Y. Botros, A. Facchetti, O. K. Farha, T. J. Marks and J. F. Stoddart, *J. Am. Chem. Soc.*, 2018, **140**, 11402-11407.
257. A. Feng, Y. Wang, J. Ding, R. Xu and X. Li, *Curr. Drug Deliv.*, 2021, **18**, 297-311.
258. S. S. Nagarkar, A. V. Desai and S. K. Ghosh, *Chem.-Asian J.*, 2014, **9**, 2358-2376.
259. C. Li, K. Wang, J. Li and Q. Zhang, *ACS Mater. Lett.*, 2020, **2**, 779-797.
260. L. Cui, X. Wang, Z. Y. Liu, Z. Q. Li, Z. W. Bai, K. Lin, J. Yang, Y. L. Cui and F. Tian, *Int. J. Biol. Macromol.*, 2023, **240**, 124370.
261. J. Zhou, G. Y. Liu, Z. J. Guo, M. Wang, C. Y. Qi, G. Chen, X. D. Huang, S. Yan and D. H. Xu, *Chem. Eng. J.*, 2023, **455**, 140167.
262. X. S. Meng, B. Gui, D. Q. Yuan, M. Zeller and C. Wang, *Sci. Adv.*, 2016, **2**, e1600480.
263. Z. Guo, Y. Zhang, Y. Dong, J. Li, S. Li, P. Shao, X. Feng and B. Wang, *J. Am. Chem. Soc.*, 2019, **141**, 1923-1927.
264. C. Yuan, X. Wu, R. Gao, X. Han, Y. Liu, Y. Long and Y. Cui, *J. Am. Chem. Soc.*, 2019, **141**, 20187-20197.
265. M. Wan, Y. Zheng, X. Dai, H. Yang, J. Zhou, J. Ou, Y. Yang, M. Liao, Z. Xia and L. Wang, *Chem. Mater.*, 2023, **35**, 609-616.
266. L. Hu, X. Zhu, C. Yang and M. Liu, *Angew. Chem. Int. Ed.*, 2022, **61**, e202114759.
267. S. Liu, M. Wang, T. Qian, H. Ji, J. Liu and C. Yan, *Nat. Commun.*, 2019, **10**, 3898.
268. Z. Chen, J. Wang, M. Hao, Y. Xie, X. Liu, H. Yang, G. I. N. Waterhouse, X. Wang and S. Ma, *Nat. Commun.*, 2023, **14**, 1106.
269. M. Calik, F. Auras, L. M. Salonen, K. Bader, I. Grill, M. Handloser, D. D. Medina, M. Dogru, F. Löbermann, D. Trauner, A. Hartschuh and T. Bein, *J. Am. Chem. Soc.*, 2014, **136**, 17802-17807.
270. X. Wu, Y. Hong, B. Xu, Y. Nishiyama, W. Jiang, J. Zhu, G. Zhang, S. Kitagawa and S. Horike, *J. Am. Chem. Soc.*, 2020, **142**, 14357-14364.
271. S. Giannini and J. Blumberger, *Acc. Chem. Res.*, 2022, **55**, 819-830.
272. S. Kandambeth, V. Venkatesh, D. B. Shinde, S. Kumari, A. Halder, S. Verma and R. Banerjee, *Nat. Commun.*, 2015, **6**, 6786.
273. F. Beuerle and B. Gole, *Angew. Chem. Int. Ed.*, 2018, **57**, 4850-4878.
274. R. Chen, Y. Wang, Y. Ma, A. Mal, X. Gao, L. Gao, L. Qiao, X. Li, L. Wu and C. Wang, *Nat. Commun.*, 2021, **12**, 1354.
275. X. Ran, P. Guo, C. Liu, Y. Zhu, C. Liu, B. Wang, J. Zhang, S. Xie and L. Yuan, *Molecules*, 2023, **28**, 662.
276. D. Guo and Y. Liu, *Acc. Chem. Res.*, 2014, **47**, 1925-1934.
277. D. Guo and Y. Liu, *Chem. Soc. Rev.*, 2012, **41**, 5907-5921.
278. Y. Pan, X. Hu and D. Guo, *Angew. Chem. Int. Ed.*, 2021, **60**, 2768-2794.
279. C. Chen, X. Ni, H. Tian, Q. Liu, D. Guo and D. Ding, *Angew. Chem. Int. Ed.*, 2020, **59**, 10008-10012.
280. C. Wieser, C. B. Dieleman and D. Matt, *Coord. Chem. Rev.*, 1997, **165**, 93-161.
281. W. Maes and W. Dehaen, *Chem. Soc. Rev.*, 2008, **37**, 2393-2402.
282. O. Santoro and C. Redshaw, *Coord. Chem. Rev.*, 2021, **448**, 214173.
283. A. Ovsyannikov, S. Solovieva, I. Antipin and S. Ferlay, *Coord. Chem. Rev.*, 2017, **352**, 151-186.
284. G. Sachdeva, D. Vaya, C. M. Srivastava, A. Kumar, V. Rawat, M. Singh, M. Verma, P. Rawat and G. K. Rao, *Coord. Chem. Rev.*, 2022, **472**, 214791.
285. I. Ling and C. L. Roston, *Coord. Chem. Rev.*, 2018, **375**, 80-105.
286. L. Mutihac, J. H. Lee, J. S. Kim and J. Vicens, *Chem. Soc. Rev.*, 2011, **40**, 2777-2796.
287. M. Schulz, A. Gehl, J. Schlenkrich, H. A. Schulze, S. Zimmermann and A. Schaate, *Angew. Chem. Int. Ed.*, 2018, **57**, 12961-12965.
288. U. Jeong, N. A. Dogan, M. Garai, T. S. Nguyen, J. F. Stoddart and C. T. Yavuz, *J. Am. Chem. Soc.*, 2019, **141**, 12182-12186.
289. Y. Liu, X. Zhang, K. Li, Q. Peng, Y. Qin, H. Hou, S. Zang and B.-Z. Tang, *Angew. Chem. Int. Ed.*, 2021, **60**, 22417-22423.
290. R. Ha, F. Liu, J. Li, M. He, J. Lan, B. Wang, J. Sun, X. Liu, X. Ding and W. Shi, *ACS Appl. Mater. Interfaces*, 2023, **15**, 5657–5666.
291. J. Xu, W. Liu, L. Jiang, X. Jing, L. Liu and Z. Li, *Small*, 2023, **19**, 2304989.
292. Y. Li, W. Miao, M. He, C. Li, H. Gu and X. Zhang, *Ore Geol. Rev.*, 2023, **155**, 105356.
293. H. Liu, Z. Huang, K. Wen and B. Jiang, *Chin. J. Org. Chem.*, 2014, **34**, 316-324.
294. Y. Tang, H. Zhang and J. Ying, *Int. Geol. Rev.*, 2010, **52**, 964-976.
295. J. Zheng, M. Tang and Y. Hu, *Angew. Chem. Int. Ed.*, 2016, **55**, 12538-12542.
296. S. Z. Andersen, V. Colic, S. Yang, J. A. Schwalbe, A. C. Nielander, J. M. McEnaney, K. Enemark-Rasmussen, J. G. Baker, A. R. Singh, B. A. Rohr, M. J. Statt, S. J. Blair, S. Mezzavilla, J. Kibsgaard, P. C. K. Vesborg, M. Cargnello, S. F. Bent, T. F. Jaramillo, I. E. L. Stephens, J. K. Norskov and I. Chorkendorff, *Nature*, 2019, **570**, 504.
297. J. Zheng and Y. Hu, *ACS Appl. Mater. Interfaces*, 2018, **10**, 4113-4120.
298. E. A. Symons, *Sep. Sci. Technol.*, 1985, **20**, 633-651.
299. S. Navalón, A. Dhakshinamoorthy, M. Alvaro, B. Ferrer and H. García, *Chem. Rev.*, 2022, **123**, 445–490.
300. B. Xiang, J. Gong, Y. Sun, W. Yan, R. Jin and J. Li, *J. Membr. Sci.*, 2024, **691**, 122247.
301. E. A. Dolgopolova, A. M. Rice, C. R. Martin and N. B. Shustova, *Chem. Soc. Rev.*, 2018, **47**, 4710-4728.
302. K. I. Assaf and W. M. Nau, *Chem. Soc. Rev.*, 2015, **44**, 394-418.
303. H. Nie, Z. Wei, X. Ni and Y. Liu, *Chem. Rev.*, 2022, **122**, 9032-9077.
304. S. Funk and J. Schatz, *J. Incl. Phenom. Macrocycl. Chem.*, 2020, **96**, 1-27.
305. F. Biedermann, W. M. Nau and H. J. Schneider, *Angew. Chem. Int. Ed.*, 2014, **53**, 11158-11171.
306. L.-L. Tan, M.-Y. Wei, L.-Shang and Y.-W. Yang, *Adv. Funct. Mater.*, 2021, **31**, 26.

307. L. Zhu, M. Zhu and Y.-L. Zhao, *ChemPlusChem*, 2017, **82**, 30-41.
308. E. Y. Chernikova and D. V. Berdnikova, *Chem. Commun.*, 2020, **56**, 15360-15376.
309. J. Liang, V. Gvilava, C. Jansen, S. Öztürk, A. Spiess, J. Lin, S. Xing, Y. Sun, H. Wang and C. Janiak, *Angew. Chem. Int. Ed.*, 2021, **60**, 15365-15370.
310. Q. Li, J. Sun, B. Yang, H. Wang, D. Zhang, D. Ma and Z.-T. Li, *Chin. Chem. Lett.*, 2022, **33**, 1988-1992.
311. X. Chi, X. Ji, D. Xia and F. Huang, *J. Am. Chem. Soc.*, 2015, **137**, 1440-1443.
312. K. Jie, Y. Zhou, E. Li and F. Huang, *Acc. Chem. Res.*, 2018, **51**, 2064-2072.
313. C. Li, *Chem. Commun.*, 2014, **50**, 12420-12433.
314. B. Shi, K. Jie, Y. Zhou, J. Zhou, D. Xia and F. Huang, *J. Am. Chem. Soc.*, 2016, **138**, 80-83.
315. H. Zhang, Z. Liu, F. Xin and Y.-L. Zhao, *Coord. Chem. Rev.*, 2020, **420**, 213425.
316. Z. Li, Z. Shen, Y. Pei, S. Chao and Z. Pei, *Chem. Commun.*, 2023, **59**, 989-1005.
317. Y. Wu, J. Zhou, E. Li, M. Wang, K. Jie, H. Zhu and F. Huang, *J. Am. Chem. Soc.*, 2020, **142**, 19722-19730.
318. Y. Wu, Q. Li, J. Cao, Y. Liu, Z. Wang, L. Shangguan and H. Zhu, *ACS Appl. Nano Mater.*, 2021, **4**, 11126-11133.
319. Q. Li, Y. Wu, Y. Liu, L. Shangguan, B. Shi and H. Zhu, *Org. Lett.*, 2020, **22**, 6662-6666.
320. Q. Li, Y. Wu, J. Cao, Y. Liu, Z. Wang, H. Zhu, H. Zhang and F. Huang, *Angew. Chem. Int. Ed.*, 2022, **61**, e202202381.
321. J. Cao, Y. Wu, Q. Li, W. Zhu, Z. Wang, Y. Liu, K. Jie, H. Zhu and F. Huang, *Chem. Sci.*, 2022, **13**, 7536-7540.
322. M. Yan and J. Zhou, *Molecules*, 2023, **28**, 1470.
323. H.-C. Zhang and Y.-L. Zhao, *Chem.-Eur. J.*, 2013, **19**, 16862-16879.
324. H. Zhu, Q. Li, Z. Gao, H. Wang, B. Shi, Y. Wu, L. Shangguan, X. Hong, F. Wang and F. Huang, *Angew. Chem. Int. Ed.*, 2020, **59**, 10868-10872.
325. B. Zhao, J. Wang, L. Shao, Y. Wu, M. Li, B. Hua and F. Huang, *Chem. Commun.*, 2023, **59**, 10432-10435.
326. P. Li, Y. Chen and Y. Liu, *Chin. Chem. Lett.*, 2019, **30**, 1190-1197.
327. Y. Fang, Y. Deng and W. Dehaen, *Coord. Chem. Rev.*, 2020, **415**, 213313.
328. N. L. Strutt, H. C. Zhang and J. F. Stoddart, *Chem. Commun.*, 2014, **50**, 7455-7458.
329. Z. Liu, H. Zhang and J. Han, *Org. Biomol. Chem.*, 2021, **19**, 3287-3302.
330. M. Cheng, Q. Wang, Y. Cao, Y. Pan, Z. Yang, J. Jiang and L. Wang, *Tetrahedron Lett.*, 2016, **57**, 4133-4137.
331. K. Omoto, S. Tashiro and M. Shionoya, *Chem. Sci.*, 2019, **10**, 7172-7176.
332. G. Brancatelli, S. Geremia, C. Gaeta, P. Della Sala, C. Talotta, M. De Rosa and P. Neri, *Crystengcomm*, 2016, **18**, 5045-5049.
333. S. G. Mitchell, C. Streb, H. N. Miras, T. Boyd, D. L. Long and L. Cronin, *Nat. Chem.*, 2010, **2**, 308-312.
334. W. Meng, S. Kondo, T. Ito, K. Komatsu, J. Pirillo, Y. Hijikata, Y. Ikuhara, T. Aida and H. Sato, *Nature*, 2021, **598**, 298.
335. E. L. Spitler and W. R. Dichtel, *Nat. Chem.*, 2010, **2**, 672-677.
336. Y. Du, H. Yang, J. M. Whiteley, S. Wan, Y. Jin, S. H. Lee and W. Zhang, *Angew. Chem. Int. Ed.*, 2016, **55**, 1737-1741.
337. H. Yonezawa, S. Tashiro, T. Shiraogawa, M. Ehara, R. Shimada, T. Ozawa and M. Shionoya, *J. Am. Chem. Soc.*, 2018, **140**, 16610-16614.
338. R. Yu, Y. Ying, R. Gao and Y. Long, *Angew. Chem. Int. Ed.*, 2019, **58**, 3706-3714.
339. L. Dong, Z. Gao and N. Lin, *Prog. Surf. Sci.*, 2016, **91**, 101-135.
340. B. An, J. Zhang, K. Cheng, P. Ji, C. Wang and W. Lin, *J. Am. Chem. Soc.*, 2017, **139**, 3834-3840.
341. T. Zeng, X. Zhang, S. Wang, H. Niu and Y. Cai, *Environ. Sci. Technol.*, 2015, **49**, 2350-2357.
342. A. Saura-Sanmartin, A. Martinez-Cuezva, D. Bautista, M. R. B. Marzari, M. A. P. Martins, M. Alajarin and J. Berna, *J. Am. Chem. Soc.*, 2020, **142**, 13442-13449.
343. A. Saura-Sanmartin, A. Martinez-Cuezva, M. Marin-Luna, D. Bautista and J. Berna, *Angew. Chem. Int. Ed.*, 2021, **60**, 10814-10819.
344. A. Saura-Sanmartin, G. Cutillas-Font, A. Martinez-Cuezva, M. Alajarin, F. Esteban-Betegón, P. Pena-Sánchez, F. Gándara and J. Berna, *Chem. Commun.*, 2024, **60**, 6431-6434.
345. T. Takata, N. Kihara and Y. Furusho, in *Polymer Synthesis*, Springer-Verlag Berlin, Berlin, 2004, **171**, 1-75.
346. Q. Chen, J. Sun, P. Li, I. Hod, P. Z. Moghadam, Z. S. Kean, R. Q. Snurr, J. T. Hupp, O. K. Farha and J. F. Stoddart, *J. Am. Chem. Soc.*, 2016, **138**, 14242-14245.
347. L. Feng, Y. Qiu, Q. Guo, Z. Chen, J. S. W. Seale, K. He, H. Wu, Y. Feng, O. K. Farha, R. D. Astumian and J. F. Stoddart, *Science*, 2021, **374**, 1215.
348. K. Lu, A. L. Peláez, L. Wu, Y. Cao, C. Zhu and H. Fu, *Inorg. Chem.*, 2019, **58**, 1794-1805.
349. H. Yang, Y. Du, S. Wan, G. D. Trahan, Y. Jin and W. Zhang, *Chem. Sci.*, 2015, **6**, 4049-4053.
350. Y. Yang, P. Zhang, L. Hao, P. Cheng, Y. Chen and Z. Zhang, *Angew. Chem. Int. Ed.*, 2021, **60**, 21838-21845.
351. Z. Yang, J. Liu, Y. Li, G. Zhang, G. Xing and L. Chen, *Angew. Chem. Int. Ed.*, 2021, **60**, 20754-20759.
352. A. M. Evans, A. Giri, V. K. Sangwan, S. N. Xun, M. Bartnof, C. G. Torres-Castanedo, H. B. Balch, M. S. Rahn, N. P. Bradshaw, E. Vitaku, D. W. Burke, H. Li, M. J. Bedzyk, F. Wang, J. L. Brédas, J. A. Malen, A. J. H. McGaughey, M. C. Hersam, W. R. Dichtel and P. E. Hopkins, *Nat. Mater.*, 2021, **20**, 1142.
353. C. Li, J. Liu, H. Li, K. Wu, J. Wang and Q. Yang, *Nat. Commun.*, 2022, **13**, 2357.
354. L. Zhai, Z. Xie, C. Cui, X. Yang, Q. Xu, X. Ke, M. Liu, L. Qu, X. Chen and L. Mi, *Chem. Mater.*, 2022, **34**, 5232-5240.
355. X. Chen, D. Zhang, H. Zhang, CN104478946-A; CN104478946-B, issued on 07 Dec 2018.
356. K. Choi, H. S. Lee, S. I. Jang, K. M. Choi, H. Lee, WO2021154038-A1; KR2021097272-A, issued on 09 Aug 2021.
357. H. G. Ji, Y. A. Park, Y. J. Kang, S. Y. Son, K. Jin, S. S. Yeon, S. Son, Y. Jiang, N. Piao, H. Ji, WO2021112437-A1; KR2021071296-A; CN115066229-A; EP4070781-A1; US2023018579-A1; JP2023504888-W; EP4070781-A4, issued on 31 Jan 2024.
358. Y. Ji, H. Luo, J. Chen, CN113209952-A; CN113209952-B, issued on 29 Apr 2022.
359. W. Qian, F. Meng, H. Peng, Z. Guo, J. Xiao, L. Wu, X. Zhang, J. Zhang, CN106619522-A; CN106619522-B, issued on 12 Nov 2019.
360. Y. Xu, X. Chen, W. Zhang, S. Li, L. Chen, X. Shen, CN109799159-A; CN109799159-B, issued on 28 May 2021.
361. Y. Yao, H. Guo, J. Wang, Y. Ding, D. Wang, B. Lu, CN113185660-A; CN113185660-B, issued on 22 Aug 2023.
362. L. Zhang, H. He, Y. Chen, C. Min, Z. Liu, J. Li, CN111747923-A; CN111747923-B, issued on 06 Dec 2022.

Yitao Wu

Yitao Wu was born in Tongxiang, Zhejiang, China in 1996. He received his B.S. (2019) degree from Zhejiang University of Technology. Then he joined the group of Prof. Feihe Huang at Zhejiang University and received his Ph.D. (2024) degree in chemistry. His current research is macrocycle-based metal–organic frameworks.

Meiqi Tang

Meiqi Tang was born in Taian, Liaoning, China in 1998. She received her B.S. (2020) degree and M.S. (2023) degree from Zhejiang University. Her current research is focusing crystalline framework materials and responsive polymer materials.

Michael L. Barsoum

Michael L. Barsoum was born in Moorestown, New Jersey in 1997. He received a joint B.S./M.S. degree in Materials Science and Engineering from Drexel University (2021). He joined Prof. Omar K. Farha and Prof. Vinayak Dravid's groups in 2021 as a graduate student and Ryan Fellow. His research is focusing on the *in situ* electron microscopy study of MOFs for direct air capture (DAC) of CO_2.

Zhijie Chen

Zhijie Chen was born in Fuzhou, Fujian, China. He received his B.S. (2012) degree from Shanghai Jiao Tong University under the supervision of Prof. Yong Cui, and Ph.D. (2018) degree from King Abdullah University of Science and Technology under the supervision of Prof. Mohamed Eddaoudi. He was a postdoctoral researcher in Prof. Omar K. Farha's group at Northwestern University from 2018 to 2021. He joined the Department of Chemistry at Zhejiang University as a ZJU100 Young Professor in 2022. His research interest is related to the synthesis of functional porous materials, as well as their structure-property relationships.

Feihe Huang

Feihe Huang is Qiushi Distinguished Professor of Zhejiang University. His current research is focusing on supramolecular chemistry. Awards and honors he has received include Chinese Chemical Society AkzoNobel Chemical Sciences Award, The Cram Lehn Pedersen Prize in Supramolecular Chemistry, Royal Society of Chemistry Polymer Chemistry Lectureship award, and Bruno Werdelmann Lectureship Award. His publications have been cited more than 42372 times. His h-index is 109. He sits/sat on the Advisory Boards of *JACS*, *Chem. Soc. Rev.*, *Chem. Commun.*, *Macromolecules*, *ACS Macro. Lett.*, and *Polym. Chem*. He is also an Editorial Board Member of *Mater. Chem. Front.*

Data availability statements

The authors declare that all other data supporting the discussions are available in the Review. Figures reused from previously published work are with the permission from the publisher of the original source and are made clear in the manuscript.